博士論文

幼若期社会隔離と脳幹腕傍核領域慢性的活性化による脳神経回路と行動の制御

井口　理沙

1. Introduction

In this thesis, I report four studies aiming at revealing the effect of stress and stress-related neural circuits on animal behaviors and brain development. The first and second studies are related to neuronal circuit maturation in juvenile mice. In the first study, I analyzed the effect of juvenile social isolation stress on synaptic morphology and dynamics. In the second study, I assessed the roles of subunit compositions of NMDA-type glutamate receptors (NMDARs) on postnatal neural circuit remodeling. Next, I examined the effect of stress on behavior and neuronal circuit alterations. In the third study, I conducted behavioral tests to analyze the long-term impact of stress on emotion and memory formation. In the fourth study, I focused on the parabrachial nucleus (PB), a region related to chronic pain, and evaluated the effect of chronic pain on emotion and memory formation.

In the first study, I evaluated the effect of social isolation in the early development on neuronal circuit formation and maturation. The socially isolated mice have a higher ratio of synapses without postsynaptic scaffold protein PSD-95. The spine turnover rate in the socially isolated mice was not impaired and distinct from the autism spectrum syndrome (ASD) model mice, which showed enhanced spine dynamics.

In the second study, I evaluate the contribution of the ratio of NMDA receptor

2A subunit (GluN2A) and 2B subunit (GluN2B) in spine turnover in vivo. The transition of dominant GluN2 subunits from GluN2B to GluN2A occurs in the neuronal circuit maturation process. The expression ratio of GluN2A and GluN2B was manipulated by in utero electroporation, and in vivo spine dynamics were analyzed. The neurons with a modified GluN2A/GluN2B ratio showed no deficit in spine morphology and dynamics. The results suggested that the GluN2 subunit ratio is not a dominant factor for spine dynamics and may not be related to the enhanced spine turnover seen in ASD model mice.

In the third study, I evaluate the effect of juvenile socially isolation stress on the neuronal circuit. Mice that received social isolation at the juvenile stage were assessed for their behaviors related to anxiety, social interaction, and fear memory formation in the adult stage. The result showed that socially isolated mice have relatively higher escape behavior in fear memory retrieval and indicated the long-term effect of social isolation stress on behavior.

In the fourth study, I focused on the parabrachial nucleus (PB). The neuronal activity in PB contributes to various stress reactions, feeding, sleep, and pain. However, the detailed effect on emotional behavior has not yet been clarified. To study how chronic activation of PB leads to changes in memory formation and behavior, I activated neurons in PB by designer receptors exclusively activated by designer drugs system (DREADD)

in mice and evaluate their behavior. The mice with chronically activated PB showed anxiety behavior more frequently with a lower freezing rate in fear memory retrieval. Also, the mice showed enhanced activation in the amygdala CeC region besides the manipulated PB, and the *c-Fos* expression in these areas correlated with high anxiety behavior.

The precise mechanism of neural circuit impairment in ASD is under intensive investigation, but the relative contribution of genetic and environmental factors has not yet been clarified. In this study, I evaluated the long-lasting impact of early postnatal stress in the context of the neuronal circuit development in the neocortex and the behaviors related to learning and emotion. Social isolation is an established method to impose chronic stress in juvenile mice. I found immature dendritic spines and moderate changes in emotional behavior in mice with juvenile social isolation. Both spine phenotype and behavioral alterations suggested the long-lasting impact of early postnatal stress on brain function. The effect of social isolation should be mediated via multiple sensory systems, and delineation of the responsible circuit is not straightforward. Therefore, I utilized DREADD-based selective activation of the PB to evaluate the effect of activating stress-related neural circuits. Anxiety behavior induced by activation of the PB suggested the possible alterations in the stress-related circuits and increased stress

sensitivity. These results are in line with the idea that juvenile stress exposure may increase the risk of long-lasting vulnerability to adverse social conditions in adolescence.

２．Spine dynamics in socially isolated mice

２－１．Summary

Deficits in attention and emotion recognition are postulated to be associated with social isolation during the juvenile period. These behavioral impairments may be caused by miswiring of the cortical neuronal circuits during postnatal development. However, the detailed analysis of the circuit-level changes associated with social isolation has not yet been performed. To clarify this point, I analyzed the relationship between environmental factors and alternation in spine morphological characteristics and dynamics. After isolation of pups from their mothers and siblings from postnatal day (PND) 7 to 11 for 6 h per day, I performed in vivo two-photon microscopy to evaluate spine dynamics and morphology of the layer 2/3 pyramidal neurons in the somatosensory cortex at postnatal 3 weeks old. I found a reduced fraction of PSD-95-positive dendritic spines after social isolation. However, the rate of spine turnover was preserved. I conclude that neonatal social isolation impaired spine maturation but preserved their turnover. This spine phenotype is distinct from that in multiple mouse models of autism spectrum disorders.

２－２．Introduction

Development and functional maturation of neuronal circuits rely on the turnover and stabilization of dendritic spines. Previous in vivo imaging studies revealed that pyramidal neurons in the somatosensory cortex (SSC) of juvenile mice show higher spine dynamics than those in adult mice (Holtmaat et al., 2005), suggesting that more extensive remodeling of synaptic connections in the early developmental stage and the subsequent stabilization of the neuronal network in the postnatal period. Impaired spine dynamics may be related to neurodevelopmental disorders and psychiatric diseases. Autism spectrum disorder (ASD) is characterized by typical symptoms of reduced communications, repetitive behaviors, and restricted interests, which can be detected at around 3 years of age (Ecker et al., 2013; Geschwind, 2008). Multiple ASD risk genes (Huguet et al., 2013), but the complex interactions between genes and environment have not yet been clarified. Previous intravital spine imaging revealed enhanced spine turnover in pyramidal neurons in the SSC of multiple ASD model mice; patDp/+ mice, NLG R451C mice, BTBR mice (Isshiki et al., 2014) and also in model mice of ASD-related disorders; the fragile X syndrome and the Rett syndrome (Jiang et al., 2013; Nagaoka et al., 2016; Pan et al., 2010). These observations support the idea that ASD model mice and human patients may share similar neuronal circuit defects, especially in the stability of

synaptic connections.

Whether the deficit in spine dynamics is shared in other developmental and psychiatric disorders is an important question to be answered. Human genome studies on psychiatric disorders have been highly effective in identifying responsible genes. However, environmental factors have been shown to be as important as the genetic factors in the etiology of psychiatric disorders (Carr et al., 2013; Maguire et al., 2015; Platt et al., 2013). Social isolation, such as neglect and social rejection, has been reported to be a possible risk factor that affects brain functions and may increase the risk of developing multiple psychiatric disorders (Insel & Fernald, 2004). Isolation of mice from their mothers and siblings in the juvenile stage has been used as a model of neglect and social rejection in humans. Previous studies revealed that social isolation in mice induces altered neocortical neural circuits, glial responses, and behavior (Makinodan et al., 2012; Miyazaki et al., 2012; Tada et al., 2016; Takatsuru et al., 2009; Yamamuro et al., 2018). Neonatal mice develop skills of social communication through the tactile sensation with mothers and siblings, together with ultrasonic vocalization (Pasciuto et al., 2015), which is processed in the SSC and the auditory cortex, triggering their remodeling and maturation (Holtmaat & Svoboda, 2009). The previous study showed that neonatal social isolation protocol as in this study can cause disruption of experience-dependent synaptic

delivery of AMPA receptors and aberrant neuronal circuit formation at neuronal pathway from the somatosensory cortex layer 4 to layer 2/3 (Miyazaki et al., 2014). This study also reported that the isolated mice have attenuated sensitivity of whiskers by field excitatory postsynaptic currents (f EPSC) recording in the somatosensory cortex layer 2/3 neurons of the barrel column to the deflection of principal whiskers. The socially isolated mice are also known to have abnormal behavior dependent on whisker-barrel function. Therefore, I performed in vivo two-photon imaging of dendritic spines and evaluated the possible alterations of spine dynamics in the SSC after social isolation. After social isolation, spines without a major postsynaptic scaffolding protein PSD-95 increased, while the rate of both addition and elimination of spines was preserved. Thus, social isolation and ASD-related genetic alterations impact the neuronal network differently, with the former inhibiting the maturation of dendritic spines by inhibiting PSD-95 accumulation, while the latter enhancing the turnover of dendritic spines.

２－３．Materials and Methods

After social isolation of mice at the juvenile stage, in vivo two-photon imaging of dendritic spines was performed at 3 weeks postnatal using the thin-skull imaging technique. After in vivo imaging, mice were transcardially perfused for fixation, and the

neuronal morphology was analyzed after sectioning and confocal imaging of the dendrites filled with DsRed2 fluorescent protein.

Mice

Timed pregnant mice of the strain C57Bl/6 J (Japan SLC, Inc.) were maintained with a fixed 12 h light-dark cycle (light period, 8:00 - 20:00, dark period, 20:00 - 8:00). Food and water were provided ad libitum. Animal experiments followed the institutional guidelines of the University of Tokyo.

In utero electroporation

Plasmid transduction into the progenitors of layer 2/3 neurons in the SSC was achieved by in utero electroporation (Isshiki et al., 2014). The DNA solution was prepared by mixing β-actin promoter-LoxP-STOP-LoxP-DsRed2 (1.5 μg/μl), β-actin-promoter-LoxP-STOP-LoxP-PSD-95-EGFP (PSD-95-EGFP; PSD-95 tagged with EGFP, 1 μg/μl), and β-actin-promoter-Cre (10 ng/μl).

Social isolation

Social isolation was performed by separating male pups from mothers and

siblings from 10:00 to 16:00 in the second postnatal weeks (PND7 to 11). A small container (6 cm in diameter, 9 cm in height) with bedding tips was used to keep each pup in isolation on a heating pad at 35ºC. Individual pups were kept at a distance of approximately 2 m from the mothers and siblings. After social isolation, pups were returned to the original cages of the mother and siblings.

Surgery

The method of preparing a thinned-skull window was as described previously (Isshiki et al., 2014).

In vivo imaging

The mouse with a thinned-skull window was placed under an upright scanning microscope (FV-300, Olympus) equipped with a pulsed laser (MaiTai HP, Spectra-Physics) and a ×25 water immersion objective lens (XLPlan N, numerical aperture (NA) 1.05, Olympus). The procedure of in vivo two-photon spine imaging was as previously described (Isshiki et al., 2014).

Confocal imaging

Mice at PND 11 or postnatal 3 weeks were transcranial perfused with a phosphate buffer containing 4 % paraformaldehyde and 0.2 % glutaraldehyde. The brains were postfixed in the same fixative for 4 h before and sectioned into 50 μm thick slices using a vibratome (VT1200, Olympus). Slices stained with Hoechst 33342 (Dojindo) were imaged with a fluorescence microscope (BX51, Olympus). Dendritic spines and dendrites of the pyramidal neurons filled with DsRed2 in the layer 2/3 of the SSC were imaged using an FV1000 confocal laser-scanning microscope (Olympus) with a ×30 silicon lens (UPlanSApo, NA 1.05, Olympus).

Data analysis

Images were analyzed with ImageJ (NIH, http://rsb.info.nih.gov/il). Spine dynamics were quantitated as previously described (Isshiki et al., 2014). Dendritic protrusions were classified as either spines or filopodia, with filopodia defined as long protrusions with smaller diameters and without PSD-95 puncta and detectable heads. Protrusions judged as filopodia were excluded from spine counting.

Spine turnover rates were calculated as follows;

Spine gain rate (%) = $N_{gain} / \{(N_{total1}+N_{total2})/2\}$

Spine loss rate (%) = N_{loss} /{((N_{total1}+N_{total2})/2}

N_{total1} and N_{total2} are the total spine numbers in the first and the second imaging days.

N_{loss} and N_{gain} are the numbers of spines that were eliminated or appeared.

Spine density was calculated as the spine number divided by the dendrite length in each image. The filopodia fraction was calculated as follows;

Filopodia fraction at day0 or 2 (%) = filopodia number (day0 or 2) /spine number (day0 or 2)

Filopodia fraction (%) = (The filopodia fraction at day0 + The filopodia fraction at day2)/2

The criteria in a previous report were used to classify PSD-95-EGFP-positive spines (Isshiki et al., 2014).

I analyzed dendritic morphology by measuring the number of branching points and spine density in both apical and basal dendrites. In the apical dendrites, the closest secondary dendritic segments from the soma were selected (3 segments at PND11 and 4 segments at PND23-25). The branching points of the secondary dendritic segments in the basal dendrites were also manually selected. Spine densities in these secondary dendritic segments (starting from the proximal branch points and ending at the distal branch points or at the distance of 77 μm from the proximal branching points) were calculated using the

spine numbers and the segment lengths. In projection images, the areas of spine heads were measured and taken as spine head sizes. The level of statistical significance was set at $P < 0.05$ as * and $P < 0.01$ as **. All statistical analyses were performed using Graph pad prism software (version 6.0 for windows, GraphPad Software, San Diego, USA). The data are presented as mean ± s.e.m..

２－４．Results

Neonatal social isolation increased PSD-95-negative spines of the layer 2/3 pyramidal neurons in the SSC

The layer 2/3 pyramidal neurons in the mouse SSC were transfected with expression plasmids of DsRed2 and PSD-95-EGFP by in utero electroporation. After delivery of pups that had received in utero electroporation, I performed social isolation by separating male pups from the mother and siblings in the second postnatal weeks old. The social isolation protocol was similar to the protocol with neonatal rats (Tada et al., 2016), which negatively regulated translocation of glutamate receptor subunits (amino3-hydroxy-5-methyl-4-isoxazolepropionic acid: AMPA-type receptors), suppressed the activity of cofilin / ADF (actin-depolymerizing factor) in the frontal and sensory cortex, and enhanced the social dominance (Tada et al., 2017). After social isolation, I performed

in vivo two-photon microscopy of dendritic spines at 3 weeks old postnatal through thin skull windows over the SSC. The same dendrites were identified, and spine turnover rates were calculated from two images taken with the interval of two days (Fig. 1A–B). Spine turnover rates did not show significant difference between control and mice after social isolation (Gain rate; Control = 7.031 ± 0.650, n = 42 segments from 6 mice, Isolation = 7.029 ± 1.001, n = 44 segments from 5 mice, t = 0.001, P = 0.999, unpaired Student's *t*-test, Lost rate; Control = 8.894 ± 0.978, n = 42 segments from 6 mice, Isolation = 8.829 ± 1.245, n = 44 segments from 5 mice, t = 0.042, P = 0.968, unpaired Student's *t*-test; Fig. 1C). The total spine density of socially isolated group was similar to that without manipulation (Control = 0.7385 ± 0.078, n = 42 segments from 6 mice, Isolation = 0.675 ± 0.059, n = 44 segments from 5 mice, t = 0.625, P = 0.548, unpaired Studen*t*'s t-test; Fig. 1D). The filopodia fractions also did not show significant difference (Control = 0.952 ± 0.237, n = 42 segments from 6 mice, Isolation = 0.974 ± 0.277, n = 44 segments from 5 mice, t = 0.062, P = 0.952, unpaired Student's *t*-test; Fig. 1E). Furthermore, the overall rate of protrusion turnover, including spines and filopodia, did not show a statistical difference between the two groups (data not shown). Finally, I investigated the degree of maturation of spines by the presence of PSD-95-EGFP clusters within spines. I utilized in vivo two-photon images on the first day to calculate the intensity ratio of EGFP versus

DsRed2 within spines, which was further normalized by the EGFP/DsRed2 intensity ratio within dendritic shafts. Spines without PSD-95-EGFP clusters were more frequent in mice after social isolation (Control = 10.88 ± 0.723, n = 36 segments from 5 mice, Isolation = 23.19 ± 0.655, n = 39 segments from 4 mice, $t = 12.28$, $P < 0.01$, unpaired Student's *t*-test; Fig. 1F). These observations are consistent with the idea that neonatal social isolation prevents synaptic translocation of the prominent postsynaptic scaffolding protein without affecting spine turnover rate.

Modest morphological alterations of dendrites induced by neonatal social isolation in the layer 2/3 pyramidal neurons of the SSC

Quantitative analysis of spine dynamics indicated preservation of spine turnover after social isolation, but inhibition of spine maturation by preventing synaptic translocation of PSD-95. Does social isolation also affect the maturation of dendritic arborization? To test this, I next measured multiple parameters of dendritic morphology after social isolation. The time points of analysis were set at PND11 (just after the social isolation) and at PND23–25 (at the timing of in vivo spine imaging) (Fig. 2A). The cortical layers were visualized by the Hoechst staining of the cellular nucleus, and I found similar patterns of the cortical layers in both groups after social isolation (Fig. 2B). To obtain the detailed morphology of dendrites in the histological sections, I performed

confocal microscopic observation of the layer 2/3 pyramidal neurons in the SSC (Fig. 2C–D). The numbers of the primary basal branches between control mice and mice after social isolation did not show a significant difference (Fig. 3A, refer to Table 1). There were no systematic changes in the branching numbers at the secondary apical and basal branch points (Fig. 3B, refer to Table 1). Next, the positions of the secondary branch points were compared between control and socially isolated mice in both apical and basal dendrites of the layer 2/3 pyramidal neurons. The distance between the secondary branch points and the soma was moderately longer in mice after social isolation at two time points (PND11 and PND23–25) (Fig. 3C, refer to Table 1). The spine density in the apical and basal secondary dendrites showed a trend of subtle increase in mice after social isolation at postnatal 3 weeks old (Fig. 4A, refer to Table 2). The spine head size showed a modest difference in the basal dendrites at PND23–25 (Fig. 4B, refer to Table 2). In summary, neonatal social isolation does not induce profound alterations in the pyramidal neuron morphology. Still, it may cause moderate changes in the morphology of dendrites and spine density both acutely after social isolation and in the late stage of postnatal development at PND23-25.

２－５．Discussion

The histological analyses of dendritic morphology in this study indicate the suppression of spine maturation in the SSC by social isolation. I utilized PSD-95-EGFP as a marker that reflects the extent of maturation of dendritic spines, as previous studies reported clear roles of PSD-95 in the maturation of excitatory synapses and spines. PSD-95 is a prominent scaffolding protein highly enriched in the postsynaptic membrane of the excitatory synapses. Glutamate receptor content in synapses, spine volume, and efficacy of synaptic transmission are enhanced by exogenous expression of PSD-95 (El-Husseini et al., 2002; Elias et al., 2008). Time-lapse imaging studies confirmed the simultaneous accumulation of PSD-95 at the postsynaptic site and synaptophysin, a major synaptic vesicle protein, at the opposing presynaptic site, supporting the idea of PSD-95 as a reliable marker of synaptic junctions (Okabe et al., 2001). Loss of PSD-95 clusters was temporally coupled with subsequent spine loss in vivo (Cane et al., 2014). These reports collectively indicate functional roles of PSD-95 in spine maturation and guarantee PSD-95-EGFP as a reliable marker of spine maturation. Thus, an increase of PSD-95-EGFP-negative spines after social isolation suggests that the connection between neurons in the SSC remains immature in SSC.

Histological analyses of the pyramidal neuron dendrites in this study found not

negligible but moderate alterations in dendrite morphology in mice after social isolation. Nevertheless, social isolation modulated several morphological parameters, including spine density, branching positions of the basal dendrites, and spine head size. These results of in vivo imaging and histological analyses indicate that neonatal social isolation impacts specific components of dendritic and synaptic properties, especially in spine maturation, without changing spine dynamics.

The immature spine phenotype I found in mice after social isolation is consistent with previous studies, which showed impairment of AMPA receptor targeting to synapses (Miyazaki et al., 2012) caused by cofilin/ADF-mediated stabilization of actin cytoskeleton within spines (Tada et al., 2017). Upregulation of corticosteroids triggered by the stress of social isolation is postulated to be linked to synapse impairment (Miyazaki et al., 2012). Consistent with this model, when glucocorticoid was administered repeatedly from PND 30 to 40, this treatment induced enhancement of spine turnover in the barrel cortex (Liston & Gan, 2011). Both AMPA receptor synapse translocation and recruitment of PSD-95 into spines can be taken as indicators of spine synapse maturation. Therefore, the reduced fraction of PSD-95-containing spines found in this study may also be explained by stress-induced upregulation of corticosteroids and subsequent cofilin-mediated actin stabilization within spines.

In this study I labeled PSD-95 in SSC neurons by in utero electroporation. The overexpression of PSD-95 is known to affect neuronal development and synaptic transmission (El-Husseini et al., 2000; Gray et al., 2006). I can't rule out the possibility of overexpression of PSD-95 in this study. However, for the analysis of PSD-95 expression ratio in the layer 2/3 pyramidal neurons of the somatosensory cortices, the same method was applied to both the control mice and the socially isolated mice. Therefore I interpreted the result of the low expression of PSD-95-EGFP within the spines in the socially isolated mice group over the control group as an immature neuronal circuit formation by the social isolation manipulation.. It is necessary to examine if the socially isolated mice show a trend to have a low expression of endogenous PSD-95 within spines in their somatosensory cortices. To assess the expression of endogenous protein, the immunostaining of fixed brainal slices is a conventional method. However, dense molecule structures of PSD components would make the PSD-95 antibody hard to reach to the endogenous PSD-95 binding sites (Okabe, 2007). A pepsin pretreatment on slices prior to immunostaining may improve detection of PSD-95 (Fukuya & Watanabe, 2000). Another method for the assessment of an endogenous protein expression will be accomplished by using recombinant antibody-like proteins, Fibronectin intrabodies generated with mRNA display (FingRs) (Gross et al, 2013). PSD-95-FingRs-GFP can

bind to PSD-95 at the SH3-GK domain, which mediates intra- and intermolecular interactions (McGee et al., 2001) without affecting morphologies or electrophysiological properties in the transfected neurons. While the immunostaining method is used to analyze the PSD-95 expression pattern after social isolation in fixed brainal slices, this PSD-95 labeling method with FingRs would enable to analyze the endogenous PSD-95 expressions both before and after social isolation by in vivo imaging. Because PSD-95-FingR-GFP labels the MAGUK proteins SAP-102 and SAP-97 in cultured cells, further considerations of PSD-95-FingRs-GFP expression efficiency and interpreting would be required for quantitative analysis of endogenous PSD-95 negative spine ratio. The analysis on the endogenous PSD-95 expression in SSC of the socially isolated mice is expected to verify the immature neuronal circuit formation by the social isolation manipulation. A previous study reported decreased spine formation and increased spine loss in layer 5 pyramidal neurons after social isolation (Takatsuru et al., 2009). The discrepancy in spine dynamics from our study may be explained by either the protocol of social isolation, pyramidal neuron types, or the developmental stage of neurons examined for spine turnover. Previous studies reported that social isolation could induce aberrant social behavior, which may be considered a potential model for ASD (Zelikowsky et al., 2018). Multiple ASD model mice showed enhanced spine dynamics in cortical pyramidal

neurons. However, any prominent effect on spine dynamics could not be detected after social isolation in this study, suggesting that ASD and social isolation cause independent impairments in the cortical neural network.

The medial prefrontal cortex (mPFC) and limbic system such as the hippocampus are enriched with glucocorticoid receptors and may play a role in regulating emotion (Jacobson, 2005). A previous study reported that socially isolated juvenile rats showed a small spine density in mPFC and the hippocampus at postnatal 8 weeks old (Silva-Gómez et al., 2003). In mPFC, as well as in SSC, spine density is controlled by glucocorticoid (Liu & Aghajanian, 2008), which also down-regulates glutamate receptor expression and suppresses its function (Yuen et al., 2012) after social isolation. Another study also reported that social isolation reduced complexity in both apical and basal dendrites in the rat mPFC (Wang et al., 2012). Thus, social isolation negatively regulates the complexity of dendritic arborization and the spine density of pyramidal neurons in the neocortex and the hippocampus. Interestingly, social isolation is reported to have different effects on dendritic alterations in mPFC, basolateral amygdala, and nucleus accumbens (Wang et al., 2012). Further investigations on neuronal connectivity in multiple brain areas and its relationship to glucocorticoid signaling may reveal mechanisms of circuit-level alterations triggered by social isolation.

３．Relationship between NMDA receptor subunit composition and in vivo spine dynamics

３－１．Summary

NMDA-type glutamate receptors (NMDARs) in dendritic spines are involved in both synaptic maturation and plasticity in brain regions related to learning and memory. The modification of NMDAR subunit GluN2A and GluN2B was reported to be related to psychiatric disorders and thought to be their risk genes. The GluN2A and GluN2B expression ratio (GluN2A/2B) is known to become higher in many brain regions with brain maturation. Each subunit of NMDARs has different roles, as the GluN2A subunit may accelerate spine maturation, while GluN2B is proposed to have roles in increasing flexibility in neuronal circuit formation, though it is not yet proved in vivo. In this study, I evaluated the effect of modulating the GluN2A/2B ratio on spine dynamics. We manipulated the GluN2A/2B ratio in vivo by in utero electroporation of plasmid constructs for GluN2A knockdown or GluN2B overexpression and measured spine turnover by two-photon microscopy through the open skull window. We found that manipulation GluN2A/2B ratio does not affect spine dynamics in vivo, suggesting that enhanced spine turnover in multiple ASD model mice is not driven by altered GluN2A/2B ratio.

3－2．Introduction

A large number of synapses are formed in the early postnatal period, but only a fraction of newly formed spines is stabilized, and the rest are eliminated. The regulation of spine turnover is critical for proper neuronal circuit formation, and its impairment is thought to be related to psychiatric disorders. NMDAR subunits GluN2A and GluN2B are good candidates for the regulatory components of spine dynamics. NMDARs have many functional domains, including zinc ion (Zn^{2+}) allosteric domain, glutamate-binding domain, and glycine/D-serine- binding domain to control calcium ion (Ca^{2+}) influx. NMDARs are composed of four subunits, including two mandatory GluN1 subunits and two GluN2 subunits. Subunit composition determines the cation channel properties, ligand affinity, and voltage-dependence of the receptor (Paoletti & Neyton, 2007). GluN2B is a dominant subunit in the early developmental stage but gradually replaced by GluN2A during brain maturation (Sans et al., 2000).

Interestingly the transition from GluN2B to GluN2A occurs when the increase in synaptic density stops. GluN2A and GluN2B subunits have different structures in intracellular C-terminal domains (CTD). GluN2B CTD is known to have interaction with activated the calcium (Ca^{2+}) /calmodulin-dependent kinase Ⅱ (CaMKII), but GluN2A CTD doesn't. Transgenic mice lacking GluN2A or GluN2B show learning deficits, high

anxiety, and loss of intentional behavior. Behavior analysis of transgenic mice with the CTD region replaced between GluN2A and GluN2B revealed that GluN2A and GluN2B CTDs are related to motor performance or anxiety behavior.

Previous studies have shown NMDAR dysfunction in psychiatric disorders. Chronic administration of NMDAR agonist, D-cycloserin, is beneficial in autism spectrum disorder (ASD), especially for some symptoms, including reduced social behavior, impaired concentration, and excess activity (Urbano et al., 2014). Also, single-nucleotide polymorphism (SNP) analysis has shown that GRIN2A and GRIN2B genes are related to psychiatric disorders (Yoo et al., 2012). De novo mutation in GluN2A is known to be linked to schizophrenia (Tarabeux et al., 2011), and de novo mutation in GluN2B is related to ASD (Kenny et al., 2014; O'Roak et al., 2011, 2012).

The expression ratio of GluN2A and GluN2B has been proposed to regulate spine morphology and function, contributing to the proper wiring of neurons (Gambrill & Barria, 2011). This study reported manipulation of GluN2A and GluN2B expression by in utero electroporation, together with miniature excitatory postsynaptic currents (mEPSC) recording and in vitro live-cell imaging analysis in hippocampus slice culture. These experiments revealed that early expression of GluN2A induced reduction in synaptic number, size, and dynamics. On the other hand, GluN2B overexpression

enhanced spine formation and elimination.

To date, many morphological and electrophysiological studies on culture cells or brain slices examined NMDAR function. However, NMDAR subunit function in vivo at the early developmental stage has not yet been clarified. In this study, in vivo imaging of neurons with a modified ratio of GluN2A/2B was performed to evaluate spine dynamics at the juvenile stage. We hypothesized that spine dynamics are enhanced by reducing the GluN2A/2B expression. However, I found that spine dynamics were resistant to the manipulation of the GluN2A/2B ratio, suggesting the existence of NMDAR-independent signaling pathways involved in the regulation of spine dynamics in vivo.

３－３．**Materials and methods**

Mice

The details of the animal purchase, maintenance in the animal facility were described in section 2.　E14 Jcl:ICR mice were used for in utero electroporation. All procedures of animal handling and treatment followed the institutional guidelines of the University of Tokyo.

DNA plasmid vector construction

Progenitor cells of layer 2/3 neurons in the SSC were transfected using in utero electroporation as described previous section. DNA solution was prepared by mixing β-actin promoter-LoxP-STOP-LoxP-DsRed2 (1.5 μg/μl), β-actin-promoter-LoxP-STOP-LoxP-PSD-95-EGFP (1 μg/μl), and βactin-promoter-Cre (10 ng/μl). β-actin promotor GluN1-1a vector, β-actin promotor-LoxP-STOP-LoxP-EGFP-GluN2A vector, β-actin promotor-LoxP-STOP-LoxP-EGFP-GluN2B vector was prepared for in utero electroporation. β-actin promotor GluN1-1a vector was created from CMV promotor GluN1-1a vector. β-actin promotor-LoxP-STOP-LoxP-EGFP-GluN2A vector and β-actin promotor-LoxP-STOP-LoxP-EGFP-GluN2B vector were also generated from pCI-EGFP-NR2a wt (Addgene Plasmid #45445) and pCI-EGFP-NR2b wt (Addgene Plasmid #45447).

pSilencer GluN2A siRNA Expression vector and pSilencer GluN2A siRNA Expression control vector was created using pSilencer 2.0-U6 (Ambion).

Target sense sequences are shown below.

5’-gatccggatccgacatccacgttcttcaagagagaacgtggatgtcggatccttttttggaaa-3’

5’-agcttttccaaaaaaggatccgacatccacgttctctcttgaagaacgtggatgtcggatccg-3’

Control target sense sequences are shown below.

5’-gatccggatgcgacttccaggttcttcaagagagaacctggaagtcgcatccttttttggaaa-3’

5’-agcttttccaaaaaaggatgcgacttccaggttctctcttgaagaacctggaagtcgcatccg-3’

For DNA plasmid purification, I used Quiagen MaX prep (Qiagen) and Quick Gene Plasmid kit SII (Kurabo).

Transfection

COS-7 cell on 3.5cm dish with PLL (1 mg/μl) coat were transfected DNA plasmid vector (2.5 μg) with Lipofectamine 3000 (Thermofisher) (OPTIMEM 560 μl/dish, P3000 4 μl/dish, Lipofectamine 3000 12 μl/dish). Two days later, transfected COS-7 cells were fixed with 2% PFA and analyzed for mPFC fluorescence and EGFP fluorescence with a confocal laser-scanning microscope (FV-1000, Olympus) equipped with a silicon lens (UPlanSApo, ×30, NA 1.05, Olympus).

In utero electroporation

Progenitor cells of layer 2/3 neurons in the SSC were transfected using in utero electroporation as described in section 2 and previous study (Isshiki et al., 2014). DNA solution for each mouse was prepared as below;

Control mice: βactin promotor-LoxP-STOP-LoxP-DsRed (final concentration 1 μg/μl),

β-actin-promoter-Cre (final concentration 10 ng/μl).

GluN1-1a mice: βactin promoto-LoxP-STOP-LoxP-GluN1-1a (final concentration 1 μg/μl), βactin promotor-LoxP-STOP-LoxP-DsRed (final concentration 1 μg/μl), β-actin-promoter-Cre (final concentration 10 ng/μl).

GluN1-1a + EGFP-GluN2B mice: βactin promotor-LoxP-STOP-LoxP-GluN1-1a (final concentration 1 μg/μl), βactin promotor-LoxP-STOP-LoxP-stop EGFP-GluN2B (final concentration 1 μg/μl), βactin promotor-LoxP-STOP-LoxP-DsRed (final concentration 1 μg/μl), β-actin-promoter-Cre (final concentration 10 ng/μl).

Control si-RNA mice: Human U6 promoter pSilencer GluN2A siRNA Expression control vector (final concentration 2 μg/μl), βactin promotor-LoxP-STOP-LoxP-EGFP (final concentration 1 μg/μl), β-actin-promoter-Cre (final concentration 10 ng/μl)

GluN2A si-RNA mice: Human U6 promoter pSilencer GluN2A siRNA Expression vector (final concentration 2 μg/μl), βactin promotor-LoxP-STOP-LoxP-EGFP (final concentration 1 μg/μl), β-actin-promoter-Cre (final concentration 10 ng/μl)

Surgery

The surgery method except the in vivo imaging window preparation technique was performed as described in the material and methods part of the section 2. For the in

vivo imaging window preparation, the thin skull technique was applied in section 2 and the open skull technique was applied in section 3. Mice were anesthetized with ketamine (100 mg/kg body weight) and xylazine (10 mg/kg body weight). To fix mice to the stereotaxic instrument (Narishige), I attached a stainless tube with its diameter of 3 mm to the skull surface over the cerebellum with dental cement (Sunmedical). A circular glass with 2 ㎜-diameter and 0.17 mm-thickness was glued to another circular glass with 3 ㎜ -diameter and 0.17 mm thickness with adhesive (Norland Optical Adhesive 61U). The pair of glasses were placed on the area where the skull bone was removed over the somatosensory cortex and fixed with dental cement (Sunmedical).

In vivo imaging

In vivo imaging was conducted with mice at the age of 3 weeks or 6 weeks postnatal as described in section 2 and the previous study (Isshiki et al., 2014). A scanning microscope (FV-300, Olympus) was used for the in vivo spine imaging. The light source of two-photon excitation was a pulsed laser (MaiTai HP, Spectra-Physics). Spines were imaged by a ×25 objective lens (XLPlan N, water immersion, NA 1.05, Olympus).

Data analysis

Spine dynamics in vivo, spine gain rate and loss rate, in vivo spine density, and spine head size were quantitated according to the criteria described in section 2 and the previous study (Isshiki et al., 2014). ImageJ was used to quantitate and analyze the images (NIH, http://rsb.info.nih.gov/il).

For statistical evaluation, Student's t-test and one-way ANOVA with post hoc Turkey test were used. Data were presented as means ± s.e.m. The level of statistical significance was set at $P < 0.05$ as * and $P < 0.01$ as **. All statistical analyses were performed using Graph pad prism software (version 6.0 for windows, GraphPad Software, San Diego, USA).

３－４． Results

Confirmation of GluN2A/2B modification

The expression of GluN2A and GluN2B subunit was manipulated by in utero electroporation in the somatosensory cortex. Spine dynamics of transfected neurons were imaged by two-photon microscopy through an open skull window. At 3 weeks old, the open skull windows were installed over the somatosensory cortex. After recovery from the effects of the surgery, chronic imaging was performed in the adult stage at 6 weeks

postnatal. Hence GluN2A subunit is expressed dominantly over GluN2B at 3 weeks old, I designed GluN2A/2B modification by either GluN2A knockdown or GluN2B overexpression. GluN2A subunit expression was inhibited by GluN2A siRNA, GluN2B subunit overexpression was achieved by co-transfection of GluN1-1a and GluN2B expression vectors.

A chemical transfection method on COS-7 cell culture was used for confirmation of each transfection vector. COS-7 cells were transfected with CMV promotor GluN1-1a plus CMV promotor EGFP-GluN2A, or CMV promotor GluN1-1a plus CMV promotor EGFP-GluN2B. After EGFP immunostaining, each cell showed EGFP signal on the cell membrane (Fig. 5A). For confirmation of GluN2A knockdown by pSilencer GluN2A siRNA expression vector, I prepared three conditions of COS-7 cell transfection (Fig. 5B). The first condition was the combination of mRFP and EGFP-GluN2A expression as a control sample. The second condition was the combination of mRFP, EGFP-GluN2A, and siRNA control for the absence of effects related to non-specific siRNA expression, and the third condition was the combination of mRFP, EGFP-GluN2A and GluN2A siRNA expression for the evaluation of siRNA effects. mRPF and EGFP fluorescence in each condition was detected by confocal microscopy, and the EGFP/mRFP expression ratios were compared. GluN2A si-RNA expression results in drastic reduction in EGFP/mRFP

ratio and control si-RNA expression did not induce the reduction of the ratio (Control 1.274 ± 0.212, n = 121 cell, control si-RNA 1.537 ± 0.191, n = 127 cell, GluN2A si-RNA 0.182 ± 0.042, n = 118 cell, F (2, 363) = 16.64, P<0.001, control vs GluN2A si-RNA, P< 0.001, GluN2A si-RNA vs Control si-RNA, P < 0.001, One way ANOVA test; Fig. 5C). This result confirmed that the pSilencer GluN2A siRNA expression vector was effective in GluN2A knockdown.

For the confirmation of GluN2B overexpression, I prepared mice expressing GluN2B in the SSC by in utero electroporation and checked its expression in fixed brain slices. E14 Jcl:ICR mice were used for in utero electroporation with the combination of four plasmids of -βactin promotor-LoxP-STOP-LoxP-GluN1-1a, β-actin promotor-LoxP-STOP-LoxP-EGFP-GluN2B, β-actin promotor-LoxP-STOP-LoxP-DsRed, and β-actin-promoter-Cre. In a fixed slice of the somatosensory cortex at postnatal 3 weeks, EGFP and DsRed fluorescence signals were detected by confocal microscopy (Fig. 5D, Fig. 5E, Fig. 5F). EGFP/DsRed fluorescence ratio in GluN2B transfected mice (GluN1-1a + EGFP-GluN2B mice) is significantly higher than that in control (GluN1-1a mice), indicating successful translation of exogenous GluN2B in vivo (GluN1-1a; 0.365 ± 0.012, n = 4 mice, GluN1-1a + GluN2B; 0.624 ± 0.074, n = 4 mice, t = 3.461, P = 0.014, unpaired Student's *t*-test; Fig. 5G).

Mice with manipulated GluN2A/2B ratio show spine density and spine head size similar to the control mice

We analyzed spine density and spine head size from dendritic spine images acquired during in vivo imaging (Fig. 6A). GluN2B overexpression or GluN2A knockdown didn't induce significant changes in the spine density ($F(6, 25) = 1.014$, $P = 0.168$, one way ANOVA test; Fig 6B). Spine head sizes among groups were analyzed by one way ANOVA, which indicated statistical difference among groups ($F(6, 25) = 0.939$, $P = 0.006$, one way ANOVA test; Fig 6C). However, post hoc Turkey test confirmed statistical difference only in two combinations, GluN2A si-RNA at postnatal 3 weeks old and GluN2A si-RNA at postnatal 6 weeks old ($P < 0.01$), and GluN1-1a + EGFP-GluN2B at postnatal 3 weeks old and GluN2A si-RNA at postnatal 6 weeks old ($P = 0.014$). These two combinations only indicate the difference between groups at different ages and do not support the effect of NMDAR manipulations on spine size. Therefore, I conclude that the spine head size was not affected by changing the subunit composition of NMDARs.

Mice with manipulated GluN2A/2B ratio didn't show a drastic change in spine dynamics, but GluN2A knockdown mice showed a tendency to have a lower spine formation rate

At postnatal 3 weeks, I analyzed spine dynamics by repetitive in vivo two-photon imaging. Mice with manipulated GluN2A/2B ratio didn't show changes in spine gain rate and loss rate (Fig. 7A, Fig. 7B). GluN2A si-RNA mice showed a slightly lower spine gain rate over control mice and control si-RNA mice without statistical significance ($F(4, 20) = 0.568$, $P = 0.689$, one way ANOVA test; Fig. 7A). GluN2A si-RNA mice also showed a slightly lower spine loss rate over control mice and control si-RNA mice. Additionally, mice overexpressing GluN1-1a and EGFP-GluN2B showed a tendency of higher spine loss rate over the control mice. However, here again, no statistical difference among groups could be detected ($F(4, 20) = 0.524$, $P = 0.719$, one way ANOVA test; Fig. 7B).

At postnatal 6 weeks, GluN2A knockdown mice did not show statistical differences in both spine gain rate (GluN2A si-RNA mice 16.03 ± 1.895, $n = 3$ mice, Control si-RNA mice 11.71 ± 1.592, $n = 4$ mice, $t = 1.753$, $P = 0.14$, unpaired Student's t-test; Fig. 7C) and spine loss rate (GluN2A si-RNA mice 14.38 ± 1.443, $n = 3$ mice, Control si-RNA mice 13.13 ± 3.017, $n = 4$ mice, $t = 0.332$, $P = 0.754$, unpaired Student's *t*-test;

Fig. 7C).

3－5．Discussion

The neocortical circuits at postnatal 3 weeks are reported to contain excitatory spine synapses with abundant GluN2A subunits over GluN2B subunit (Sans et al., 2000). We manipulated the ratio of GluN2A/2B by in utero electroporation of either GluN2A knockdown or GluN2B overexpression constructs. Previous in vitro studies suggested that GluN2A and GluN2B have different functions and either inhibit or facilitate spine dynamics, respectively (Gambrill & Barria, 2011). We speculated that reduced GluN2A/2B ratio might affect spine dynamics toward enhanced spine turnover.

GluN2A/2B modification experiments were conducted by in utero electroporation. The expression constructs were confirmed by transfection into cultured non-neuronal cells or tissue sections. Mice with modified GluN2A/2B expression did not show significant changes in spine density and spine head size (Fig. 7C). This result indicates that the relative ratio of GluN2A and GluN2B can regulate NMDAR-mediated current and spine calcium dynamics, but the extent of functional regulation is not sufficient to induce noticeable changes in spine density and spine morphology. More detailed analysis of spine morphological parameters, such as spine head curvature and

spine neck width, may provide insights into the regulatory mechanisms of NMDAR subunit composition in spine shape regulation. However, this type of analysis may require sophisticated technology of super resolution spine imaging.

It is necessary to analyze the expressions of GluN2A subunit and GluN2B subunit in the somatosensory cortex of the mice which were induced to overexpress GluN2B subunit or knock down GluN2A subunit by in utero electroporation. I need to assess the possibility of the reduced expressions of GluN2B associated with GluN2A knockdown and the increased expression of GluN2A associated with GluN2B over expression. The expressions of GluN2A subunit and GluN2B subunit are able to be assessed by an electrophysiological technique (Holehonnuer et al., 2016; Miwa et al., 2008). NMDA receptor-mediated excitatory postsynaptic currents (EPSC) are extracted by application of an AMPA receptor antagonist, 6-cyano-7-nitroquinoxaline-2,3-dione (CNQX) and the GABAA receptors antagonist, picrotoxin (PTX) during whole-cell voltage-patch clamp recordings. The contribution of each GlN2A subunit and GluN2B subunit on NMDA receptor-mediated EPSC can assessed by using specific antagonists. PEAQX is an antagonist at NMDA receptors including GluN2A subunit. Ro25-6981 and ifenprodil are GluN2B selective NMDA receptor antagonists. In this study, I used open skull imaging for in vivo imaging and resulted in a higher spine turnover rate compared

to spine dynamics with thin skull imaging. A previous study also pointed out the difference in spine dynamics with two window preparation techniques and showed higher spine gain and loss in open skull imaging (Xu et al., 2007). They also showed enhanced activation of glial cells around the open skull window. In this study, the data of individual mice were highly variable, causing difficulty in the interpretation of the effects of the GluN2A/2B ratio on spine dynamics. In future analyses, it may be necessary to develop technology that enables a more drastic change in the GluN2A/2B expression ratio. This may be accomplished simply using higher concentrations of plasmid constructs for both overexpression and suppression of GluN2A or GluN2B. In the long run, I expect to introduce new technologies, such as strong neuron-specific promoters and amplification systems based on artificial trans-regulatory elements, in the manipulation of NMDAR subunit composition.

４． Behavior analysis of mice after social isolation

４－１． Summary

Social isolation or neglect in early development is postulated to increase the long-term risk of anxiety, social disability, and cognitive impairments. Social separation at the juvenile stage is a widely accepted rodent model to study human neglect and early life stress. In vivo spine imaging revealed inhibition of spine maturation in socially separated mice in the juvenile stage. Social isolation is also known to disrupt behaviors dependent on whisker-evoked sensory input. However, it is still unclear how social isolation affects emotion-related behavior at the neuronal circuitry levels. In this study, I hypothesized that juvenile social isolation in mice might lead to high anxiety, lower social interaction, and disability in memory formation in the adult stage, as reported in neglect patients. Social separation during the juvenile stage in our experimental condition did not cause a significant change in anxiety and social behavior in adult mice. Instead, isolated mice had relatively high activity in an anxiogenic environment and showed enhanced escaping activity during fear memory retrieval tests. These results suggest that long-term social isolation affects emotion and behavior after the maturation of animals.

４－２．Introduction

Lack of social interaction has various effects on early human development. Children who experienced social isolation or neglect by caregivers later exhibit enhanced information processing about negative emotions. Social isolation and early-life stress promote cognitive decline, including diminished learning ability and diminished attention (Geoffroy et al., 2016; Masson et al., 2016). These cognitive features induce hypersensitivity to stress and increase the risk of developing mental illness, including major depression, addiction, and post-traumatic stress disorder (PTSD) (Chapman et al., 2004; Faravelli, 2012; Felitti et al., 1998; Fergusson et al., 1996). Alternatively, early social isolation may attenuate stress sensitivity in adults. Indeed, studies have shown that children with adverse childhood experiences slowed down the hypothalamic-pituitary-adrenal endocrine response (HPA-axis reactivity) to acute stress during maturity (Elzinga et al., 2008). These conflicting reports indicate the importance of research clarifying the delayed effects of the childhood social environment on later brain function and neural circuit formation (Reul & de Kloet, 1985; Sapolsky et al., 1983).

Behavioral studies using animal models have been employed to study aversive and affective emotional states and behaviors. Especially, neuronal circuits underlying negative emotion-related behaviors such as avoidance or fear have been extensively

explored for decades. Fear conditioning is one of the associative forms of learning models to evaluate fear memory formation and retrieval. In fear conditioning, an emotionally neutral sensory stimulus such as context or tone is used as a conditioned stimulus (CS), and an innately aversive sensory information such as foot-shock or nausea is used as an unconditioned stimulus (US). Upon CS being associated with US presentation and fear memory of CS-US association has been formed, CS acquires an ability to induce defensive behaviors such as freezing and escaping.

The major brain regions primarily associated with fear conditioning include the amygdala, hippocampus, mPFC, and cingulate cortex. Neuronal activation in the basolateral nucleus of the amygdala (BLA) and the central nucleus of the amygdala (CeA) plays an essential role in fear memory formation in fear conditioning (Rustay et al., 2008; Vazdarjanova & Mcgaugh, 1998; Watabe et al., 2013). Learning the context requires hippocampal neural circuits. The mPFC and cingulate cortex are regions required for new memory acquisition, and pharmacological suppression of these regions attenuates the formation and recall of contextual memory (Pezze et al., 2014).

A previous study has reported early-life stress and fear memory formation are deeply related to each other. Maltreatment of the mother with insufficient bedding for nest building results in abnormal behaviors in pups, and they exhibit impaired odor leaning

and show unique avoidance behavior (Nishi et al., 2014).

To further investigate the relationship between early-life stress and emotion-related behaviors, I utilized a social separation model during the juvenile stage as a mouse model of social isolation and early-life stress, and evaluated anxiety-like behavior, social behavior, fear memory formation, and recall in the adult stage. The results indicate the adult mice after juvenile social isolation exhibit long-term behavioral impairments, including the increase in activity in an anxiogenic environment and the increase in the escaping behavior during fear memory recall.

４－３．Materials and Methods

Mice

The use of the animals was approved by the Institutional Committee for the Care and Use of Experimental Animals at the Jikei University School of Medicine. All experiments conformed to the Guidelines for Proper Conduct of Animal Experiments by the Science Council of Japan (2006) and to the guidelines recommended by the International Association for the Study of Pain (Hawkley et al., 2012; van Bodegom et al., 2017). All efforts were made to reduce the number of animals used and the suffering of the animals.

Male C57BL/6J mice (4 weeks old) were purchased from Japan SLC, Inc. (Shizuoka, Japan). The mice were provided with food and water ad libitum. The mice were group-housed (3-4 mice per cage) in the cage (197 mm width × 340 mm depth ×165 mm height, super mouse 750, Natsume Seisakusho Co., Ltd, Tokyo, Japan), and maintained on a 12 h light/dark cycle, and provided with food and water ad libitum through the study. All behavioral testing was conducted between 7:00 and 19:00.

Social isolation

Social isolation procedures were performed as described in section 2, except that isolated subjects underwent separation from the PND 7 to PND 28. The rest of the siblings remained in the home cage with their mother. To eliminate the possible effects of social interactions after weaning, the control group (N = 10) without social isolation and the isolation group (N = 10) were combined and group-reared after weaning at PND 28. The behavioral experiment was started on the PND 48 (Fig. 8A).

Experimental paradigm

The behavioral battery was designed to start from the relatively simple tests with less stress, followed by tests with complex and more stressful conditions as follows; Day

1: open field test, and three-chamber test, Day 2: fear conditioning, Day 3: contextual retrieval, Day 4: tone retrieval. All mice underwent handling for 1 week (5 min/day) before the first behavioral experiment.

The groups of mice with or without social isolation, which didn't experience open field test and three-chamber test before fear memory conditioning was designated as FC-isolation group (N = 5) or FC-control group (N = 6) (Fig. 8A), respectively.

Open field test

The mouse was placed in the center of the field (50 cm width × 50 cm depth × 30 cm height, 100 Lux, O'Hara & Co., Ltd), and the behavior was recorded for 10 minutes. The center area was set to 36 % of the bottom area. The percentage of staying time in the center area, the moving speed in all areas, and the moving distances in all areas were analyzed.

Three-chamber test

The thee-compartment testing apparatus consisted of the open field box (50 cm width × 50 cm depth × 30 cm height, 100 Lux) and was divided into three parts with two transparent acrylic boards. There were three compartments in which the mice were free

to move between: the center compartment (10 cm × 50 cm) and the left and right compartment (20 cm × 50 cm). Two identical wire baskets (7.5 cm width × 7.5 cm depth × 10 cm height) were placed at the far right and the front left corners. In the habituation session, mice were placed in the center and could move freely in the chamber containing two inverted empty baskets for 10 min. 2 h after the habituation session, in the test session, a 4-week-old male mouse (presentation mouse) was placed only in the right basket for 10 min in the same manner.

Fear conditioning

On day 2, the mice were placed in a conditioning chamber (170 mm width × 100 mm depth × 100 mm height, 200 Lux, 50 dB background white noise) surrounded by a sound-attenuating chamber (CLM3, O'Hara & Co., Ltd., Tokyo, Japan) for fear conditioning. Following to 2 minutes of observation period, the mice were conditioned with three pairings of a 20 s CS tone (CS; pure tone, 10 kHz, 65 dB) that terminated concurrently with a foot-shock (US; 0.6 mA, 2 s). Foot-shocks were delivered to the floor grid of the chamber through a shock generator (O'Hara & Co., Ltd, Tokyo, Japan). The first CS was delivered 120 s after the animal was placed in the chamber, and the inter-trial intervals were 40 s and 50 s.

Contextual retrieval test

On day 3, the mice were re-placed in the conditioning chamber, with the same environmental context of 200 Lux illumination, 50 dB background white noise, and ethanol scent. The freezing and escape behavior of the mice was recorded for 5 min.

Tone retrieval test

On day 4, the mice were placed in the retrieval chamber (with white acrylic plate walls scented with peppermint odor; 50 Lux, 60 dB background white noise). The CS presentation began 60 s after the mice were placed in the chamber, and lasted for 120 s. The freezing and escape behavior of the mice was recorded for 5 min.

Data analysis

In the three-chamber test, the total floor was divided into 5 × 5 areas with an equal area size. The 10 areas, including the presentation mouse, were designated as the Mouse Area. The 10 areas, including the empty basket, were named as the Empty Area, and the remaining areas were named as the Other Area (Fig. 9A). The 4 areas, including the presentation mouse, and the 4 areas, including the empty basket, were defined as Empty area ROI and Mouse area ROI and analyzed for social index and enter ratio. Social

index and enter ratio were calculated as below.

Social index = (Stay time Mouse – Stay time Empty) / (Stay time Mouse + Stay time Empty)

Stay time Mouse: time spent in 4 areas including mouse basket

Stay time Empty: time spent in 4 areas including empty basket

Enter ratio = the number of entries into 4 areas including mouse basket / the number of entries into 4 areas including empty basket

In fear conditioning, contextual retrieval test and tone retrieval test, mouse behavior was captured using a digital camera at 2 frames/s and freezing behavior was analyzed using Time FZ1 software (O'Hara & Co., Ltd), a package based on NIH Image. The movement of the mouse was detected by pixel-to-pixel subtraction between two subsequent frames and the behavior at each frame was defined as "freezing" or "immobility" when the total number of pixels with detectable frame-to-frame difference was less than 30. The identification of freezing and immobility behavior was pre-optimized by two in dependent human observers using C57BL/6 J mice.

I used an unpaired Student's t-test and two-way ANOVA with post hoc Bonferroni's test. The level of statistical significance was set at $P < 0.05$ as * and $P < 0.01$ as **. All statistical analyses were performed using Graph pad prism software (version

6.0 for windows, GraphPad Software, San Diego, USA). The data are presented as mean ± s.e.m.

４－４． Results

Juvenile separation did not change locomotor activity in an anxiogenic environment and social behavior of adult mice

No differences in body weight were observed between Control and Isolation groups at neither final day of social isolation (PND 28) nor the time of behavioral experiment (PND 48) (PND 28, Control = 10.674 ± 0.712, n = 7 mice, Isolation = 9.11 ± 0.867, n = 6 mice, t = 1.394, P = 0.193, PND 48, Control = 19.736 ± 0.372, n = 7 mice, Isolation = 19.808 ± 0.463, n = 6 mice, t = -0.122, P = 0.905, unpaired Student's *t*-test; Fig. 8B).

An open field test was performed to analyze the anxiety-like behavior of adult mice socially isolated in the juvenile stage. The percent time spent in the center area was similar between the control group and the isolation group (Control = 13.275 ± 1.419, n = 10 mice, Isolation = 12.648 ± 2.137, n = 10 mice, t = 0.484, P = 0.634, unpaired Student's *t*-test; Fig. 8C). No statistical difference was found in total distance traveled (Control = 4894.48 ± 402.621, n = 10 mice, Isolation = 5758.81 ± 308.122, n = 10 mice, t = -1.428,

P = 0.172, unpaired Student's *t*-test; Fig. 8D) and speed of locomotion (Control = 13.787 ± 0.434, n = 10 mice, Isolation = 15.080 ± 0.486, n = 10 mice, t =- 1.925, P = 0.070, unpaired Student's *t*-test; Fig. 8E). Thus, the social isolation in the juvenile stage did not significantly affect the anxiety-like behavior after maturation.

Next, the three-chamber test was performed to analyze the social behavior of socially isolated mice. In the three-chamber test, two baskets were diagonally set at corners of the field, and an intruder mouse was placed in one basket. Tracing of mouse location (Fig. 9A) revealed that both control and isolation groups showed differences in duration time in Mouse area, Empty area and Other area ($F(2, 36) = 134.7$, $p < 0.01$, two-way ANOVA; Fig. 9B). However, the analysis of stay time in the three regions did not show any significant differences between the control and isolation groups. The stay time ratio (social index) and number of entries ratio into the Mouse Area and the Empty Area (enter ratio) showed no significant differences between two groups (Social index: Control = 2.502 ± 0.455, n = 10 mice, Isolation = 3.047 ± 0.353, n = 10 mice, t = 0.946, P = 0.357, unpaired Student's *t*-test; Fig. 9C, Enter ratio, Control = 1.559 ± 0.201, n = 10 mice, Isolation = 1.438 ± 0.183, n = 10 mice, t = 0.443, P = 0.663, unpaired Student's t-test; Fig. 9D). Thus, the three-chamber test revealed that the social isolation in the juvenile stage did not significantly affect social behavior after maturation.

Increased escape behavior related to fear memory in mice received social isolation operations

Fear conditioning was performed to associate tone and foot-shock using mice that had completed the open field test and three-chamber test. In this fear conditioning, the tone was presented for 20 seconds, and foot-shock was presented for 2 seconds. The ends of the tone and the foot-shock were temporally aligned. Three pairs of the tone and the foot-shock were given at random intervals (Fig. 10A).

The day after fear conditioning, contextual retrieval was performed to analyze the degree of freezing in the conditioning chamber. There was no difference between the two groups in the freezing behavior (Fig. 10B, Control = 29.767 ± 5.192, n = 10 mice, Isolation = 25.95 ± 2.715, n = 10 mice, t =0.595, P = 0.56, unpaired Student's t-test; Fig. 10C) and the number of jumps, which was considered to be escape behavior (Control = 11.5 ± 1.695, n = 10 mice, Isolation = 7.1 ± 1.871, n = 10 mice, t = 1.743, P = 0.09, unpaired Student's *t*-test; Fig.10D).

The day after contextual retrieval, tone retrieval was performed. The tone previously associated with foot shock was presented in a new chamber, different from the foot shock chamber, and the degree of freezing was analyzed. The freezing responses of two groups analyzed with temporal bins of 20 s in the tone retrieval sessions revealed that

control and isolation groups showed differences in freezing ratio ($F(1, 17) = 84.46$, $p < 0.01$, two-way repeated ANOVA; Fig. 11A). However, the post hoc comparisons revealed no difference between the control and isolation groups in freezing at each bin.

On the other hand, there was an increase in the number of jumps during tone presentation in the isolation group (Control = 4.7 ± 0.99, n = 10 mice, Isolation = 7.778 ± 0.94, n = 9 mice, t = -2.256, P = 0.038, unpaired Student's *t*-test; Fig. 11C).

So far, multiple behavioral experiments were performed on each mouse according to the design of the behavioral battery. In order to clarify possible impairment in fear memory formation and recall, the control group (FC-control group) and isolation group (FC-isolation group) received fear conditioning in a naïve condition, namely on the first day without performing an open field test and a three-chamber test. In contextual retrieval, the FC-isolation group showed a similar freezing behavior to the FC-control group (Fig.12A, FC-control = 30.81 ± 5.209, n = 6 mice, FC-isolation = 31.17 ± 7.514, n = 5 mice, t = -0.04, P = 0.969, unpaired Student's *t*-test; Fig. 12B). The FC-isolation group showed higher jump number during the contextual retrieval (FC-control = 6.0 ± 1.155, n = 6 mice, FC-isolation = 16.2 ± 4.341, n = 5 mice, t = 2.475, P = 0.035, unpaired Student's *t*-test; Fig. 12C). The freezing responses of two groups analyzed with temporal bins of 20 s in the tone retrieval sessions showed differences in freezing ratio ($F(1, 9) = 20.29$, $P <$

0.01, two-way repeated ANOVA test; Fig. 12D). However, post hoc comparisons revealed no difference between the mouse groups in freezing at each bin. The freezing ratio in the FC-isolation groups showed a tendency of reduction, but without statistical significance (Fig. 12E). The number of jumps showed an increasing trend in the FC-isolation mice group (FC-Control = 5.167 ± 1.47, n = 6 mice, FC-Isolation = 10.0 ± 1.732, n = 5 mice, t = -2.128, P = 0.065, unpaired Student's *t*-test; Fig. 12F).

４－５．Discussion

From the results of the open field test, I concluded that the juvenile isolation operation tended to induce a slightly higher locomotor activity but did not affect anxiety-like behavior. From the results of contact time and frequency with new mice in the three-chamber test, there were no significant changes in social behavior caused by the juvenile isolation operation. From the results of fear memory conditioning, the fear response was largely intact after social isolation. The formation and recall of fear memory were tested by conditioning mice using foot-shock as the US associated with context and tone as CS. Contextual fear memory recall tests showed no detectable changes in freezing response in the isolation group. On the other hand, there was an increased tendency of jumping in the isolation group, which may suggest a higher tendency to escape behavior. Similarly,

in the tone retrieval test, the isolation group showed no detectable changes in freezing response, while they exhibited significantly enhanced jumping behavior.

From the above experimental results, unlike the hypothesis of this study, the juvenile social isolation operation does not profoundly affect anxiety-like behavior and sociality-related behaviors in the adult stage. The results suggested a mild increase in the general locomotor activity and slight enhancement in fear memory recall such as in Figure 12. Mice are known to take various actions as fear and anxiety response to environmental threats. It would be an interesting future study to investigate the neuronal mechanisms for other defensive behaviors in fear learning such as jumping (Pournajafi-Nazarloo et al., 2011).

Adverse environments and experiences during the neonatal period can dramatically affect the development of the HPA axis that underlies adaptive behavioral responses. Maternal separation (MS) experiments, as a model of early life stress, demonstrated that the level of corticosterone (CORT) levels and *c-Fos* expression were dependent on the different experimental conditions of MS, e.g., age of testing and frequency of repetition (Horii-Hayashi et al., 2013). Furthermore, separation conditions (isolation with or without a littermate) could also influence the results of the MS experiments. Previous studies showed that the distance traveled in the open field test

increased when rats were individually isolated for 28 days or 58 days after birth. Also, an increase in escape behavior in the context retrieval was reported in rats under the same isolation condition (Mora-Gallegos & Fornaguera, 2019). The difference in the fear memory response of the socially isolated mice shown in this study and the previous studies may be explained by the fact that the behavioral outcomes are greatly influenced by the details of the social isolation conditions, especially the difference in age and isolation period. It is also possible that the interaction with other mice during the maturation period may provide a "social buffering" effect. Social buffering is a phenomenon in which an affiliative conspecific reduces stress responses in a subject. Previous studies suggested that stress responses are ameliorated when the number of associates increases, and social buffering enhances fear memory extinction by reducing CORT levels (Kiyokawa, 2016; Kiyokawa & Hennessy, 2018; Mikami et al., 2020). Therefore, one possible interpretation of the mild deficit observed in the present study is the early life stress during juvenile stage might have been masked by social buffering effects.

From previous studies, it is proposed that social isolation enhances stress responses and causes neurological dysfunction (Hawkley et al., 2012; van Bodegom et al., 2017). All mammals share an HPA-axis reactivity that controls the production and

secretion of CORT, which function in physiological and behavioral adaptations. In the HPA endocrine response, corticotrophin-releasing hormone (CRH) and arginine vasopressin (AVP) are first secreted from the paraventricular nucleus (PVN) (Stratakis & Chrousos, 1995). CRH and AVP activate the anterior lobe of the pituitary gland and promote the secretion of adrenocorticotropic hormone (ACTH), which also stimulates the adrenal cortex to promote the secretion of corticosteroids. Corticosteroids cross the blood-brain barrier and bind to two types of receptors, the glucocorticoid receptors (GRs) and mineralocorticoid receptors (MRs), which drive gene expression related to the maturation of neurological functions such as the structural reconstruction of axons and dendrite (Datson et al., 2001; Meyer, 1983). GRs are expressed in many brain regions, especially in the hypothalamic neurons and anterior pituitary gland. On the other hand, the MR is localized in the limbic system and is exceptionally high in the hippocampus (Reul & de Kloet, 1985; Sapolsky et al., 1983).

Many studies have been conducted on the changes in the HPA endocrine response to social isolation using the serum ACTH and CORT concentration as indicators. In previous studies, there has been a substantial discrepancy in HPA responses to social isolation. Some studies showed high concentrations of serum ACTH and CORT due to social isolation (Chida et al., 2005; Dronjak et al., 2004; Ferland & Schrader, 2011; Kanitz

et al., 2004; Perelló et al., 2006; Pournajafi-Nazarloo et al., 2011; Ruscio et al., 2007; Weintraub et al., 2010). However, there are studies in which low concentrations of serum ACTH and CORT were reported (Djordjevic et al., 2010; Hermes et al., 2006; Serra et al., 2005; Weintraub et al., 2010), and also studies reporting no difference in concentration compared to group breeding (Castro & Matt, 1997; Grippo et al., 2007; Pournajafi-Nazarloo et al., 2009; Scaccianoce et al., 2006; Stowe et al., 2005; Toth et al., 2011; Weiss et al., 2004). This inconsistency among previous reports may be due to differences in model animal species, isolation start time and isolation period (Serra et al., 2007). For example, previous studies have shown that single social isolation of 1 h or daily isolation of 1 h lasting for 4 weeks significantly increases serum CORT levels, but 4 weeks of continuous social isolation had no effect (Pournajafi-Nazarloo et al., 2011).

The above experimental results suggest that the experimental condition of social isolation in the present study may induce a mild increase in general locomotor activity and fear memory recall that does not lead to substantial changes in freezing response. These experimental results are intriguing but need further confirmation of responsible brain regions linked to the observed behavioral changes. Clarification of these points may require the development of new analytical techniques in the future.

５．Behavioral analysis of the mice with chronic activation of the parabrachial nucleus (PB) region

５－１．Summary

Patients with chronic disease are at increased risk of developing psychiatric disorders as well as symptoms associated with inflammatory responses. The parabrachial nucleus (PB) in the pons has been acknowledged as a key structure to relay nociceptive information from peripheral nociceptors to the forebrain structures. However, accumulating evidence suggests that the PB also serves as a general alarm system in response to real and/or potential threat signals such as pain, hunger, bitter, cold, or thirst. The PB projects to the amygdala and the bed nucleus of the stria terminalis, both of which are related to emotional behavior. The synaptic potentiation of the PB-CeA pathway is observed in many animal models of chronic pain as well as PTSD models, the dysregulation of the PB activity may be involved in cognitive dysfunction and emotion-related behavioral disorders observed in many chronic diseases. The purpose of this study was to examine the effects of chronic activation of PB on cognitive, social, and emotional behaviors. A mouse model was established using a chemogenetic activation system, Designer Receptors Exclusively Activated by Designer Drugs (DREADD) for the chronic activation of PB. Anxiety-like behavior, sociality, fear memory formation, and pain

thresholds were analyzed in this mouse model. The results showed marked anxiety-like behavior and impaired fear memory recall after the chronic PB-activation, indicating that hyperactivity in the PB induces the circuit dysregulation related to the psychiatric disorders.

5－2．Introduction

Chronic diseases such as diabetes, arthritis, cancer, and chronic pain are known to be accompanied by mental disorders such as major depression, together with deficits in multiple cognitive domains, including attention, learning, and emotional reading (Pieretti et al., 2016). Conversely, these impairments in brain functions are known to increase the risk of systemic and chronic disorders. The mechanism of interaction between chronic diseases and emotional dysfunctions remains unclear. In this study, I focused on the PB, which has been postulated to play a key role to transmit nociceptive information from the spinal cord to the amygdala; known as the “spino-parabrachial-amygdaloid pathway”. The PB is composed of 10 subnuclei; the combined region of eight subnuclei is called the lateral parabrachial nucleus (lPB), and the combined region of the remaining two subnuclei is called the medial parabrachial nucleus (mPB). The PB receives sensory information via projections from the posterior horn nucleus of the spinal

cord, the trigeminal ganglion, the nucleus of the solitary tract (NTS) which is innervated by the nodose ganglion, and periaqueductal gray (PAG) (Krout et al., 1998). In turn, it sends projections to the capsular subdivision of the CeA (CeC) (Bernard et al., 1993), the dorsolateral bed nucleus of the stria terminalis (dl BNST), the ventromedial bed nucleus of the stria terminalis (vm BNST) (Lebow & Chen, 2016), the hypothalamus (Bester, 1997), and the dorsal horn of the medulla oblongata (Yoshida et al., 1991). These anatomical configurations put the PB into a unique position to serve as a general alarm system to detect real and/or potential danger and broadcast it to the forebrain structures.

The corticolimbic system is involved in the plastic behaviors to adapt to the constantly changing environment, and its pathophysiology is involved in behavioral malfunctions such as drug addiction and chronic pain (Baliki & Apkarian, 2015; Denk et al., 2014; Navratilova et al., 2015). Among the corticolimbic systems, the amygdala is an essential structure for the regulation of negative emotions such as fear and pain, and positive emotions such as reward (Adhikari et al., 2015; Gottfried et al., 2003; Han, 2015). The BLA functions as a field of input in the amygdala structure and receives inputs from all sensory-related brain regions and the thalamus. The CeA is predominantly composed of inhibitory neurons that produce gamma-Aminobutyric acid (GABA) as their output (GABAergic neurons), and the glutamatergic neurons in the BLA project to CeC as well

as the lateral subdivision of the CeA (CeL). The PB-CeC pathway plays an important role in fear memory formation and recall, as pharmacological inactivation of the PB attenuated fear memory formation while optogenetic activation of the PB-CeA pathway terminals serves as the US to create artificial fear memory when associated with CS. Furthermore, the two excitatory pathways, one from the PB and the other from the BLA, into the CeC are both under the activity-dependent synaptic potentiation in pre- and post-synaptic manner following robust fear memory formation (Watabe et al., 2013). Also, several chronic, as well as semi-chronic pain models, have been shown to exhibit synaptic potentiation in the PB-CeA pathway (Miyazawa et al., 2018).

Acute activation of the PB by DREADD has been reported to suppress sleep fluctuations and induce continuous arousal (Qiu et al., 2016). The external lateral subdivision of PB is known to express a high level of calcitonin gene-related peptide (CGRP). The CGRP-positive cells in the PB are necessary and sufficient for the formation of aversive memory and taste memory. Furthermore, chronic activation of CGRP-positive cells in the PB causes severe anorexia and starvation (Palmiter, 2018). Another subpopulation in the PB, which expresses oxytocin, directly projects the oxytocin-positive cells in the periventricular hypothalamus (PVH), and is involved in the regulation of water intake (Ryan et al., 2017). Yet, it is still not fully explored how the chronic

activation of the PB regulates emotion-related behaviors.

The DREADD system is a powerful tool to chronically activate or inactivate certain groups of neurons in particular brain regions. The excitatory DREADD using hM3D (Gq) increases intracellular calcium concentration (Roth, 2016), protein kinase C (PKC) activity, and Ca2+/calmodulin-dependent kinase (CaMK) activity. It promotes depolarization and increases membrane excitability. Clozapine N-oxide (CNO) is often used as a ligand for DREADD, but there is a risk of side effects due to chronic application of clozapine. To overcome this problem, deschloroclozapine (DCZ), which has been recently invented by the Minamimoto group to achieve a higher affinity and selectivity, was used in the present study (Nagai et al., 2019). It has been confirmed that the intraperitoneal administration of DCZ (1 μg per kg) to mice expressing hM3D (Gq) DREADD in the somatosensory cortex induced persistent cell firing for 150 min (Nagai et al., 2019).

The purpose of this study is to examine the effects of chronic PB activation on emotion-related behaviors. I hypothesized that mice with chronic activation of the PB exhibit increased anxiety, decreased sociality, and decreased memory formation, as in patients with chronic pain with psychiatric disorders. In the present study, I have conducted the open-field test, the three-chamber test, the fear memory conditioning test,

the von Frey filament test, and the test to the electrical foot-shock threshold, to evaluate the effects of chronic PB activation.

５－３．Materials and Methods

Mice

Four weeks old C57BL/6J male mice were purchased from Japan SLC, Inc (Shizuoka, Japan). The mice were bilaterally injected with AAV5-hSyn-hM3D(Gq)-mCherry into PB (-6.0 mm posterior to bregma, 3.2 mm from skull surface, 1.3 mm lateral to the midline) as DREADD group. Other mice were injected with AAV2.5-hSynapsin-EGFP-WPRE-bGHPB or AAVDJ-Syn-mCherry into the bilateral PB as a control group. Each AAV was injected 250 μl at a speed 50 μl/minutes.

DREADD ligand administration

DREADD ligand deschloroclozapine (DCZ, 10 μg/kg) was administered to both groups by intraperitoneal injection twice per day for 8 days before the behavioral experiment and on the day of the behavioral experiment (Fig. 13A). Behavioral experiments were conducted an hour after DCZ administration, and only the data recorded within an hour and 40 minutes after administration were analyzed. There is no difference

in body weight at the first day of the behavioral experiment between the two groups (Control = 103.2 ± 2.798, n = 10 mice, DREADD = 103.2 ± 0.713, n = 14 mice, t = 0.012, P = 0.990, unpaired Student's t-test; Fig. 13B).

Experimental paradigm

DCZ administration was started 13 days after the AAV injection, and behavioral experiments were started 21 days later. The methods for behavior analyses including open field test, three-chambered test, fear conditioning, context retrieval and tone retrieval were followed as previously described in the materials and methods part of the section 4. Open field test and von flay test were conducted on day 1, fear conditioning, generalized fear memory conditioning, and three-chamber test were conducted on day 2, contextual retrieval, generalized tone retrieval, and shock intensity test were performed on day 3, tone retrieval test was performed on day 4. The pre-experimentation handling was started one week before the first behavioral test. The open field test, three-chamber test, fear conditioning, contextual retrieval, and tone retrieval were performed as described in the previous sections.

Generalized fear conditioning

On day 2, the mice were placed in the conditioning chamber and exposed to tone with foot shock association (CS+) and tone without foot shock association (CS-) for generalized fear conditioning. Training was conducted with interleaved presentations of three paired tones CS+ (65 dB, 4 kHz, 20 s) that co-terminated with foot shock as US (0.3 mA, 2 s), and three unpaired tones CS- (65 dB, 12.5 kHz with 2 Hz, 20 s) with variable inter-trial intervals for generalized fear conditioning. Three pairings were conducted with CS+ and CS- alternatively and the whole sequence was repeated twice. Specifically, the CS+ was presented at 270, 440 and 570 s and was paired with a foot shock, whereas the CS- occurred at 370, 520 and 660 s. The context was set by presenting white noise at 50 dB, illuminance of 200 lux, and with ethanol scent. Tone without foot shock association (CS-) and tone with foot shock association (CS+) were presented to mice.

Generalized fear retrieval

On day 3, the tone not associated with a foot shock (CS-) was presented to the mice in the same manner as that in tone retrieval, and freezing behavior was evaluated. Four hours later, the response to the tone associated with a foot shock (CS+) was assessed. The chambers were set to provide different contexts in the two retrievals; the CS+

retrieval context (white acrylic plate walls scented with peppermint odor; 50 Lux, 60 dB background white noise), or CS- retrieval context (with stripe patterns walls and, on the floor, different texture like a filter paper, scented with muscat odor; 50 Lux, 60 dB background white noise) The tone discrimination was calculated using the following equations:

Tone discrimination = {(CS+ FZ ratio) - (CS- FZ ratio)} / {(CS+FZ ratio) + (CS- FZ ratio)}

CS+ FZ ratio = freezing ratio at CS+ tone retrieval, CS+ 20 second presentation (bin4)

CS- FZ ratio = freezing ratio at CS- tone retrieval, CS- 20 second presentation (bin4)

Analysis for paw withdrawal threshold in response to mechanical stimulation

The von Frey filament test was performed with plastic filaments with a flat tip of 0.008, 0.02, 0.04, 0.07, 0.16, 0.4, 0.6, 1.0, and 2.0 G was applied perpendicularly to the plantar surface of the left and right hind paws, and the threshold value for repellent behavior was analyzed as describes in previous study (Christensen et al., 2019).

Analysis for paw withdrawal threshold in response to electrical foot-shock

Foot shocks with different intensities of 0.02, 0.04, 0.06, 0.08, 0.1, 0.12, 0.14, 0.16, 0.18, 0.2, 0.22, and 0.24 mA were given for 2 s at 30 s intervals. The thresholds for

retreating, flinching, vocalization, and jumping were measured from the video recording.

Data analysis

I used unpaired Student's t-test and two-way ANOVA with post hoc Bonferroni's test. The level of statistical significance was set at $P < 0.05$ as * and $P < 0.01$ as **. All statistical analyses were performed using Graph pad prism software (version 6.0 for windows, GraphPad Software, San Diego, USA). The data are presented as mean ± s.e.m.

5－4．Results

Chronic activation of the PB region did not affect pain threshold

The PB is an important region for pain stimulus transmission. Therefore, changes in pain recognition ability may be partly responsible for the results of the above-mentioned fear memory formation and recall. To verify this possibility, I analyzed the threshold of mechanical pain and electrical pain. The PB of DREADD group mice was chronically activated. The mechanical pain threshold in the foot was analyzed by the manual von Frey test. There was no significant difference between the two groups in the mechanical pain threshold for the average of both feet (Control = 0.876 ± 0.126, n = 8 mice, DREADD = 0.998 ± 0.123, n = 13 mice, t = 0.656, P = 0.575, unpaired Student's

t-test; Fig. 13C). The electrical pain threshold of the foot was verified using a continuous increase in the foot shock current from 0 mA by 0.02 mA steps under the condition of 2 s duration and 30 s intervals. The current at which the mouse showed flinching, vocalization, and jump was recorded. There was no significant difference between the two groups in the electrical pain threshold in any of the responses (Flinching, Control = 0.043 ± 0.004, n = 8 mice, DREADD = 0.38 ± 0.004, n = 8 mice, t = 0.78, P = 0.448, Vocalization, Control = 0.068 ± 0.005, n = 8 mice, DREADD = 0.078 ± 0.005, n = 8 mice, t = -1.44, P = 0.172, jump, Control = 0.125 ± 0.011, n = 8 mice, DREADD = 0.098 ± 0.012, n = 8 mice, t = 1.706, P = 0.11, unpaired Student's *t*-test; Fig. 13D).

Chronic activation of PB resulted in a marked increase in anxiety-like behavior

An open field test was performed to analyze anxiety-like behavior in mice chronically activated in PB. First, behaviors were analyzed one hour after single DCZ injection (i.p.) to test whether acute stimulation of PB changes anxiety-like behaviors. Mice with acute DREADD showed enhanced anxiety-like behaviors, such as shorter center time (Acute-Control = 14.71 ± 1.37, n = 10 mice, Acute-DREADD = 6.825 ± 2.857, n = 10 mice, t = 2.488, P = 0.023, unpaired Student's *t*-test; Fig. 14A) and shorter total distance (Acute-Control = 4020 ± 242.5, n = 10 mice, Acute-DREADD = 2269 ± 285.4,

n = 10 mice, t = 4.675, P < 0.01, unpaired Student's *t*-test; Fig. 14B). DREADD mice didn't show difference in locomotion speed (Acute-Control = 12.13 ± 0.39, n = 10 mice, Acute-DREADD = 13.87 ± 0.898, n = 10 mice, t = 1.777, P = 0.092, unpaired Student's *t*-test; Fig. 14C).

Next, anxiety-like behavior was measured after chronic activation of PB. The center time was remarkably decreased in the DREADD group (Control = 10.789 ± 0.923, n = 15 mice, DREADD = 4.289 ± 1.09, n = 15 mice, t = 4.552, P < 0.01, unpaired Student's *t*-test; Fig. 14D). In addition, the total distance was decreased (Control = 4500.17 ± 227.321, n = 15 mice, DREADD = 3303.61 ± 392.531, n = 15 mice, t = 2.638, P = 0.015, unpaired Student's *t*-test; Fig. 14E), while the locomotion speed was increased (Control = 12.821 ± 0.242, n = 15 mice, DREADD = 15.235 ± 0.289, n = 15 mice, t = -4.141, P < 0.01, unpaired Student's *t*-test; Fig. 14F) in the DREADD group. These results indicate that chronic activation of PB induces a marked increase in anxiety-like behavior. For sociability analysis, I traced mouse location (Fig. 15A) in three-chamber test chamber and revealed that both control and DREADD groups showed differences in duration time in Mouse area, Empty area and Other area (F (2, 28) = 102.5, P < 0.01, two-way ANOVA test; Fig. 15B). However, the post hoc comparisons showed no statistical difference between control and isolation groups in stay time at three locations (Fig. 15B). The social

index and enter ratio into the Mouse area and the Empty area showed no significant differences between two groups (Social index: Control = 2.018 ± 0.409, n = 8 mice, DREADD = 1.401 ± 0.66, n = 8 mice, t = 0.793, P = 0.441, unpaired Student's *t*-test; Fig. 15C, Enter ratio, Control = 1.214 ± 0.105, n = 8 mice, DREADD = 1.203 ± 0.137, n = 8 mice, t = 0.061, P = 0.953, unpaired Student's *t*-test; Fig. 15D). These results indicate that chronic activation of PB did not significantly impair social behavior.

Chronic activation of PB reduced freezing for fear memory retrieval

After completing the open-field test and the three-chamber test, fear conditioning was performed to evaluate the ability to associate tone and foot shock. The DREADD group consistently showed higher freezing behavior before the presentation of tone and shock (Fig. 16A).

The day after fear conditioning, contextual retrieval was performed to examine whether fear memory associated with the context was formed. However, no significant difference was observed in freezing rate (Fig. 16B, Control = 34.633 ± 4.427, n = 10 mice, DREADD = 43.24 ± 3.703, n = 14 mice, t = 1.493, P = 0.15, unpaired Student's *t*-test; Fig. 16C) and jump number, which was interpreted as escape behavior (Control = 9.8 ± 2.756, n = 10 mice, DREADD = 6.643 ± 1.633, n = 14 mice, t = 0.986, P = 0.34, unpaired

Student's *t*-test; Fig. 16D).

Next, I evaluated fear memory associated with an auditory stimulus. In the tone retrieval test, the tone associated with foot shock was presented in a new environmental context, and the degree of freezing was analyzed. The freezing responses of two groups analyzed with temporal bins of 20 s in the tone retrieval sessions revealed that control and isolation groups showed differences in freezing ratio ($F(1, 22) = 27.05$, $P < 0.01$, two-way ANOVA test; Fig. 17A). The post hoc comparisons revealed no difference in freezing rate between mouse groups at bin4, which corresponds to the initial 20 s of the tone presentation (Control = 45.25 ± 6.163, n = 10 mice, DREADD = 34.821 ± 5.192, n = 14 mice, t = 1.295, P = 0.211, unpaired Student's *t*-test; Fig.17B). The DREADD group continued freezing after the completion of tone presentation, showing a remarkable increase compared to the control group (Control = 18.25 ± 3.417, n = 10 mice, DREADD = 46.607 ± 4.551, n = 14 mice, t = -4.983, $P < 0.01$, unpaired Student's *t*-test; Fig.17C). There was no statistical difference in the jump number between the control and DREADD groups (Control = 8 ± 1.719, n = 10 mice, DREADD = 5.571 ± 0.732, n = 14 mice, t =1.3, P = 0.21, unpaired Student's *t*-test; Fig.17D). Enhanced anxiety of DREADD mice may be linked to the increased freezing ratio at later time bins after tone presentation.

Since the DREADD group consistently showed a continuous increase in freezing

time throughout the tone retrieval session, it was considered that the freezing reaction might be a reaction that does not depend on the tone presentation. Therefore, I verified the discrimination ability of shock-associated tone by generalized fear conditioning. In generalized fear conditioning, two types of sound cues were presented, and only one of them was associated with a foot shock. The tones with or without foot shock were presented for two minutes after 24 h and 26 h after the conditioning. The freezing responses to the tone associated with a foot shock analyzed with temporal bins of 20 s in the tone retrieval sessions revealed that control and isolation groups showed differences in freezing ratio ($F(1, 20) = 53.85$, $P < 0.01$, two-way repeated ANOVA test; Fig. 18A). Bonferroni post hoc analysis showed DREADD mice showed significant lower freezing behavior during tone presentation at bin4 (Fig. 18A). Importantly, the freezing response at the time bin corresponding to the presentation of the conditioned tone (bin4) was markedly suppressed in the DREADD group (Control = 58.75 ± 4.39, n = 12 mice, DREADD = 41.75 ± 6.541, n = 10 mice, t = 2.22, P = 0.038, unpaired Student's *t*-test; Fig. 18B). There was no significant difference in the number of jumping (Control = 5.25 ± 0.986, n = 12 mice, DREADD = 6.9 ± 0.912, n = 10 mice, t = -1.548, P = 0.241, unpaired Student's *t*-test; Fig. 18C). In response to the tone without foot shock, CS-, the control and DREADD groups showed statistically no differences in freezing ratio (F (1,

20) = 1.156, P = 0.295, two-way repeated ANOVA test; Fig. 18D). In response to the tone without foot shock, CS-, the control and DREADD groups showed statistically no differences in freezing ratio (Control = 30.21 ± 4.851, n = 12 mice, DREADD = 27.75 ± 4.88, n = 10 mice, t = 0.354, P = 0.727, unpaired Student's *t*-test; Fig. 18E). The tone discrimination index, calculated from the freezing ratio to CS+ and CS-, was not statistically different between the control and DREADD groups, while a trend of the lower index in the DREADD group was noticed (Control = 0.34 ± 0.076, n = 12 mice, DREADD = 0.172 ± 0.102, n = 10 mice, t = 1.351, P = 0.192, unpaired Student's *t*-test; Fig. 18F).

５－５．Discussion

In the present study, I found that the mice with chronic activation of the PB exhibited a marked increase in anxiety-like behavior. This enhanced anxiety may explain the trend of higher freezing ratio before the "tone-foot shock paring period" during the fear conditioning. The DREADD group showed no difference in social interaction behaviors.

Regarding the pain-related behaviors, no detectable changes were observed in the mechanical nociceptive threshold and the threshold to the electrical foot-shock in the

DREADD group. These results suggest that the chronic activation of PB did not affect the peripheral and/or spinal reflex-level of the nociceptive threshold, which is detected by the von Frey filament test, but more predominantly affected the central nervous system. An alternative explanation of the nociceptive threshold shown in this study is that the PB is composed of mixed populations of neurons, and the net effects of their activation have resulted in no change in nociceptive reflex. In support of this notion, a recently published study reported that prolonged optogenetic activation of glutamatergic PB neurons induces chronic hyperalgesia, while prolonged optogenetic activation of GABAergic PB neurons prevents the development of hypersensitivity induced by neuropathic pain (Sun et al., 2020).

Because the DREADD mice exhibit significantly enhanced anxiety-like behaviors measured in the open field test, it is difficult to interpret the fear conditioning results, which utilize immobility (freezing) as an outcome. Nevertheless, in the context-dependent fear memory test, there were no detectable changes in the freezing behaviors. In the tone retrieval test, the DREADD mice exhibited a trend of enhanced freezing behavior even before the tone-presentation, although the freezing rate did not dramatically change after tone presentation. From these results, it was suspected that the DREADD group might have a diminished ability to associate tone and foot shock. To test

this possibility, I performed a fear memory generalization paradigm, in which mice are exposed to two types of tones; the tone associated with a foot shock (CS+) and the tone without association (CS-). DREADD mice showed a similar freezing ratio in CS- tone retrieval, as seen in control mice. However, in CS+ retrieval, the DREADD mice showed a drastically lower freezing response than control mice. These results suggest that the DREADD mice have attenuated fear memory formation and/or retrieval, and that the DREADD mice have relatively lower ability in tone discrimination of CS+ and CS-. The DREADD mice did not show a deficit in mechanical and electrical pain threshold of hind paws, which suggests lower fear response during the tone retrieval session may result from memory formation and retrieval process, rather than peripheral nociceptive or spinal reflex level mechanisms.

The PB is also proposed to play a key role in the regulation of food intake, but no change in body weight was observed in this study. Because the intraperitoneal DCZ injection was performed during the daytime, a potential decrease in food intake induced by DCZ may have been compensated by feeding behavior during the active night period.

The PB-CeA pathway is a glutamatergic excitatory projection (Sato et al., 2015). Previous studies have shown that acute optogenetic activation of this excitatory projection induces negative emotion-related behaviors such as anxiety, depression, and aversive

behavior in rats (Hama et al., 2015). On the other hand, optogenetic activation of excitatory projections of the amygdala BLA-CeA pathway induces a decrease in anxiety-like behavior and a decreased threshold in thermal stimulation. Simultaneous optogenetic activation of the PB-CeA pathway and the amygdala BLA-CeA pathway did not result in negative emotion-related behavioral changes (Cai et al., 2018). Thus, acute activation of excitatory projection from PB to CeA activates negative behavior, while acute activation of excitatory projection from BLA to CeA suppresses negative behavior. These distinct functions may be explained by the difference in the target areas of the two excitatory projections. The BLA projects to a wide range of CeA including CeC, CeL, and CeM, while PB projection is restricted predominantly to the CeC with minor branches to CeL. The results presented in this section indicated that the activity in the PB regulates anxiety-related behavior and fear-related memory.

In the present study, DCZ has been applied for 8 consecutive days in an attempt to induce synaptic plasticity in the relevant pathways during daily activities using sensory information as CS. However, the behavioral outcomes seemed to be different from those of mice that received optogenetic stimulation for long-term potentiation (LTP) induction at the PB-CeA terminals, which exhibited enhanced generalization to the CS (-), exaggerated fear memory when paired with the weak US, and little changes with general

anxiety (Tohyama et al., personal communications). There are several possibilities to explain these superficially conflicting results; First, synaptic plasticity requires the coincident activities of pre- and post-synaptic neurons. Therefore, chronic activation of the presynaptic PB neurons is not sufficient to induce LTP in the PB-CeA pathway in the present study. Second, the PB sends projections not only to the CeA, but many other brain regions including the bed nucleus of the stria terminalis (BNST), VMH, and PAG. Therefore, the behavioral phenotypes in the present study are the combinatory effects of chronic activations in multiple brain regions and circuitries. Third, some metaplastic changes are induced during the chronic treatment period of the consecutive 8 days, so that LTP induced in the early phase might have been de-potentiated in the later phase. It would be an important future study to clarify these possibilities. To approach the first possibility, ex vivo electrophysiological experiments are required together with both DREADD and opsins expressed in the PB. The input/output analysis of the light-evoked synaptic weight would reveal if the LTP-like phenomenon induced in the PB-CeC pathways. To examine the second possibility, whole-brain level analysis is necessary, part of which is examined in Chapter 5. The third possibility can be tested by examining the time course of behavioral changes. The preliminary results showed that acute excitatory DREADD induces anxiety-like behaviors in a similar manner to those in the present study. Because

the PB is composed of heterogeneous cell populations, a cell-type specific and intersectional approach would be desired to further dissect out the circuitry mechanisms in the future study.

６．Correlation analysis of behavior and neuronal activation in mice with chronic activation of the PB region

６－１．Summary

Chronic activity in the parabrachial nucleus (PB) region has been shown to induce marked anxiety-like behavior and fear memory attenuation. In addition to the PB region, multiple neuronal circuits indirectly activated by efferent from the PB should be identified for the comprehensive understanding of the brain regions involved in the behavioral outcomes. The candidate brain regions include the CeC, BNST, BLA, and mPFC. In order to clarify the correlation between the activity of each brain region, I combined a chemogenetical activation system, Designer Receptors Exclusively Activated by Designer Drugs (DREADD) and a large-scale imaging and detection of *c-Fos*-positive neurons by both conventional immunostaining of tissue sections and a large volume detection of cells using Ab Sca*l*e. We found that the chemogenetic activation of PB induced wide-spread activation of neurons in multiple target brain areas, together with increased correlation of neuronal activity among the central nuclei of the amygdala. Correlational analysis between the neuronal activation in brain regions and behavioral performance revealed correlation between anxiety and the neuronal activities in PB, CeC, and BLA, indicating that the activity in the amygdala region may be an important

component that drives behavioral changes.

6－2．Introduction

Expression of the IEGs is used as an indicator of neural activity. IEGs regulate the expression of many downstream transcription factors (Herdegen & Leah, 1998; Knapska & Kaczmarek, 2004) related to variable cellular functions (Lanahan & Worley, 1998). More than 100 genes are classified as IEGs (Minatohara et al., 2016; Sheng et al., 1995), but the genes expressed in nerve cells are limited (Sheng et al., 1995). *c-Fos* is a typical IEG in nerve cells, and *c-Fos* expression is triggered by cyclic adenosine monophosphate (cAMP) and Ca^{2+} through the activation of the cAMP response element binding protein (CREB) / the cAMP response element (CRE) complex. The *c-Fos* protein dimerizes with the Jun family protein and constitutes the transcription factor AP-1 (Chiu et al., 1988; Pennypacker, 1995). The correlation between *c-Fos* expression and learning behavior is observed not only during learning (Kaczmarek, 1990; Tischmeyer et al., 1990) but also during memory recall (Bravo-Rivera et al., 2015; Gallo et al., 2018; Kubik et al., 2007; López de Armentia, 2007; Maviel et al., 2004).

Since it was shown that the chronic activity in the PB region induces a marked increase in anxiety-like behavior and a decrease in fear memory, the brain regions related

to this behavioral change were examined by *c-Fos* immunoreactivity. The brain regions with increased *c-Fos* immunoreactivity include the central amygdala CeA, the BNST, the BLA, and the mPFC after chronic activation of the PB region. In particular, the increased activity in the amygdala region was correlated with the extent of behavioral changes.

６－３．Materials and Methods

Mice

Mice examined at section 6 were prepared as previously described in section 5. AAVDJ-Syn-mCherry or AAV5-hSyn-hM3D(Gq)-mCherry was injected bilaterally into the PB region of 4-week-old male B6/J mice to prepare the control group and the DREADD group, respectively. Two weeks later, DCZ (10 μg / kg) was administered twice per day for 8 days, and each behavioral experiment (open field test, generalized FC, CS-, and CS+ retrieval) was performed an hour after DCZ administration. DCZ was administered for 2 days after the end of the behavioral experiment.

Immunostaining

DCZ was administered an hour before fixation. Perfusion fixation was performed with an initial application of 10 ml of 0.01 M PBS and subsequent application

of 40 ml of 4 % PFA. The dissected brains were further fixed in the same fixative overnight. 50 μm thick sections were prepared by vibratome (VT1000, Leica). Sections were treated overnight at room temperature with a blocking solution containing 1 % BSA and 0.5 % triton. The sections were incubated with anti-*c-Fos* primary antibody (Rabbit polyclonal / ab190289, Lot GR3271743-1, Abcam) overnight at a dilution of 1: 5000. Next, the samples were incubated with the secondary antibody (Goat Anti Rabbit Alexa Fluor 488 / ab150077, Abcam) for 2 hours at room temperature with a dilution of 1: 350. The stained sections were observed with a confocal microscope (FV3000, Olympus), and *c-Fos*-positive cells were measured with ImageJ software.

Ab Sca*l*e for *c-Fos* Immunostaining

Brain slices with the thickness of 300 μm from control (n = 1 mouse) and DREADD mice (n = 1 mouse) were made by vibratome（VT1200S, Leica）. Ab Sca*l*e Immunostaining method was as described previously (Hama et al., 2015). The following primary and secondary antibodies were used. Anti *c-Fos* antibody (Polyclonal rabbit purified antibody, #226003, Lot 6-72, 1:100 dilution, Synaptic Systems), Alexa Fluor 488-conjugated goat anti-rabbit polyclonal antibody (# A-11008, 1:200 dilution, Invitrogen). For nuclear staining, Hoechst dye (Hoechst 33342, 1:200 dilution, Dojindo)

was used.

Data analysis

Pearson's r values for the *c-Fos*-positive cell density between the two regions were determined (Tanimizu et al., 2017). Similarly, the correlation between *c-Fos*-positive cell density and the total time spent in the central area during the open field test was evaluated by the Person r values. We also assessed the correlation between *c-Fos*-positive cell density and the freezing time in the 20 seconds after tone presentation in the generalized fear conditioning with a similar strategy. For *c-Fos* expression analysis with the Ab Sca*l*e method, *c-Fos* immunoreactivity and Hoechst signal were detected by a confocal microscope (Nikon Eclipse Ti A1-A, Nikon) with a low-magnification objective lens (x10, NA 0.45, air, Olympus). Acquired images were analyzed with ImageJ. Images were acquired in a 16-bit gray range. Thresholds for fluorescence brightness of anti- *c-Fos* immunoreactivity were adjusted to reduce the background intensity. Images of *c-Fos*-positive cells in the PB, the amygdala CeC, the amygdala BLA, prefrontal cortex mPFC, and dm BNST, dl BNST, vm BNST were analyzed. For the determination of the anatomical regions, I followed the stereotaxic coordinates of the mouse brain by G. Paxinos and K. B. J. Franklin (Academic Press, 2008) and previous publications (Cai et

al., 2014; Kovács et al., 2018; Tanimizu et al., 2017). The *c-Fos* positive neuron density of DREADD mice was normalized by the *c-Fos* positive neuron average density of the control mice.

６－４．Results

Chronic activation of the PB region results in the activation of the amygdala

After the behavioral experiment, the animals were maintained for two days, with 10 μg/kg of DCZ administration twice per day. On the next day, an hour after administration of 10 μg/kg of DCZ, perfusion fixation was performed, and the *c-Fos* expression pattern in each brain region was analyzed. mCherry positive neurons in PB (Fig. 19A) and *c-Fos*-positive neurons in multiple regions, including PB and amygdala regions, were detected by confocal microscopy (Fig. 19B).

A marked increase in *c-Fos*-positive cell density in the DREADD group was observed in the PB region and the CeC region (PB, Control = 100 ± 22.538, n = 4 mice, DREADD = 484.15 ± 87.243, n = 4 mice, t = -4.263, P = 0.018, CeC, Control = 100 ± 39.777, n = 4 mice, DREADD = 249.706 ± 42.643, n = 4 mice, t = -2.567, P = 0.043, unpaired Student’s t-test; Fig. 19C).

Interregional correlations of *c-Fos*-positive cell densities were presented based

on Pearson's r for correlations of the positive cell densities between two brain regions (Fig. 19D). In the control group, a positive correlation was found between the CeC, the CeL, and the CeM, which constitute the amygdala central core CeA. It was shown that the CeL has a strong positive correlation with the mPFC and dl BNST. Furthermore, the amygdala CeM has a strong positive correlation with the amygdala BLA. In turn, BLA is positively correlated with the amygdala CeM, the mPFC, and the dm BNST. The BNST region is composed of the dm BNST, the dl BNST, and the vm BNST. There exists a high correlation between dm BNST and dl BNST, the correlations between vm BNST and other BNST regions were low. The three pairs of regions showed robust negative correlations in the control group; the PB and the amygdala CeC, the amygdala CeC and the vm BNST, and the amygdala CeL and the vm BNST.

In the DREADD group, more positive correlations between brain regions were observed. Compared to the control group, there were positive correlations among 6 brain regions; the PB, the amygdala CeC, the amygdala CeL, the amygdala CeM, the mPFC, and the dl BNST. In the mPFC and the dl BNST, the correlation with the amygdala region became strong in a positive direction, and the vm BNST also showed higher correlations with other regions. In the DREADD group, there was no tendency of increased correlation of the amygdala BLA with several other regions, including the PB, the amygdala CeC,

CeL, and CeM.

Next, to assess *c-Fos* expression in the broader areas, I performed *c-Fos* immunostaining in thick slices using the Ab Sca*l*e method and obtained fluorescence signals with confocal microscopy. The *c-Fos* immuno signals were detected in the entire thickness of the slices (Fig. 20A, Fig. 20B). As a result, a large number of *c-Fos*-positive cells could be extracted and counted in the larger areas of multiple brain regions compared to the previous *c-Fos*-positive cells analysis in thin slices (the average number of counted *c-Fos* positive cells in Figure 19C control mice: PB 23, CeC 7, CeL 11, CeM 23, BLA 68, mPFC 30, dm BNST 30, dl BNST 39, vm BNST 62, The number of counted *c-fos* positive cells in Figure 21B: PB 39, CeC 37, CeL 48, CeM 28, BLA 89, mPFC 192, dm BNST 124, dl BNST 68, vm BNST 320). In this analysis with thick slices, increases in the number of *c-Fos*-positive cells in the amygdala sub-regions (CeM, CeL, CeC, and BLA) in DREADD mice were confirmed. In addition to the amygdala, this Ab Sca*l*e-based analysis also enabled to show increased *c-Fos*-positive neurons in the thalamic nucleus (Fig. 21A, Fig. 21B).

Relationship between induced PB activation and anxiety-like behavior

Relationships between the behavioral data and the regional density of *c-Fos*-

positive cells were analyzed based on the data from 8 animals, 4 from the Control group and 4 from the DREADD group. First, the center times measured in the open field test were evaluated for their correlation with the regional density of *c-Fos*-positive cells. I found that the time spent in the center area showed a weak negative correlation with the *c-Fos* positive cell density in multiple brain regions. (Fig. 22A and B, correlation coefficient Pearson's r values; PB = -0.689, CeC = -0.749, CeL = -0.294, CeM = -0.103, BLA = -0.579, mPFC = -0.125, dm BNST = 0.492, dl BNST = 0.181, vm BNST = -0.419). The weak correlations found in the PB and the CeC were consistent with the decreased center times and the increased *c-Fos*-positive cell densities in the DREADD group relative to the values in the Control group (Fig. 22A). These results suggest that there was a positive correlation between anxiety-like behavior and PB activation. However, more extensive statistical evaluation was hindered by the small number of samples in the current study.

Next, the freezing behavior of mice in response to the CS+ tone, which had been conditioned with foot shock, in the behavioral paradigm of generalized fear memory retrieval was evaluated if this fear-related response shows any correlation with the regional density of *c-Fos*-positive cells. The freezing rate after tone presentation in the tone retrieval test showed a trend of negative correlation with the *c-Fos*-positive cell

density in the PB, CeC, and BLA. (Fig. 22C and D, correlation coefficient Pearson's r values; PB = -0.245, CeC = -0.078, CeL = 0.425, CeM = 0.608, BLA = -0.315, mPFC = 0.403, dm BNST = 0.383, dl BNST = 0.447, vm BNST = 0.232). The observed tendency of the weak correlation may be derived from both the higher *c-Fos*-positive cell densities and the lower freezing rate in the PB of the DREADD group (Fig. 22C). Nevertheless, this trend of negative correlation in the freezing behavior was less obvious compared with the extent of correlation between the open field test and the *c-Fos*-positive cell density shown in Fig. 22B.

６－５．Discussion

In the previous Section, I reported the behavioral changes associated with the chronic chemogenetic activation of the PB without providing the data showing the extent of the PB activation. By taking the advantage of the neuronal activity marker *c-Fos*. I could successfully confirm the effective activation of a large number of neurons in the PB. In addition, an increase in *c-Fos* positive cell density was also observed in the CeC, which receives projections from the PB.

The Ab Sca*l*e method enabled detection of *c-Fos*-positive cells in a large volume and confirmed the increased *c-Fos*-positive cell density in the PB and CeC of the

DREADD mouse, showing the overall consistency with the results of conventional immunostaining method. This Ab Sca*l*e method also showed the increased density of *c-Fos*-positive cells in the thalamic nucleus of the DREADD mouse. The thalamic nucleus is known to receive neuronal projection from the PB (Qui et al., 2016) and this study suggested the chronic activation of this projection may be involved in the behavioral characteristic of the DREADD group.

I performed an interregional comparison of the *c-Fos*-positive cell density and generated matrices of Pearson's r for both the control and DREADD groups. The activity of the PB is correlated with the CeC, CeL, and CeM. Although the PB showed lower correlations with the CeL and CeM, they increased the correlations by the chronic activation of the PB by DREADD. On the other hand, there is little correlation between the PB and BLA, even in the DREADD group.

The correlational analysis between the activated brain regions and behavioral parameters in this study provided more information about the neural circuit activation involved in behavioral regulation. A weak negative correlation between the time spent in the center area and the activated cell density in the PB and CeC suggests the possible involvement of these two brain regions in the upregulation of behaviors related to anxiety. However, the interpretation of my data may not be straightforward in terms of the

comparison with previous optogenetic studies of the PB. Namely, the previous studies revealed that the optogenetic activation of the excitatory or inhibitory neurons in the lateral PB did not affect anxiety-like behavior in the open field test (Sun et al., 2020). This inconsistency may be caused by the technical difference between optogenetics and chemogenetics. Indeed, the optogenetic activation of the BLA-CeA pathway was shown to induce an anxiolytic effect (Tye et al., 2011). Furthermore, the afferent projections to the CeA were revealed to serve opposite functions in the regulation of anxiety-like behavior; the PB-CeA pathway is involved in an anxiogenic effect, while the PB-BLA input is involved in an anxiolytic effect (Cai et al., 2018). Furthermore, the genetically defined neural circuits in the BLA to the CeA were shown to regulate the negative or positive emotional behaviors (Kim et al., 2017). These previous publications indicate the complex outcomes of the exogenous activation of the neural circuits involving the PB, CeA, and BLA. To reveal the precise mechanism of emotional valence, I should utilize cell type- and neural circuit-specific strategies such as the Cre- or Flp- dependent gene expression technology.

The correlation between the freezing behavior in the fear memory recall and the *c-Fos*-positive cell densities of the PB and the CeC was even less prominent compared with the correlation with the open field test. More experiments are required in the future

to confirm if the differential behavioral outcomes after chronic PB activation in two types of fear-related responses are indeed driven by the differential neural circuit activation. Nevertheless, specific behavioral outputs may show consistent activity patterns in multiple brain regions, which can be detected by correlational analysis between region-specific neuronal activity patterns and animal behavior.

Based on the above observation, I conclude that the chronic activation of the PB increases the activity in a wide range of brain regions, including the CeC, and this increased activity in the amygdala-related brain regions may be involved in the increase of anxiety. In the formation of fear memory and its retrieval, it is known that two independent pathways are involved; one is the direct pathway from the PB region to the CeC. The other is the indirect path from the spino-thalamic tract to the CeA via the somatosensory cortex or thalamus as well as LA/BLA (Watabe et al., 2013). Therefore, one intriguing possibility is that the balance of the two pathways, the direct and the indirect pathways, plays a role in the proper regulation of emotion-like behaviors via the activation of the CeC. The chronic activation of the PB region might have induced excess enhancement of the direct pathway, which disrupted the balance of the two pathways, leading to pathological behavior. It would be an important future study to examine this hypothesis by selective activation or inhibition of the direct or indirect pathways in the

future.

7. Discussion

In this thesis, I first analyzed the effect of social isolation on the development and maturation of neuronal circuits and brain function. The studies showed immature neuronal circuit formation and increased escape behavior by social isolation stress. The phenomenon is thought to be due to the stress response in the endocrine system via the hypothalamus-pituitary-adrenal (HPA) axis. To study the molecular mechanism of synaptic dynamics, I evaluated the possible contribution of NMDA receptor subunit composition to synaptic maturation and turnover. The mice with altered GluN2A/GluN2B ratio show normal spine dynamics. Further improvement in the experimental condition and quantitative analysis in the future may clarify the contribution of NMDA receptors in controlling synapse dynamics. In the latter half of this thesis, the relationship between stress and the mechanism of neuronal circuit maturation was evaluated by social isolation and chronic activation of the PB region. Behavioral tests have revealed that the PB region is strongly involved in anxiety-like behavior and fear memory retrieval. The extent of the behavioral changes was correlated with the activation of the PB and amygdala CeC. For further study on neuronal circuits associated with disorders in emotion-related behavior, it is required to study the function of the neuronal projection from PB to CeC and also the pathway from the amygdala BLA to CeC via cortex.

8. Acknowledgment

Studies in section 1. “Spine dynamics in socially isolated mice” were supported by Grants-in-Aid for Scientific Research (17H01387 and 18H04727 to S.O.), Core Research for Evolutional Science and Technology from the Japan Science and Technology Agency (JPMJCR14W2 to S.O.), the Project for Elucidating and Controlling Mechanisms of Aging and Longevity from the Japan Agency for Medical Research and Development (17gm5010003 to S.O.), and the UTokyo Center for Integrative Science of Human Behavior (CiSHuB).

I appreciate Prof. Shigeo Okabe, Dr. Shinji Tanaka, Dr. Yutaro Kashiwagi and other students and staff at the Department of Cellular Neurobiology, The University of Tokyo. I also appreciate Prof. Kenichi Ohki, Dr. Masato Uemura, Dr. Satoru Kondo, Dr. Fumiaki Kishino (Department of Physiology, The University of Tokyo) for the support of the open skull imaging, Prof. Ayako Watabe, Dr. Kaori Mikami, Dr. Masashi Nagase, Dr. Takashi Nagashima, Dr. Suguru Tohyama, Dr. Mieko Morishima (Institute of Clinical Medicine and Research, The Jikei University School of Medicine) for the technical instruction and support for the behavioral experiments.

9. Reference

Adhikari, A., Lerner, T. N., Finkelstein, J., Pak, S., Jennings, J. H., Davidson, T. J., Ferenczi, E., Gunaydin, L. A., Mirzabekov, J. J., Ye, L., Kim, S. Y., Lei, A., & Deisseroth, K. (2015). Basomedial amygdala mediates top-down control of anxiety and fear. *Nature*, *527*(7577), 179–185.

Baliki, M. N., & Apkarian, A. V. (2015). Nociception, pain, negative moods, and behavior selection. *Neuron, 87*(3), 474–491.

Bernard, J. -F, Alden, M., & Besson, J. M. (1993). The organization of the efferent projections from the pontine parabrachial area to the amygdaloid complex: A phaseolus vulgaris leucoagglutinin (PHA-L) study in the rat. *J. Comp. Neurol.*, *329*(2), 201–229.

Bester, H., Matsumoto, N., Besson, J. M., Bernard, J. F. (1997). Further evidence for the involvement of the spinoparabrachial pathway in nociceptive processes: a c-Fos study in the rat. *J. Comp. Neurol., 383*(4), 439–458.

Bravo-Rivera, C., Diehl, M. M., Roman-Ortiz, C., Rodriguez-Romaguera, J., Rosas-Vidal, L. E., Bravo-Rivera, H., Quiñones-Laracuente, K., & Do-Monte, F. H. (2015). Long-range GABAergic neurons in the prefrontal cortex modulate behavior. *J. Neurophysiol.*, *114*(3), 1357–1359.

Cai, H., Haubensak, W., Anthony, T. E., & Anderson, D. J. (2014). Central amygdala PKC-δ+

neurons mediate the influence of multiple anorexigenic signals. *Nat. Neurosci.*, *17*(9), 1240–1248.

Cai, Y. Q., Wang, W., Paulucci-Holthauzen, A., & Pan, Z. Z. (2018). Brain circuits mediating opposing effects on emotion and pain. *J. Neurosci.*, *38*(28), 6340–6349.

Cane, M., Maco, B., Knott, G., & Holtmaat, A. (2014). The relationship between PSD-95 clustering and spine stability In Vivo. *J. Neurosci.*, *34*(6), 2075–2086.

Carr, C. P., Martins, C. M. S., Stingel, A. M., Lemgruber, V. B., & Juruena, M. F. (2013). The role of early life stress in adult psychiatric disorders. *J. Nerv. Ment. Dis.*, *201*(12), 1007–1020.

Castro, W. L. R., & Matt, K. S. (1997). Neuroendocrine correlates of separation stress in the Siberian dwarf hamster (Phodopus sungorus). *Physiol. Behav.*, *61*(4), 477–484.

Chapman, D. P., Whitfield, C. L., Felitti, V. J., Dube, S. R., Edwards, V. J., & Anda, R. F. (2004). Adverse childhood experiences and the risk of depressive disorders in adulthood. *J. Affect. Disord.*, *82*(2), 217–225.

Chida, Y., Sudo, N., & Kubo, C. (2005). Social isolation stress exacerbates autoimmune disease in MRL/lpr mice. *J. Neuroimmunol.*, *158*(1–2), 138–144.

Chiu, R., Boyle, W. J., Meek, J., Smeal, T., Hunter, T., & Karin, M. (1988). The c-fos protein interacts with c-Jun AP-1 to stimulate transcription of AP-1 responsive genes. *Cell*,

54(4), 541–552.

Christensen, S. L., Hansen, R. B., Storm, M. A., Olesen, J., Hansen, T. F., Ossipov, M., Izarzugaza, J. M. G., Porreca, F., Kristensen, D. M. (2019). Von Frey testing revisited: Provision of an online algorithm for improved accuracy of 50% thresholds. *Eur. J. Pain*, *24*(4), 783–790.

Curzon, P., Rustay, N. R. & Browman, K. E. (2009). Cued and contextual fear conditioning for rodents. *Methods of behavioral analysis in neuroscience, 2nd ed.,* chapter 2.

Datson, N. A., van der Perk, J., de Kloet, E. R., & Vreugdenhil, E. (2001). Identification of corticosteroid-responsive genes in rat hippocampus using serial analysis of gene expression. *Eur. J. Neurosci.*, *14*(4), 675–689.

Denk, F., McMahon, S. B., & Tracey, I. (2014). Pain vulnerability: A neurobiological perspective. *Nat. Neurosci. 17*(2), 192–200.

Djordjevic, A., Adzic, M., Djordjevic, J., & Radojcic, M. B. (2010). Chronic social isolation suppresses proplastic response and promotes proapoptotic signalling in prefrontal cortex of Wistar rats. *J. Neurosci. Res.*, *88*(11), 2524-2533.

Dronjak, S., Gavrilović, L., Filipović, D., & Radojčić, M. B. (2004). Immobilization and cold stress affect sympatho-adrenomedullary system and pituitary-adrenocortical axis of rats exposed to long-term isolation and crowding. *Physiol. Behav.*, *81*(3), 409–415.

Ecker, C., Spooren, W., & Murphy, D. G. M. (2013). Translational approaches to the biology of autism: false dawn or a new era. *Mol. Psychiatry, 18*(4), 435–442.

El-Husseini, A. E. D., Schnell, E., Chetkovich, D. M., Nicoll, R. A., Bredt, D. S. (2000) PSD-95 involvement in maturation of excitatory synapses. *Science*, *290*(5495), 1364–1368

El-Husseini, A. E. D., Schnell, E., Dakoji, S., Sweeney, N., Zhou, Q., Prange, O., Gauthier-Campbell, C., Aguilera-Moreno, A., Nicoll, R. A., & Bredt, D. S. (2002). Synaptic strength regulated by palmitate cycling on PSD-95. *Cell*, *108*(6), 849–863.

Elias, G. M., Elias, L. A. B., Apostolides, P. F., Kriegstein, A. R., & Nicoll, R. A. (2008). Differential trafficking of AMPA and NMDA receptors by SAP102 and PSD-95 underlies synapse development. *Proc. Natl. Acad. Sci. U. S. A.*, *105*(52), 20953–20958.

Elzinga, B. M., Roelofs, K., Tollenaar, M. S., Bakvis, P., van Pelt, J., & Spinhoven, P. (2008). Diminished cortisol responses to psychosocial stress associated with lifetime adverse events. A study among healthy young subjects. *Psychoneuroendocrinology*, *33*(2), 227–237.

Faravelli, C., Lo, S. C., Godini L., Lelli, L., Benni, L., Pietrini, F., Lazzeretti, L., Talamba, G. A., Fioravanti, G., Ricca, V. (2012). Childhood stressful events, HPA axis and anxiety disorders. *World J. Psychiatry*, *2*(1), 13-25

Felitti, V. J., Anda, R. F., Nordenberg, D., Williamson, D. F., Spitz, A. M., Edwards, V., Koss, M. P., & Marks, J. S. (1998). Relationship of childhood abuse and household dysfunction to many of the leading causes of death in adults: the adverse childhood experiences (ACE) study. *Am. J. Prev. Med.*, *14*(4), 245–258.

Fergusson, D. M., Horwood, L. J., & Lynskey, M. T. (1996). Childhood sexual abuse and psychiatric disorder in young adulthood: II. psychiatric outcomes of childhood sexual abuse. *J. Am. Acad. Child Adolesc. Psychiatry*, *35*(10), 1365–1374.

Ferland, C. L., & Schrader, L. A. (2011). Cage mate separation in pair-housed male rats evokes an acute stress corticosterone response. *Neurosci. Lett.*, *489*(3), 154–158.

Fukaya, M., & Watanabe, M. (2000). Improved immunohistochemical detection of postsynaptically located PSD-95/SAP90 protein family by protease section pretreatment: a study in the adult mouse brain. *J. Comp. Neurol, 426*(4), 572-586.

Gambrill, A. C., & Barria, A. (2011). NMDA receptor subunit composition controls synaptogenesis and synapse stabilization. *Proc. Natl. Acad. Sci. U. S. A.*, *108*(14), 5855–5860.

Gallo, F. T., Katche, C., Morici, J. F., Medina, J. H., & Weisstaub, N. V. (2018). Immediate early genes, memory and psychiatric disorders: Focus on c-Fos, Egr1 and Arc. *Front. Behav. Neurosci. 12*(79), 1-16.

Geoffroy, M. C., Pinto Pereira, S., Li, L., & Power, C. (2016). Child neglect and maltreatment and childhood-to-adulthood cognition and mental health in a prospective birth cohort. *Am. Acad. Child Adolesc. Psychiatry*, *55*(1), 33-40.

Geschwind, D. H. (2008). Autism: many genes, common pathways? *Cell 135*(3), 391–395.

Gottfried, J. A., O'Doherty, J., & Dolan, R. J. (2003). Encoding predictive reward value in human amygdala and orbitofrontal cortex. *Science*, *301*(5636), 1104–1107.

Gray, N. W., Weimer, R. M., Bureau, I., Svoboda, K. (2006). Rapid redistribution of synaptic PSD-95 in the neocortex in vivo. *PLoS. Biol., 4*(11), 2066- 2075.

Grippo, A. J., Gerena, D., Huang, J., Kumar, N., Shah, M., Ughreja, R., & Sue Carter, C. (2007). Social isolation induces behavioral and neuroendocrine disturbances relevant to depression in female and male prairie voles. *Psychoneuroendocrinology*, *32*(8–10), 966–980.

Gross, G. G., Junge, J. A., Mora, R. J., Kwon, H. B., Olson, C. A., Takahashi, T. T., Liman, E. R., Ellis-Davies, G. C., McGee, A. W., Sabatini, B. L., Roberts, R. W., Arnold, D. B. (2013). Recombinant probes for visualizing endogenous synaptic proteins in living neurons. *Neuron*, *78*(6), 971-85.

Hama, H., Hioki, H., Namiki, K., Hoshida, T., Kurokawa, H., Ishidate, F., Kaneko, T., Akagi, T., Saito, T., Saido, T., & Miyawaki, A. (2015). ScaleS: An optical clearing palette for

biological imaging. *Nat. Neurosci.*, *18*(10), 1518–1529.

Hawkley, L. C., Cole, S. W., Capitanio, J. P., Norman, G. J., & Cacioppo, J. T. (2012). Effects of social isolation on glucocorticoid regulation in social mammals. *Horm. Behav., 62*(3), 314–323.

Herdegen, T., & Leah, J. D. (1998). Inducible and constitutive transcription factors in the mammalian nervous system: control of gene expression by Jun, Fos and Krox, and CREB/ATF proteins. *Brain Res. Brain Res. Rev., 28*(3), 370–490.

Hermes, G. L., Rosenthal, L., Montag, A., & McClintock, M. K. (2006). Social isolation and the inflammatory response: sex differences in the enduring effects of a prior stressor. *Am. J. Physiol. Regul. Integr. Comp. Physiol.*, *290*(2), R273-R282.

Holehonnur, R., Phensy, A. J., Kim, L. J., Milivojevic, M., Vuong, D., Daison, D. K., Alex, S., Tiner, M., Jones, L. E., Kroener, S., Ploski, J. E. (2016). Increasing the GluN2A/GluN2B ratio in neurons of the mouse basal and lateral amygdala inhibits the modification of an existing fear memory trace. *J. Neurosci., 36*(36), 9490-504.

Holtmaat, A. J. G. D., Trachtenberg, J. T., Wilbrecht, L., Shepherd, G. M., Zhang, X., Knott, G. W., & Svoboda, K. (2005). Transient and persistent dendritic spines in the neocortex in vivo. *Neuron*, *45*(2), 279–291.

Holtmaat, A. J. G. D., & Svoboda, K. (2009). Experience-dependent structural synaptic

plasticity in the mammalian brain. *Nat. Rev. Neurosci.*, *10*(9), 647–658.

Horii-Hayashi, N., Sasagawa, T., Matsunaga, W., Matsusue, Y., Azuma, C., & Nishi, M. (2013). Developmental Changes in Desensitisation of c-Fos Expression Induced by Repeated Maternal Separation in Pre-Weaned Mice. *J. Neuroendocrinol.*, *25*(2), 158–167.

Huguet, G., Ey, E., & Bourgeron, T. (2013). The genetic landscapes of autism spectrum disorders. *Annu. Rev. Genomics Hum. Genet., 14*, 191–213

Insel, T., & Fernald, R. (2004). How the brain processes social information: searching for the social brain. *Annu. Rev. Neurosci.*, *27*, 697–722.

Isshiki, M., Tanaka, S., Kuriu, T., Tabuchi, K., Takumi, T., & Okabe, S. (2014). Enhanced synapse remodelling as a common phenotype in mouse models of autism. *Nat. Commun.*, *5*(4742), 1-15.

Jacobson, L. (2005). Hypothalamic-pituitary-adrenocortical axis regulation. *Endocrinol. Metab. Clin. North Am., 34*(2), 271–292.

Jiang, M., Ash, R. T., Baker, S. A., Suter, B., Ferguson, A., Park, J., Rudy, J., Torsky, S. P., Chao, H. T., Zoghbi, H. Y., & Smirnakis, S. M. (2013). Dendritic arborization and spine dynamics are abnormal in the mouse model of MECP2 duplication syndrome. *J. Neurosci.*, *33*(50), 19518–19533.

Kaczmarek, L. , N. E. (1990). C-fos protooncogene expression and neuronal plasticity. *Acta. Neurobiol. Exp*. *50*(4-5),173-179

Kanitz, E., Tuchscherer, M., Puppe, B., Tuchscherer, A., & Stabenow, B. (2004). Consequences of repeated early isolation in domestic piglets (Sus scrofa) on their behavioural, neuroendocrine, and immunological responses. *Brain Behav. Immun.*, *18*(1), 35–45.

Kenny, E. M., Cormican, P., Furlong, S., Heron, E., Kenny, G., Fahey, C., Kelleher, E., Ennis, S., Tropea, D., Anney, R., Corvin, A. P., Donohoe, G., Gallagher, L., Gill, M., & Morris, D. W. (2014). Excess of rare novel loss-of-function variants in synaptic genes in schizophrenia and autism spectrum disorders. *Mol. Psychiatry*, *19*(8), 872–879.

Kim, J., Zhang, X., Muralidhar, S., LeBlanc, S. A., & Tonegawa, S. (2017). Basolateral to central amygdala neural circuits for article basolateral to central amygdala neural circuits for appetitive behaviors. *Neuron*, *93*(6), 1464-1479.

Kiyokawa, Y. (2017). Social odors: alarm pheromones and social buffering. *Curr. Top. Behav. Neurosci.*, 30, 47–65.

Kiyokawa, Y., & Hennessy, M. B. (2018). Comparative studies of social buffering: a consideration of approaches, terminology, and pitfalls. *Neurosci. Biobehav. Rev.*, 86, 131–141.

Knapska, E., & Kaczmarek, L. (2004). A gene for neuronal plasticity in the mammalian brain: Zif268/Egr-1/NGFI-A/ Krox-24/TIS8/ZENK? *Prog. Neurobiol.*, *74*(4), 183–211.

Kovács, L. Á., Schiessl, J. A., Nafz, A. E., Csernus, V., & Gaszner, B. (2018). Both basal and acute restraint stress-induced c-Fos expression is influenced by age in the extended amygdala and brainstem stress centers in male rats. *Front. Aging Neurosci. 10*(248), 1-20.

Krout, K. E., Jansen, A. S. P., & Loewy, A. D. (1998). Periaqueductal gray matter projection to the parabrachial nucleus in rat. *J. Comp. Neurol.*, *401*(4), 437–454.

Kubik, S., Miyashita, T., & Guzowski, J. F. (2007). Using immediate-early genes to map hippocampal subregional functions. *Learn. Mem., 14*(11), 758–770.

Lanahan, A., & Worley, P. (1998). Immediate-early genes and synaptic function. *Neurobiology of Learning and Memory*, *70*(1–2), 37–43.

Lebow, M. A., & Chen, A. (2016). Overshadowed by the amygdala: The bed nucleus of the stria terminalis emerges as key to psychiatric disorders. *Molecular Psychiatry*, *21*(4), 450–463.

Liston, C., & Gan, W. B. (2011). Glucocorticoids are critical regulators of dendritic spine development and plasticity in vivo. *Proc. Natl. Acad. Sci. U. S. A.*, *108*(38), 16074–16079.

Liu, R. J., & Aghajanian, G. K. (2008). Stress blunts serotonin- and hypocretin-evoked EPSCs in prefrontal cortex: Role of corticosterone-mediated apical dendritic atrophy. *Proc. Natl. Acad. Sci. U. S. A.*, *105*(1), 359–364.

López de Armentia, M., Sah, P. (2007). Bidirectional synaptic plasticity at nociceptive afferents in the rat central amygdala. *J. Physiol.*, 581(3), 961–970.

Maguire, S. A., Williams, B., Naughton, A. M., Cowley, L. E., Tempest, V., Mann, M. K., Teague, M., & Kemp, A. M. (2015). A systematic review of the emotional, behavioural and cognitive features exhibited by school-aged children experiencing neglect or emotional abuse. *Child Care Health Dev., 41*(5), 641–653.

Makinodan, M., Rosen, K. M., Ito, S., & Corfas, G. (2012). A critical period for social experience-dependent oligodendrocyte maturation and myelination. *Science*, *337*(6100), 1357–1360.

Masson, M., East-Richard, C., & Cellard, C. (2016). A meta-analysis on the impact of psychiatric disorders and maltreatment on cognition. *Neuropsychology*, *30*(2), 143–156.

Maviel, T., Durkin, T. P., Menzaghi, F., & Bontempi, B. (2004). Sites of neocortical reorganization critical for remote spatial memory. *Science*, *305*(5680), 96–99.

McGee, A. W., Dakoji, S. R., Olsen, O., Bredt, D. S., Lim, W. A., Prehoda, K. E. (2001) Structure of the SH3-guanylate kinase module from PSD-95 suggests a mechanism for

regulated assembly of MAGUK scaffolding proteins. *Mol. Cell.*, 8(6), 1291–1301.

Meyer, J. (1983). Early adrenalectomy stimulates subsequent growth and development of the rat brain. *Exp. Neurol.*, *82*(2), 432–446.

Mikami, K., Kiyokawa, Y., Ishii, A., & Takeuchi, Y. (2020). Social buffering enhances extinction of conditioned fear responses by reducing corticosterone levels in male rats. *Horm. Behav., 118*(104654), 1-7.

Minatohara, K., Akiyoshi, M., & Okuno, H. (2016). Role of immediate-early genes in synaptic plasticity and neuronal ensembles underlying the memory trace. *Front. Mol. Neurosci.*, *8*(78), 1-11.

Miwa, H., Fukaya, M., Watabe, A. M., Watanabe, M., & Manabe, T. (2008). Functional contributions of synaptically localized NR2B subunits of the NMDA receptor to synaptic transmission and long-term potentiation in the adult mouse CNS. *J. Physiol., 586*(10), 2539–2550.

Miyazaki, T., Kunii, M., Tada, H., Sano, A., Kuroiwa, Y., Goto, T., Malinow, R., & Takahashi, T. (2012). Developmental AMPA receptor subunit specificity during experience-driven synaptic plasticity in the rat barrel cortex. *Brain Res.*, *1435*, 1–7.

Miyazawa, Y., Takahashi, Y., Watabe, A. M., & Kato, F. (2018). Predominant synaptic potentiation and activation in the right central amygdala are independent of bilateral

parabrachial activation in the hemilateral trigeminal inflammatory pain model of rats. *Mol. Pain*, *14*, 1-21.

Mora-Gallegos, A., & Fornaguera, J. (2019). The effects of environmental enrichment and social isolation and their reversion on anxiety and fear conditioning. *Behav. Processes*, *158*, 59–69.

Nagai, Y., Miyakawa, N., Takuwa, H., Hori, Y., Oyama, K., Ji, B., Takahashi, M., Huang, X. P., Slocum, S. T., DiBerto, J. F., Xiong, Y., Urushihata, T., Hirabayashi, T., Fujimoto, A., Mimura, K., English, J. G., Liu, J., Inoue, K. I., Kumata, K., … Minamimoto, T. (2020). Deschloroclozapine, a potent and selective chemogenetic actuator enables rapid neuronal and behavioral modulations in mice and monkeys. *Nat. Neurosci.*, *9*, 1157-1167.

Nagaoka, A., Takehara, H., Hayashi-Takagi, A., Noguchi, J., Ishii, K., Shirai, F., Yagishita, S., Akagi, T., Ichiki, T., & Kasai, H. (2016). Abnormal intrinsic dynamics of dendritic spines in a fragile X syndrome mouse model in vivo. *Sci. Rep.*, *6*(26651), 1-11.

Navratilova, E., Atcherley, C. W., & Porreca, F. (2015). Brain circuits encoding reward from pain relief. *Trends Neurosci., 38*(11), 741–750.

Nishi, M., Horii-Hayashi, N., & Sasagawa, T. (2014). Effects of early life adverse experiences on the brain: Implications from maternal separation models in rodents.

Front. Neurosci., *8*(166), 1-6.

Okabe, S., Miwa, A., & Okado, H. (2001). Spine formation and correlated assembly of presynaptic and postsynaptic molecules. *J. Neurosci.*, *21*(16), 6105–6114.

Okabe, S. (2007). Molecular anatomy of the postsynaptic density. *Mol. Cell Neurosci. 34*(4), 503-518.

O'Roak, B. J., Deriziotis, P., Lee, C., Vives, L., Schwartz, J. J., Girirajan, S., Karakoc, E., MacKenzie, A. P., Ng, S. B., Baker, C., Rieder, M. J., Nickerson, D. A., Bernier, R., Fisher, S. E., Shendure, J., & Eichler, E. E. (2011). Exome sequencing in sporadic autism spectrum disorders identifies severe de novo mutations. *Nat. Genet., 43*(6), 585–589.

O'Roak, B. J., Vives, L., Fu, W., Egertson, J. D., Stanaway, I. B., Phelps, I. G., Carvill, G., Kumar, A., Lee, C., Ankenman, K., Munson, J., Hiatt, J. B., Turner, E. H., Levy, R., O'Day, D. R., Krumm, N., Coe, B. P., Martin, B. K., Borenstein, E., … Shendure, J. (2012). Multiplex targeted sequencing identifies recurrently mutated genes in autism spectrum disorders. *Science*, *338*(6114), 1619–1622.

Palmiter, R. D. (2018). The parabrachial nucleus: CGRP neurons function as a general alarm. *Trends Neurosci.*, *41*(5), 280–293.

Pan, F., Aldridge, G. M., Greenough, W. T., & Gan, W. B. (2010). Dendritic spine instability

and insensitivity to modulation by sensory experience in a mouse model of fragile X syndrome. *Proc. Natl. Acad. Sci. U. S. A., 107*(41), 17768–17773.

Paoletti, P., & Neyton, J. (2007). NMDA receptor subunits: function and pharmacology. *Curr. Opin. Pharmacol.*, *7*(1), 39–47.

Pasciuto, E., Borrie, S. C., Kanellopoulos, A. K., Santos, A. R., Cappuyns, E., D'Andrea, L., Pacini, L., & Bagni, C. (2015). Autism Spectrum Disorders: Translating human deficits into mouse behavior. *Neurobiol. Learn. Mem., 124*, 71–87.

Pennypacker, K. R. (1995). AP-1 transcription factor complexes in CNS disorders and development. *J. Fla. Med. Assoc., 82*(8), 551–554.

Perelló, M., Chacon, F., Cardinali, D. P., Esquifino, A. I., & Spinedi, E. (2006). Effect of social isolation on 24-h pattern of stress hormones and leptin in rats. *Life Sci.*, *78*(16), 1857–1862.

Pezze, M., McGarrity, S., Mason, R., Fone, K. C., & Bast, T. (2014). Too little and too much: Hypoactivation and disinhibition of medial prefrontal cortex cause attentional deficits. *J. Neurosci.*, *34*(23), 7931–7946.

Platt, B., Kadosh, K. C., & Lau, J. Y. F. (2013). The role of peer rejection in adolescent depression. *Depress. Anxiety, 30*(9), 809-821

Pournajafi-Nazarloo, H., Partoo, L., Sanzenbacher, L., Paredes, J., Hashimoto, K., Azizi, F.,

& Sue Carter, C. (2009). Stress differentially modulates mRNA expression for corticotrophin-releasing hormone receptors in hypothalamus, hippocampus and pituitary of prairie voles. *Neuropeptides*, *43*(2), 113–123.

Pournajafi-Nazarloo, H., Partoo, L., Yee, J., Stevenson, J., Sanzenbacher, L., Kenkel, W., Mohsenpour, S. R., Hashimoto, K., & Carter, C. S. (2011). Effects of social isolation on mRNA expression for corticotrophin-releasing hormone receptors in prairie voles. *Psychoneuroendocrinology*, *36*(6), 780–789.

Qiu, M. H., Chen, M. C., Fuller, P. M., & Lu, J. (2016). Stimulation of the Pontine Parabrachial Nucleus Promotes Wakefulness via Extra-thalamic Forebrain Circuit Nodes. *Curr. Biol.*, *26*(17), 2301–2312.

Reul, J. M. H. M., & de Kloet, E. R. (1985). Two receptor systems for corticosterone in rat brain: Microdistribution and differential occupation. *Endocrinology*, *117*(6), 2505–2511.

Roth, B. L. (2016). DREADDs for Neuroscientists. *Neuron*, *89*(4), 683–694.

Ruscio, M. G., Sweeny, T., Hazelton, J., Suppatkul, P., & Sue Carter, C. (2007). Social environment regulates corticotropin releasing factor, corticosterone and vasopressin in juvenile prairie voles. *Horm. Behav.*, *51*(1), 54–61.

Ryan, P. J., Ross, S. I., Campos, C. A., Derkach, V. A., & Palmiter, R. D. (2017). Oxytocin-receptor-expressing neurons in the parabrachial nucleus regulate fluid intake. *Nat.*

Neurosci., *20*(12), 1722–1733.

Sans, N., Petralia, R. S., Wang, Y. X., Blahos, J., Hell, J. W., & Wenthold, R. J. (2000). A developmental change in NMDA receptor-associated proteins at hippocampal synapses. *J. Neurosci.*, *20*(3), 1260–1271.

Sapolsky, R. M., McEwen, B. S., & Rainbow, T. C. (1983). Quantitative autoradiography of [3H]corticosterone receptors in rat brain. *Brain Research*, *271*(2), 331–334.

Sato, M., Ito, M., Nagase, M., Sugimura, Y. K., Takahashi, Y., Watabe, A. M., & Kato, F. (2015). The lateral parabrachial nucleus is actively involved in the acquisition of fear memory in mice. *Mol. Brain*, *8*(22), 1-15.

Scaccianoce, S., del Bianco, P., Paolone, G., Caprioli, D., Modafferi, A. M. E., Nencini, P., & Badiani, A. (2006). Social isolation selectively reduces hippocampal brain-derived neurotrophic factor without altering plasma corticosterone. *Behav. Brain Res.*, *168*(2), 323–325.

Serra, M., Pisu, M. G., Floris, I., & Biggio, G. (2005). Social isolation-induced changes in the hypothalamic-pituitary-adrenal axis in the rat. *Stress*, *8*(4), 259–264.

Serra, M., Sanna, E., Mostallino, M. C., & Biggio, G. (2007). Social isolation stress and neuroactive steroids. *Eur. Neuropsychopharmacol.*, *17*(1), 1–11.

Sheng, H. Z., Lin, P. X., & Nelson, P. G. (1995). Combinatorial expression of immediate

early genes in single neurons. *Brain. Res. Mol. Brain. Res.*, *30*(2), 196–202.

Silva-Gómez, A. B., Rojas, D., Juárez, I., & Flores, G. (2003). Decreased dendritic spine density on prefrontal cortical and hippocampal pyramidal neurons in postweaning social isolation rats. *Brain Res.*, *983*(1–2), 128–136.

Stowe, J. R., Liu, Y., Curtis, J. T., Freeman, M. E., & Wang, Z. (2005). Species differences in anxiety-related responses in male prairie and meadow voles: The effects of social isolation. *Physiol. Behav.*, *86*(3), 369–378.

Stratakis, C. A., & Chrousos, G. P. (1995). Neuroendocrinology and Pathophysiology of the Stress System. *Ann. N. Y. Acad. Sci.*, *771*(1), 1–18.

Sun, L., Liu, R., Guo, F., Wen, M. qing, Ma, X. lin, Li, K. yuan, Sun, H., Xu, C. lin, Li, Y. yuan, Wu, M. yin, Zhu, Z. gang, Li, X. jian, Yu, Y. qin, Chen, Z., Li, X. yao, & Duan, S. (2020). Parabrachial nucleus circuit governs neuropathic pain-like behavior. *Nat. Commun.*, *11*(1), 5974, 1-21.

Tada, H., Miyazaki, T., Takemoto, K., Jitsuki, S., Nakajima, W., Koide, M., Yamamoto, N., Taguchi, A., Kawai, H., Komiya, K., Suyama, K., Abe, H., Sano, A., & Takahashi, T. (2017). Social isolation suppresses actin dynamics and synaptic plasticity through ADF/cofilin inactivation in the developing rat barrel cortex. *Sci. Rep.*, *7*(1), 8471, 1-10.

Tada, H., Miyazaki, T., Takemoto, K., Takase, K., Jitsuki, S., Nakajima, W., Koide, M.,

Yamamoto, N., Komiya, K., Suyama, K., Sano, A., Taguchi, A., & Takahashi, T. (2016). Neonatal isolation augments Social dominance by altering actin dynamics in the medial prefrontal cortex. *Proc. Natl. Acad. Sci. U. S. A.*, *113*(45), 7097–7105.

Takatsuru, Y., Yoshitomo, M., Nemoto, T., Eto, K., & Nabekura, J. (2009). Maternal separation decreases the stability of mushroom spines in adult mice somatosensory cortex. *Brain Res.*, *1294*, 45–51.

Tanimizu, T., Kenney, J. W., Okano, E., Kadoma, K., Frankland, P. W., & Kida, S. (2017). Functional connectivity of multiple brain regions required for the consolidation of social recognition memory. *J. Neurosci.*, *37*(15), 4103–4116.

Tarabeux, J., Kebir, O., Gauthier, J., Hamdan, F. F., Xiong, L., Piton, A., Spiegelman, D., Henrion, Millet, B., Fathalli, F., Joober, R., Rapoport, J. L., Delisi, L. E., Fombonne, E., Mottron, L., Forget-Dubois, N., Boivin, M., Michaud, J. L., Drapeau, P., … Krebs, M. O. (2011). Rare mutations in N-methyl-D-aspartate glutamate receptors in autism spectrum disorders and schizophrenia. *Transl. Psychiatry*, *1*(11), e55, 1-7.

Tischmeyer, W., Kaczmarek, L., Strauss, M., Jork, R., & Matthies, H. (1990). Accumulation of c-fos mRNA in rat hippocampus during acquisition of a brightness discrimination. *Behav. Neural. Biol., 54*(2), 165–171.

Toth, M., Mikics, E., Tulogdi, A., Aliczki, M., & Haller, J. (2011). Post-weaning social

isolation induces abnormal forms of aggression in conjunction with increased glucocorticoid and autonomic stress responses. *Horm. Behav.*, *60*(1), 28–36.

Tye, K. M., Prakash, R., Kim, S. Y., Fenno, L. E., Grosenick, L., Zarabi, H., Thompson, K. R., Gradinaru, V., Ramakrishnan, C., & Deisseroth, K. (2011). Amygdala circuitry mediating reversible and bidirectional control of anxiety. *Nature*, *471*, 358–362.

Urbano, M., Okwara, L., Manser, P., Hartmann, K., Herndon, A., & Deutsch, S. I. (2014). A trial of D-cycloserine to treat stereotypies in older adolescents and young adults with autism spectrum disorder. *Clin. Neuropharmacol.*, *37*(3), 69–72.

van Bodegom, M., Homberg, J. R., & Henckens, M. J. A. G. (2017). Modulation of the hypothalamic-pituitary-adrenal axis by early life stress exposure. *Front. Cell Neurosci.*, *11*(87), 1-33.

Vazdarjanova, A., & Mcgaugh, J. L. (1998). Basolateral amygdala is not critical for cognitive memory of contextual fear conditioning. *Proc Natl Acad Sci U. S. A.*., *95*(25), 15003-15007.

Wang, Y. C., Ho, U. C., Ko, M. C., Liao, C. C., & Lee, L. J. (2012). Differential neuronal changes in medial prefrontal cortex, basolateral amygdala and nucleus accumbens after postweaning social isolation. *Brain Struct. Funct.*, *217*(2), 337–351.

Watabe, A. M., Ochiai, T., Nagase, M., Takahashi, Y., Sato, M., & Kato, F. (2013). Synaptic

potentiation in the nociceptive amygdala following fear learning in mice. *Mol. Brain*, *6*(11), 1-14.

Weintraub, A., Singaravelu, J., & Bhatnagar, S. (2010). Enduring and sex-specific effects of adolescent social isolation in rats on adult stress reactivity. *Brain Res.*, *1343*, 83–92.

Weiss, I. C., Pryce, C. R., Jongen-Rêlo, A. L., Nanz-Bahr, N. I., & Feldon, J. (2004). Effect of social isolation on stress-related behavioural and neuroendocrine state in the rat. *Behav. Brain Res.*, *152*(2), 279–295.

Xu, H. T., Pan, F., Yang, G., & Gan, W. B. (2007). Choice of cranial window type for in vivo imaging affects dendritic spine turnover in the cortex. *Nat. Neurosci.*, *10*(5), 549–551.

Yamamuro, K., Yoshino, H., Ogawa, Y., Makinodan, M., Toritsuka, M., Yamashita, M., Corfas, G., & Kishimoto, T. (2018). Social isolation during the critical period reduces synaptic and intrinsic excitability of a subtype of pyramidal cell in mouse prefrontal cortex. *Cereb. Cortex, 28*(3), 998–1010.

Yoo, H. J., Cho, I. H., Park, M., Yang, S. Y., & Kim, S. A. (2012). Family based association of GRIN2A and GRIN2B with Korean autism spectrum disorders. *Neurosci. Lett.*, *512*(2), 89–93.

Yoshida, A., Dostrovsky, J. O., Sessle, B. J., & Chiang, C. Y. (1991). Trigeminal projections to the nucleus submedius of the thalamus in the rat. *J. Comp. Neurol.*, *307*(4), 609–625.

Yuen, E. Y., Wei, J., Liu, W., Zhong, P., Li, X., & Yan, Z. (2012). Repeated stress causes cognitive impairment by suppressing glutamate receptor expression and function in prefrontal cortex. *Neuron*, *73*(5), 962–977.

Zelikowsky, M., Hui, M., Karigo, T., Choe, A., Yang, B., Blanco, M. R., Beadle, K., Gradinaru, V., Deverman, B. E., & Anderson, D. J. (2018). The neuropeptide Tac2 controls a distributed brain state induced by chronic social isolation stress. *Cell*, *173*(5), 1265-1279.

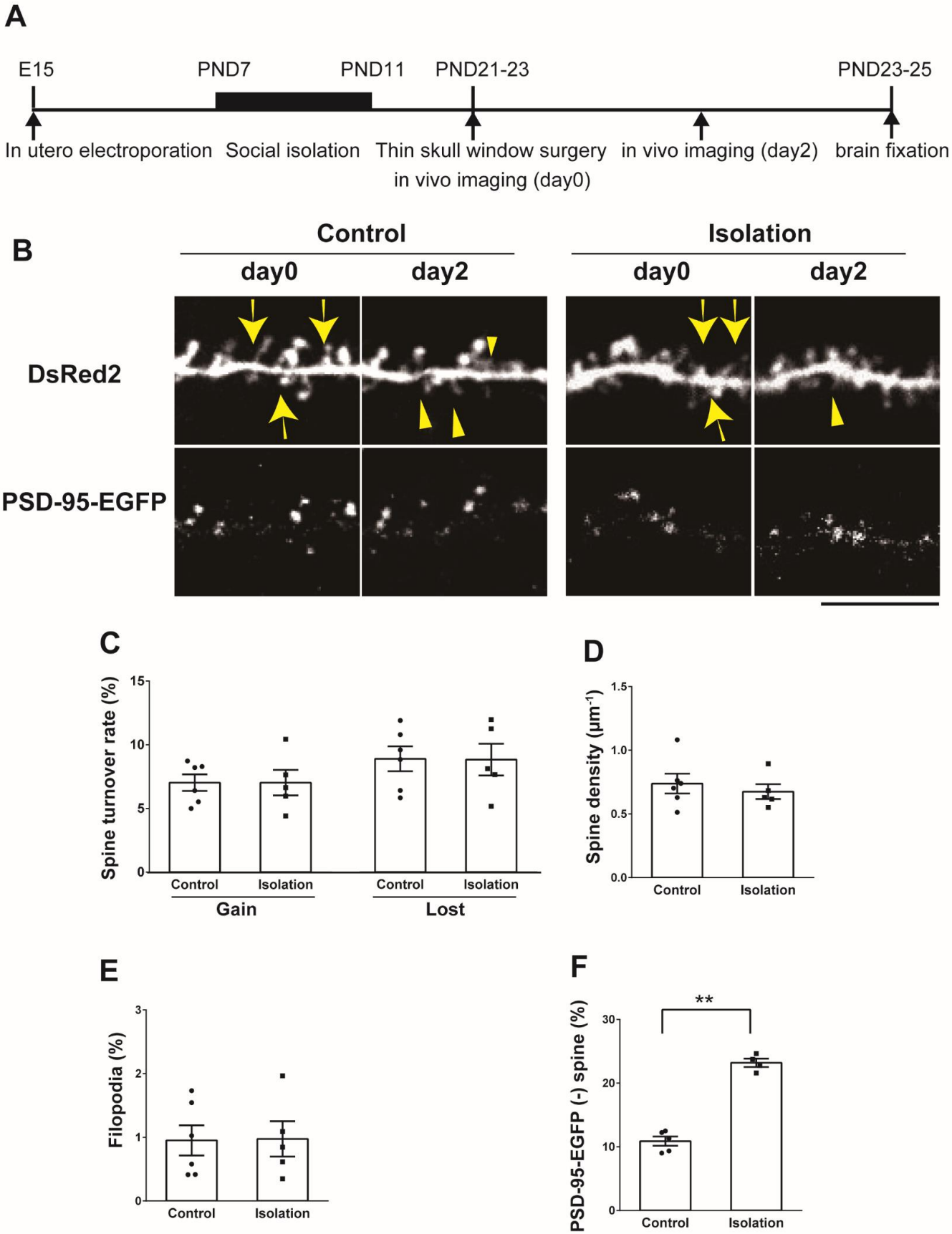

Figure 1

Figure legend was shown in next page.

Figure 1. in vivo spine dynamics PSD-95-EGFP expression in juvenile socially isolated mice SSC the layer 2/3 pyramidal neurons

(A) Timeline of in utero electroporation, social isolation, thin skull window surgery, in vivo imaging, brain fixation.

(B) In vivo imaging of dendrites expressing DsRed2 and PSD-95-EGFP in control mice (Control) and socially isolated mice (Isolation). Arrowheads and arrows point gained spines and lost spines.

(C - F) The spine turnover rate (C), spine density (D), the fraction of filopodia (E) and the fraction of spines without PSD-95-EGFP clusters (F) in control mice (Control) and socially isolated mice (Isolation) analyzed in in vivo imaging. ((C, D, E); Control n = 6 (mice), Isolation n = 5 (mice), (F); Control n = 5 (mice), Isolation n = 4 (mice))

Data are presented as mean ± s. e. m. ** $p < 0.01$, unpaired Student's *t*-test scale bar 10 μm (B).

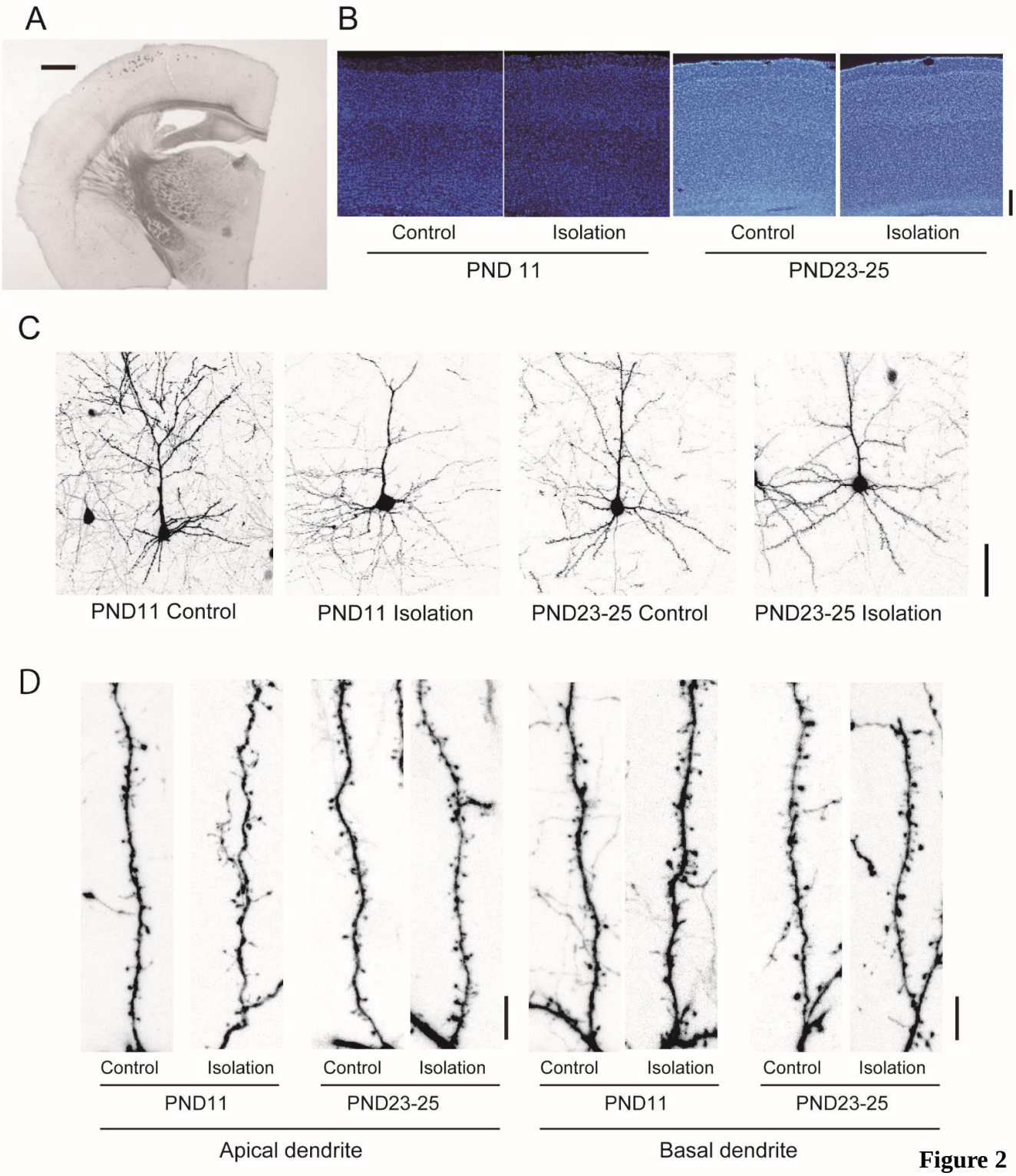

Figure 2

Figure 2. Images of SSC layer 2/3 pyramidal neurons of socially isolated mice fixed slice

(A) Image of layer 2/3 pyramidal neurons expressing DsRed2 in the somatosensory cortex (SSC) of PND23-25 control mice.
(B) The cortical regions in fixed brain slices of were stained by Hoechst dye for nuclear staining.
(C) Images of dendritic arborization in the layer 2/3 neuron expressing DsRed2 in the SSC.
(D) Higher magnification images of apical and basal dendrites with different experimental conditions were shown.
PND11 control mice (PND11 Control), PND11 socially isolated mice (PND11 Isolation), PND23-25 control mice (PND23-25 Control), and PND23–25 socially isolated mice (PND23–25 Isolation)
Each image was a maximal intensity projection made from Z stuck Images by ImageJ.
Scale bars; 100 μm (A), 200 μm (B), 50 μm (C) and 10 μm (D).

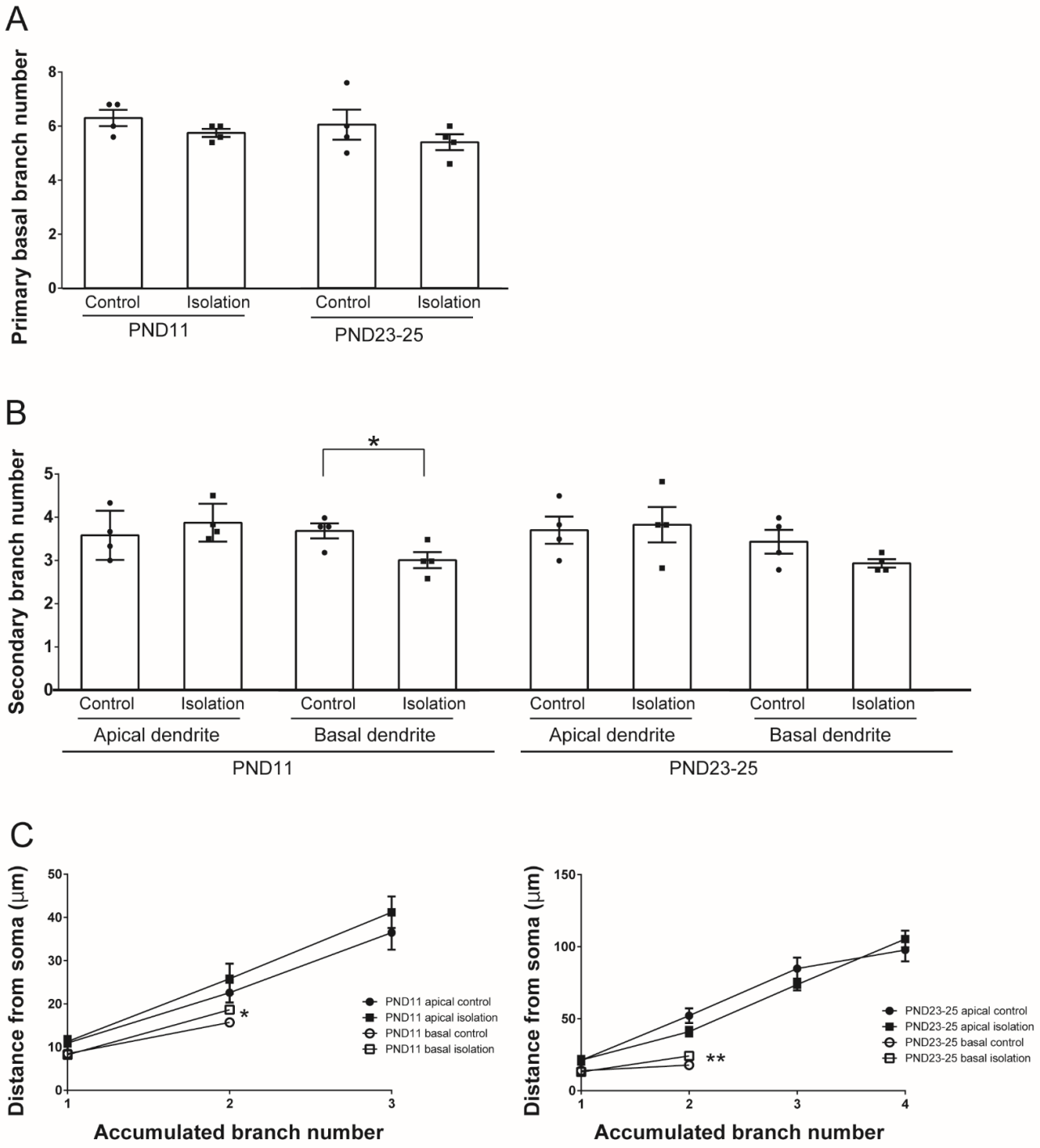

Figure 3

Figure legend was shown in next page.

Figure 3. The morphological analysis of dendrite branching in the SSC layer 2/3 pyramidal neurons after juvenile social isolation

(A) The numbers of primary branches in the basal dendrites with different experimental conditions. (PND11 control mice (PND11 Control) cell n = 20, mice n = 4; PND11 socially isolated mice (PND11 Isolation) cell n = 20, mice n = 4; PND23-25 control mice (PND23-25 Control) cell n = 20, mice n = 4; PND23-25 socially isolated mice (PND23-25 Isolation) cell n = 20, mice n = 4)
(B) The numbers of secondary branches of the secondary apical dendrites and secondary basal dendrites with different experimental conditions. (secondary apical dendrites; PND11 control mice (PND11 Control) cell n = 24, mice n = 4; PND11 socially isolated mice (PND11 Isolation) cell n = 24, mice n = 4; PND23-25 control mice (PND 23-25 Control) cell n = 24, mice n = 4; PND23-25 socially isolated mice (PND23-25 Isolation) cell n = 24, mice n = 4; secondary basal dendrites; PND11 control mice (PND11 Control) cell n = 20, mice n = 4; PND11 socially isolated mice (PND11 Isolation) cell n = 20, mice n = 4; PND23-25 control mice (PND23-25 Control) cell n = 20, mice n = 4; PND23-25 socially isolated mice (PND23-25 Isolation) cell n = 20, mice n = 4)
(C) The distance from soma to the branching positions of the secondary apical dendrites and the secondary basal dendrites. The two (basal dendrites), three (apical dendrites at PND11) or four (apical dendrites at PND23-25) successive branch points from the soma were selected at PND11 and PND23-25. All branching positions were counted manually. (secondary apical dendrites; PND11 control mice (PND11 Control) cell n = 24, mice n = 4; PND11 socially isolated mice (PND11 Isolation) cell n = 24, mice n = 4; PND23-25 control mice (PND23-25 Control) cell n = 24, mice n = 4; PND23-25 socially isolated mice (PND23-25 Isolation) cell n = 24, mice n = 4; secondary basal dendrites accumulated branching number 1; PND11 control mice (PND11 Control) cell n = 20, mice n = 4; PND11 socially isolated mice (PND11 Isolation) cell n = 20, mice n = 4; PND23-25 control mice (PND23-25 Control) cell n = 20, mice n = 4; PND23-25 socially isolated mice (PND23-25 Isolation) cell n = 20, mice n = 4; secondary basal dendrites accumulated branching number 2; PND11 control mice (PND11 Control) cell n = 11, mice n = 4; PND11 socially isolated mice (PND11 Isolation) cell n = 12, mice n = 4; PND23-25 control mice (PND23-25 Control) cell n = 13, mice n = 4; PND23-25 socially isolated mice (PND23-25 Isolation) cell n = 15, mice n = 4)
Data are presented as mean ± s. e. m. *$p < 0.05$, **$p < 0.01$, unpaired Student's t-test.

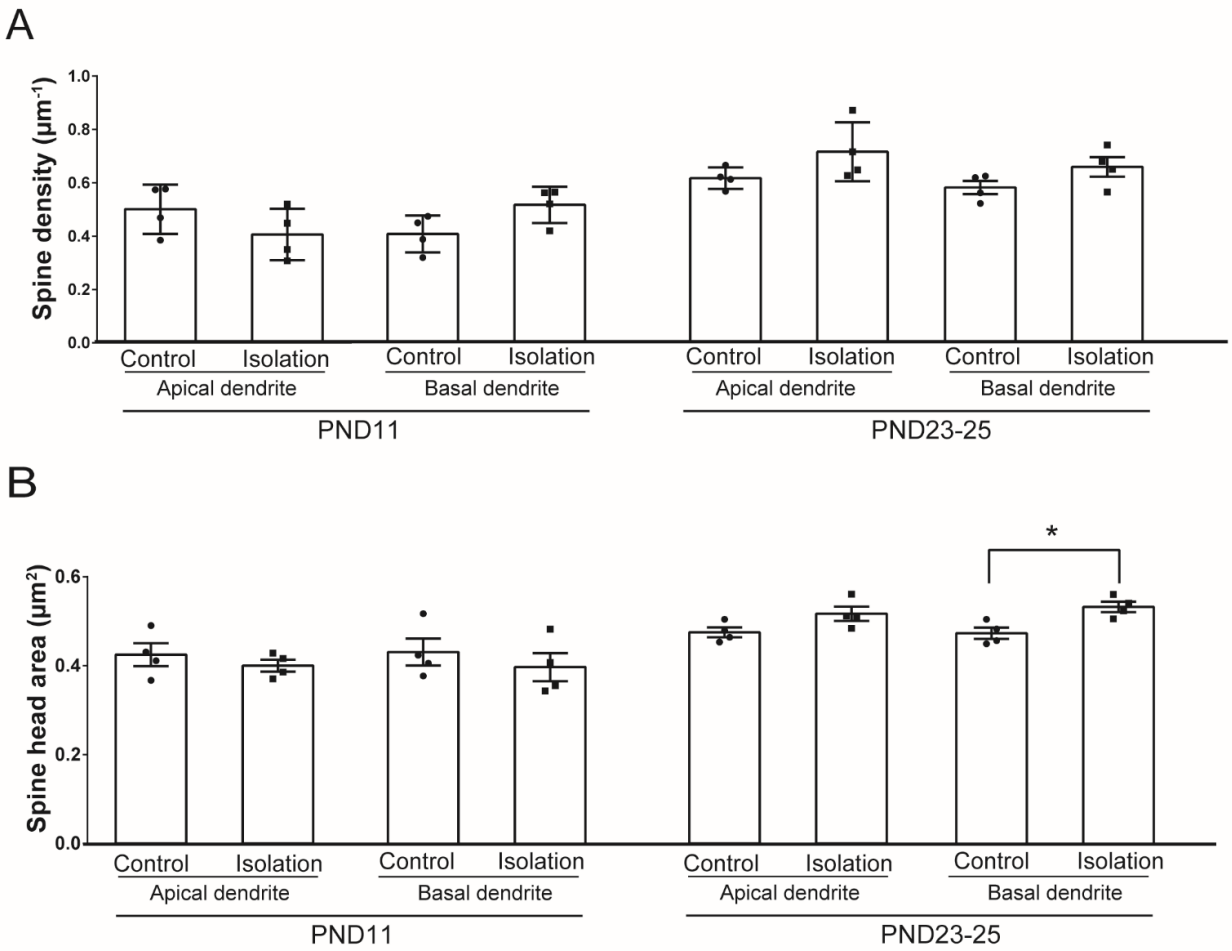

Figure 4. The morphological analysis of dendritic spine in the SSC layer 2/3 pyramidal neurons after juvenile social isolation

(A) Spine densities in the secondary apical dendrites and secondary basal dendrites of the layer 2/3 pyramidal neurons in the SSC with different experimental conditions. (PND11 control mice (PND11 Control) cell n = 20, mice n = 4; PND11 socially isolated mice (PND11 Isolation) cell n = 20, mice n = 4; PND23-25 control mice (PND23-25 Control) cell n = 20, mice n = 4; PND23-25 socially isolated mice (PND23-25 Isolation) cell n = 20, mice n = 4)
(B) The spine head areas on the secondary apical dendrites and secondary basal dendrites of the layer 2/3 pyramidal neurons in the SSC with different experimental conditions. The average spine head sizes from each mouse were plotted and used for the analysis. (PND11 apical dendrite control mice (PND11 Control) spine n = 522, mice n = 4; socially isolated mice (PND11 Isolation) spine n = 346, mice n = 4; PND11 basal dendrite control mice (PND11 Control) spine n = 488, mice n = 4; socially isolated mice (PND11 Isolation) spine n = 514, mice n = 4; PND23-25 apical dendrite control mice (PND23-25 Control) spine n = 543, mice n = 4; socially isolated mice (PND23-25 Isolation) spine n = 618, mice n = 4; PND23-25 basal dendrite control mice (PND23-25 Control) spine n = 571, mice n = 4; socially isolated mice (PND23-25 Isolation) spine n = 611, mice n = 4))
Data are presented as mean ± s. e. m. *$p < 0.05$, unpaired Student's t-test .

Table 1 Number of cell, slice, mice used for analysis in Figure 3

	Control (Mean ± s. e. m.) (Cell / Slice / Animal)	Isolation (Mean ± s. e. m.) (Cell / Slice / Animal)	t Value (df)	P Value
Figure 3A; Primary basal branch number PND11	6.300 ± 0.300 (20 / 20 / 4)	5.750 ± 0.150 (20 / 20 / 4)	1.640 (6)	0.152
Figure 3A; Primary basal branch number PND23-25	6.050 ± 0.556 (20 / 20 / 4)	5.400 ± 0.294 (20 / 20 / 4)	1.033 (6)	0.341
Figure 3B; Secondary apical branch number PND11	3.583 ± 0.285 (24 / 16 / 4)	3.875 ± 0.219 (24 / 17 / 4)	0.812 (6)	0.448
Figure 3B; Secondary apical branch number PND23-25	3.708 ± 0.315 (24 / 15 / 4)	3.833 ± 0.408 (24 / 13 / 4)	0.243 (6)	0.816
Figure 3B; Secondary basal branch number PND11	3.700 ± 0.173 (20 / 16 / 4)	3.025 ± 0.184 (20 / 15 / 4)	2.669 (6)	0.037
Figure 3B; Secondary basal branch number PND23-25	3.450 ± 0.275 (20 / 17 / 4)	2.950 ± 0.096 (20 / 15 / 4)	1.715 (6)	0.137
Figure 3C; Secondary apical branch position PND11 Accumulated branch number 1	10.94 ± 1.621 (24 / 16 / 4)	11.30 ± 1.207 (24 / 17 / 4)	0.177 (6)	0.866
Figure 3C; Secondary apical branch position PND11 Accumulated branch number 2	22.60 ± 2.295 (24 / 16 / 4)	25.82 ± 3.472 (24 / 17 / 4)	0.773 (6)	0.469
Figure 3C; Secondary apical branch position PND11 Accumulated branch number 3	36.49 ± 3.946 (24 / 16 / 4)	41.20 ± 3.657 (24 / 17 / 4)	0.877 (6)	0.414
Figure 3C; Secondary basal branch position PND11 Accumulated branch number 1	8.476 ± 0.644 (20 / 16 / 4)	8.230 ± 0.338 (20 / 15 / 4)	0.338 (6)	0.747
Figure 3C; Secondary basal branch position PND11 Accumulated branch number 2	15.71 ± 0.321 (11 / 11 / 4)	18.65 ± 0.837 (12 / 12 / 4)	3.284 (6)	0.017
Figure 3C; Secondary apical branch position PND23-25 Accumulated branch number 1	21.13 ± 3.068 (24 / 15 / 4)	21.34 ± 1.802 (24 / 13 / 4)	0.059 (6)	0.955
Figure 3C; Secondary apical branch position PND23-25 Accumulated branch number 2	52.13 ± 5.108 (24 / 15 / 4)	41.00 ± 3.360 (24 / 13 / 4)	1.820 (6)	0.119
Figure 3C; Secondary apical branch position PND23-25 Accumulated branch number 3	84.86 ± 7.588 (24 / 15 / 4)	73.73 ± 4.026 (24 / 13 / 4)	1.296 (6)	0.243
Figure 3C; Secondary apical branch position PND23-25 Accumulated branch number 4	97.74 ± 7.911 (20 / 15 / 4)	105.3 ± 5.814 (20 / 13 / 4)	0.770 (6)	0.471
Figure 3C; Secondary basal branch position PND23-25 Accumulated branch number 1	13.97 ± 0.860 (20 / 17 / 4)	13.10 ± 1.477 (20/ 15 / 4)	0.509 (6)	0.629
Figure 3C; Secondary basal branch position PND23-25 Accumulated branch number 2	17.80 ± 1.184 (13 / 12 / 4)	24.20 ± 1.136 (15 / 14 / 4)	3.902 (6)	0.008

Unpaired student t-test

Table 1

Table 2 Number of cell, slice, mice and total dendrite length used for analysis in Figure 4

	Control (Mean ± s. e. m.) (Cell / Slice / Animal)	Isolation (Mean ± s. e. m.) (Cell / Slice / Animal)	t Value (df)	P Value
Figure 4A; Apical spine density PND11 (μm^{-1})	0.500± 0.046 (20 segments / 20 / 20 / 4)	0.406 ± 0.048 (20segments / 20 / 20 / 4)	1.419 (6)	0.206
Figure 4A; Apical spine density PND23-25 (μm^{-1})	0.613 ± 0.020 (20 segments / 20 / 20 / 4)	0.712 ± 0.056 (20 segments / 20 / 20 / 4)	1.682 (6)	0.144
Figure 4A; Basal spine density PND11 (μm^{-1})	0.404± 0.035 (20 segments / 20 / 20 / 4)	0.513 ± 0.034 (20 segments / 20 / 20 / 4)	2.251 (6)	0.065
Figure 4A; Basal spine density PND23-25 (μm^{-1})	0.613 ± 0.037 (20 segments / 20 / 20 / 4)	0.704 ± 0.048 (20 segments / 20 / 20 / 4)	1.509 (6)	0.182
Figure 4B; Apical spine size PND11	(522 spines / 20 / 20 / 4)	(346 spines / 20 / 20 / 4)		> 0.05
Figure 4B; Apical spine size PND23-25	(543 spines / 20 / 20 / 4)	(618 spines / 20 / 20 / 4)		> 0.05
Figure 4B; Basal spine size PND11	(488 spines / 20 / 20 / 4)	(514 spines / 20 / 20 / 4)		> 0.05
Figure 4B; Basal spine size PND23-25	(571 spines / 20 / 20 / 4)	(611 spines / 20 / 20 / 4)		0.014
Figure 4A; Total dendrite length for apical spine density PND11 (μm)	1117.565	901.823		
Figure 4A; Total dendrite length for apical spine density PND23-25 (μm)	114.24	1016.302		
Figure 4A; Total dendrite length for basal spine density PND11 (μm)	919.571	893.370		
Figure 4A; Total dendrite length for basal spine density PND23-25 (μm)	962.636	889.034		

Unpaired student t-test

Table 2

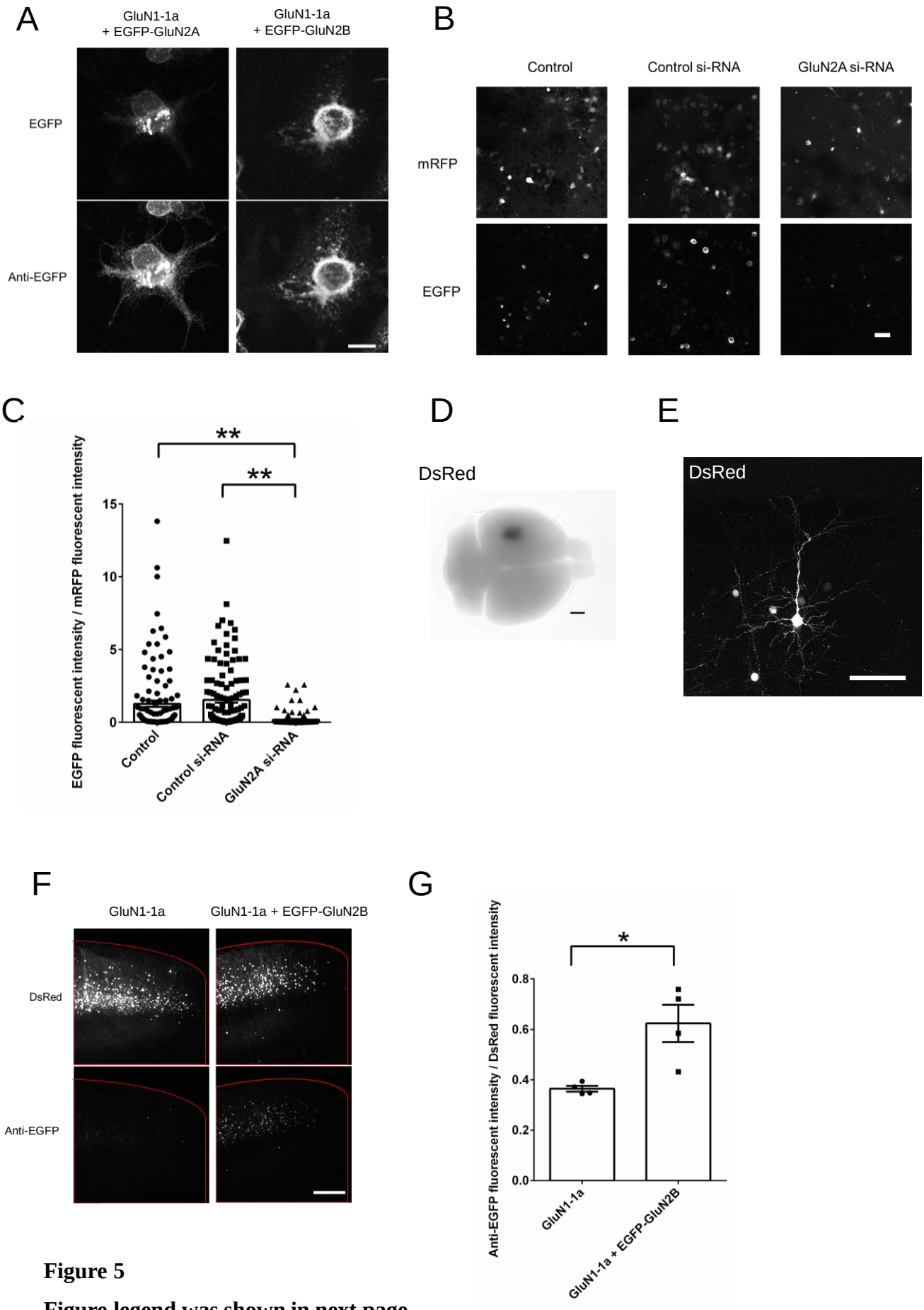

Figure 5

Figure legend was shown in next page.

Figure 5. Evaluation of expression constructs and knockdown constructs

(A) EGFP fluorescence and anti-EGFP immunoreactivity in COS-7 cells transfected with CMV promotor GluN1-1a and CMV promotor EGFP-GluN2A (GluN2A) or COS-7 cells transfected with CMV promotor GluN1-1a and CMV promotor EGFP-GluN2B (GluN2B)
(B) mRFP fluorescence and EGFP fluorescence in COS-7 cells transfected with β-actin promotor mRFP and CMV promotor EGFP-GluN2A (Control), βactin promotor mRFP, CMV promotor EGFP-GluN2A, and pSilencer control siRNA (Control si-RNA), and βactin promotor mRFP, CMV promotor EGFP-GluN2A, and pSilencer GluN2A siRNA (GluN2A si-RNA).
(C) EGFP fluorescence and mRFP fluorescence ratio in COS-7 cells expressing the combination of expression vectors and si-RNA vectors shown in (B) (Control cell n = 121, Control si-RNA cell n = 127, GluN2A si-RNA cell n = 118)
(D) DsRed fluorescence in the fixed brain after in utero electroporation of the following four plasmids; β-actin promotor-LoxP-STOP-LoxP-GluN1-1a, β-actin promotor-LoxP-STOP-LoxP-EGFP-GluN2B, β-actin promotor-LoxP-STOP-LoxP-DsRed, and β-actin-promoter-Cre.
(E) DsRed fluorescence in the somatosensory cortex layer 2/3 pyramidal neuron detected in the brain shown in (D).
(F) DsRed fluorescence and anti-EGFP fluorescence in the somatosensory cortex expressing βactin promotor-LoxP-STOP-LoxP-GluN1-1a, βactin promotor-LoxP-STOP-LoxP-DsRed, β-actin-promoter-Cre, with or without β-actin promotor-LoxP-STOP-LoxP-EGFP-GluN2B.
(G) DsRed fluorescence and anti-EGFP fluorescence ratio in the somatosensory cortex after in utero electroporation of the combinations of plasmids shown in (F) (GluN1-1a; n = 4 mice, GluN1-1a + EGFP-GluN2B; n = 4 mice)
Each image was made from a maximal intensity projection Z stuck images by ImageJ.
Data are presented as mean ± s. e. m. *$p < 0.05$, unpaired Student's t-test and one-way ANOVA with post hoc Turkey test.
Scale bars; 20 μm (A), 100 μm (B), 1 mm (F) 100 μm (G) and 500 μm (H).

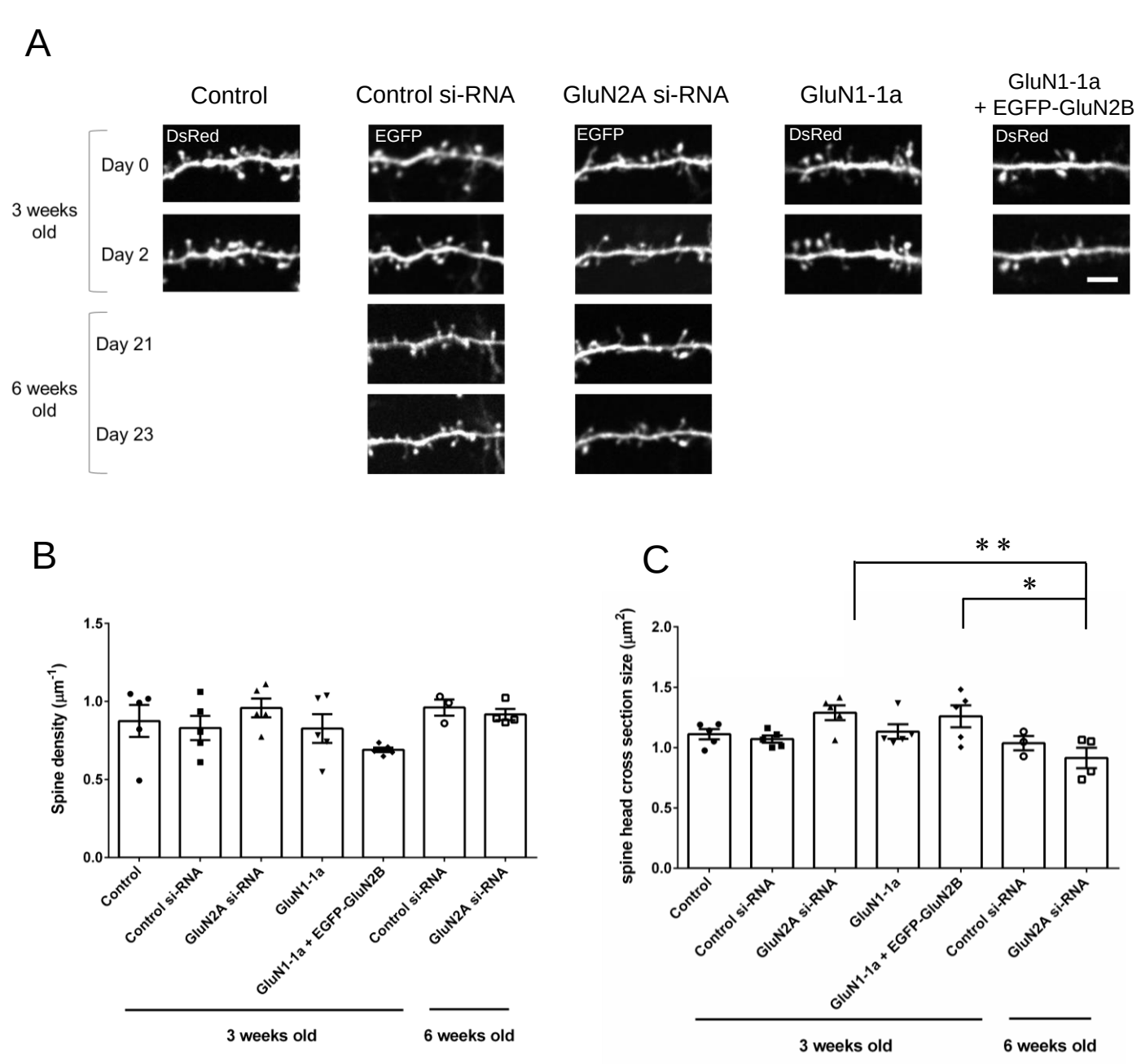

Figure 6. GLuN2A knockdown mice showed larger spine head size, but the expression of GluN2A/ 2B modification had little effect on spine density and morphology

(A) Apical dendrites of DsRed- or EGFP-positive layer 2/3pyramidal neurons in mice received in utero electroporation with the combinations of plasmids for overexpression or downregulation of GluN2 subunits. The five different types of manipulations are shown. The images of dendrites at two developmental stages, postnatal 3 weeks or postnatal 6 weeks, with an interval of two days in each developmental stage, are presented. Each image is a maximal intensity projection made from Z stuck Images by ImageJ. Scale bar; 10 μm.
(B, C) Spine density (B) or spine head cross section area (C) measured in the apical dendrites of layer 2/3 pyramidal neurons at postnatal 3 weeks or 6 weeks, with manipulations in the expression of GluN2 subunits. (Control n = 5 (mice), Control si-RNA l n = 5 (mice), GluN2A si-RNA n = 5 (mice), GluN1-1a n = 5 (mice), GluN1-1a + EGFP-GluN2B n = 5 (mice), 6 weeks old Control si-RNA n = 3 (mice), 6 weeks old GluN2A si-RNA n = 4 (mice)).
Data are presented as mean ± s. e. m. *p < 0.05, **p < 0.01, one-way ANOVA with post hoc Turkey test.

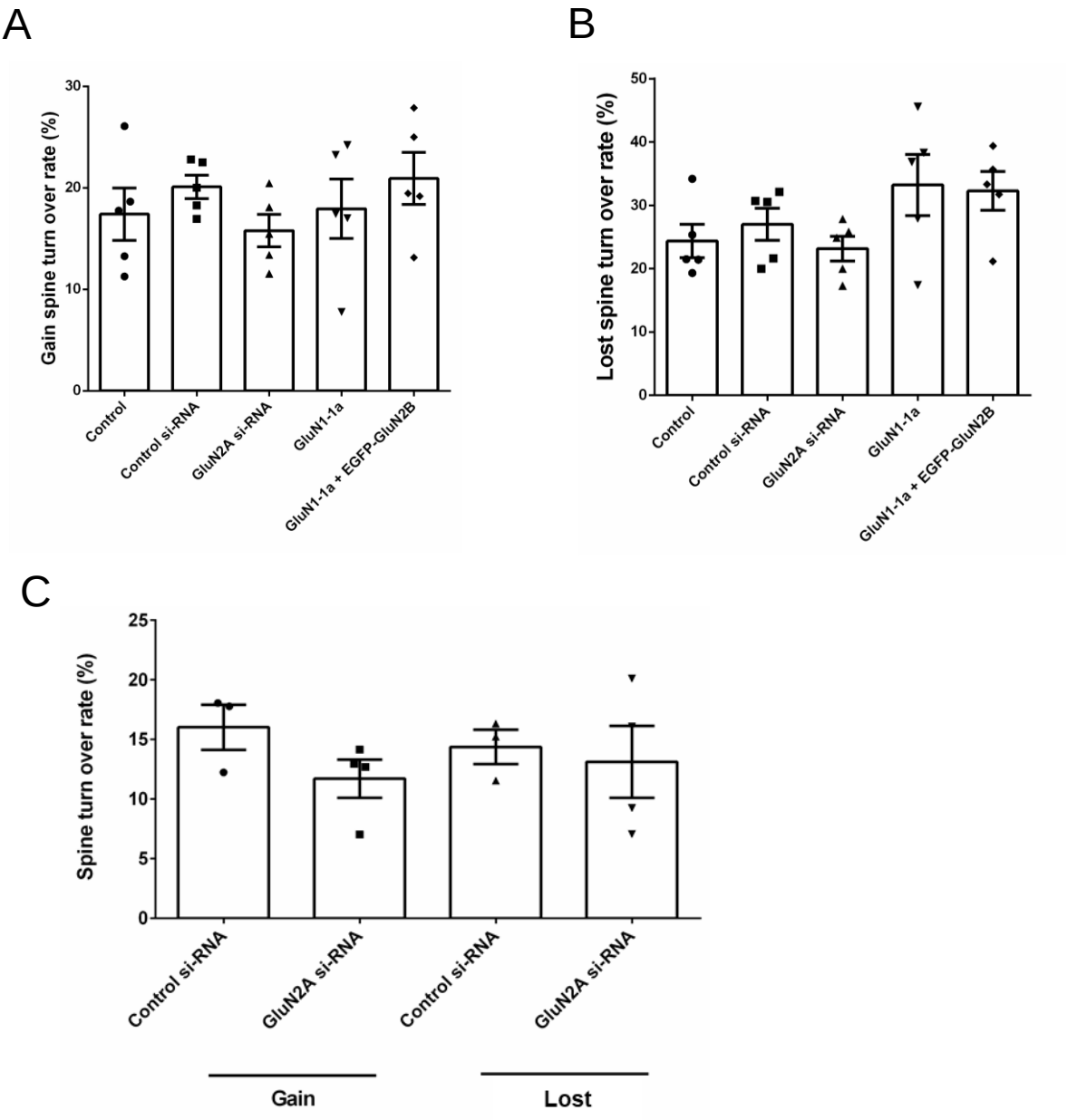

Figure 7. The effects of manipulating the expression ratio of GluN2A/2B on spine dynamics

(A, B) Rates of spine addition (A) or spine elimination (B) measured in the apical dendrites of layer 2/3 pyramidal neurons at postnatal 3 weeks, with manipulations in the expression of GluN2 subunits. (Control n = 5 (mice), Control si-RNA l n = 5 (mice), GluN2A si-RNA n = 5 (mice), GluN1-1a n = 5 (mice), GluN1-1a + EGFP-GluN2B n = 5 (mice)).
(C) Rates of spine addition and spine elimination measured in the apical dendrites of layer 2/3 pyramidal neurons at postnatal 6 weeks, with manipulations in the expression of GluN2 subunits. (Control si-RNA n = 3 (mice), GluN2A si-RNA n = 4 (mice)).
Data are presented as mean ± s. e. m., unpaired Student's t-test or one-way ANOVA test.

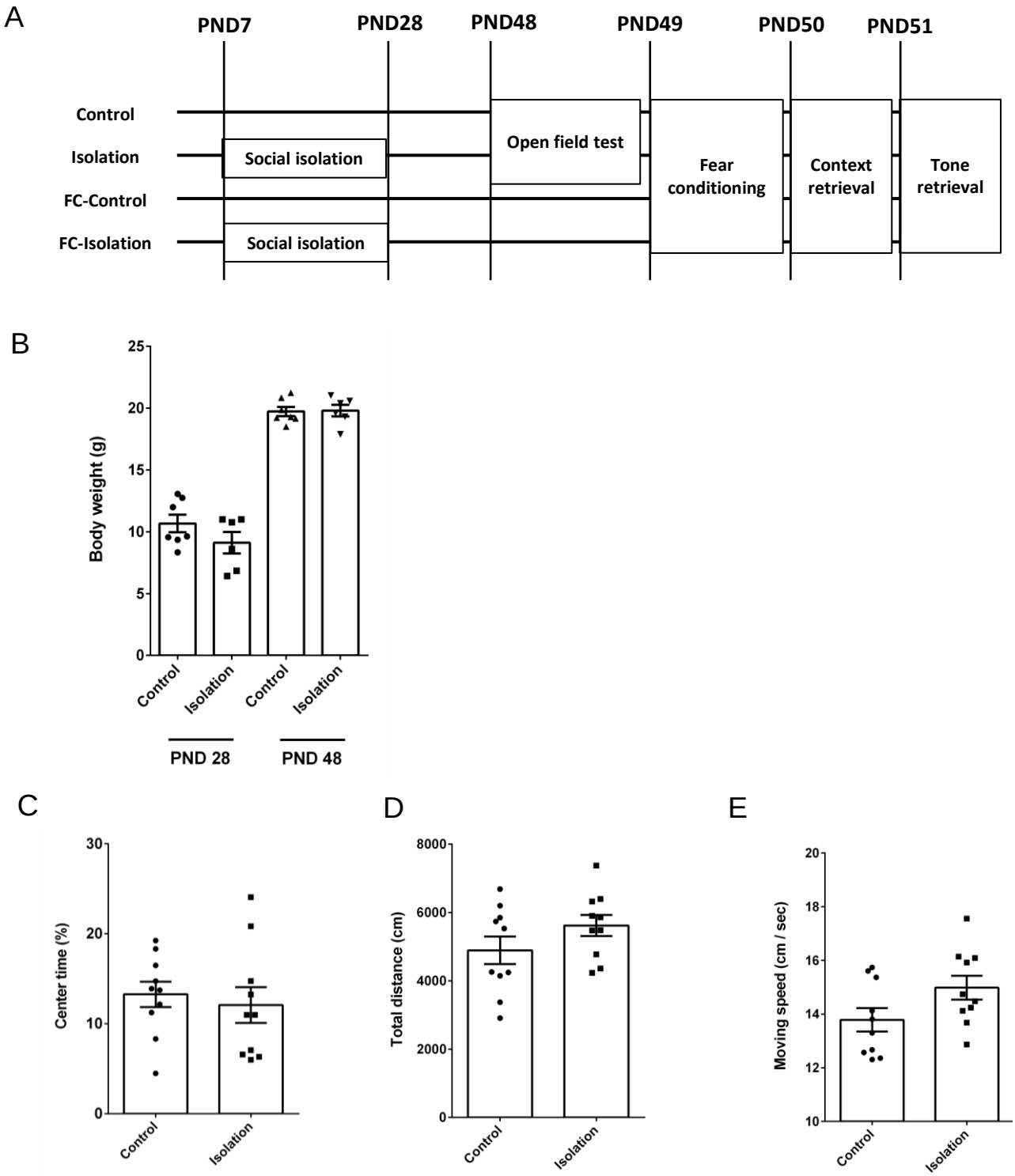

Figure 8. Analysis of anxiety-related behavior in socially isolated mice

(A) Timeline of experiments.
(B) Body weight of control mice and mice after social isolation. Body weights were measured at the end of the social isolation (PND 28) and the start of behavioral tests (PND48). (Control n = 7 (mice), Isolation n = 6 (mice))
(C-E) The ratio of time spent in the Center Area (C), the total distance traveled (D), and the speed of locomotion during 10 minutes recording of the Open field test. (Control n = 10 (mice), Isolation n = 10 (mice))
Data are presented as mean ± s. e. m. unpaired Student's t-test.

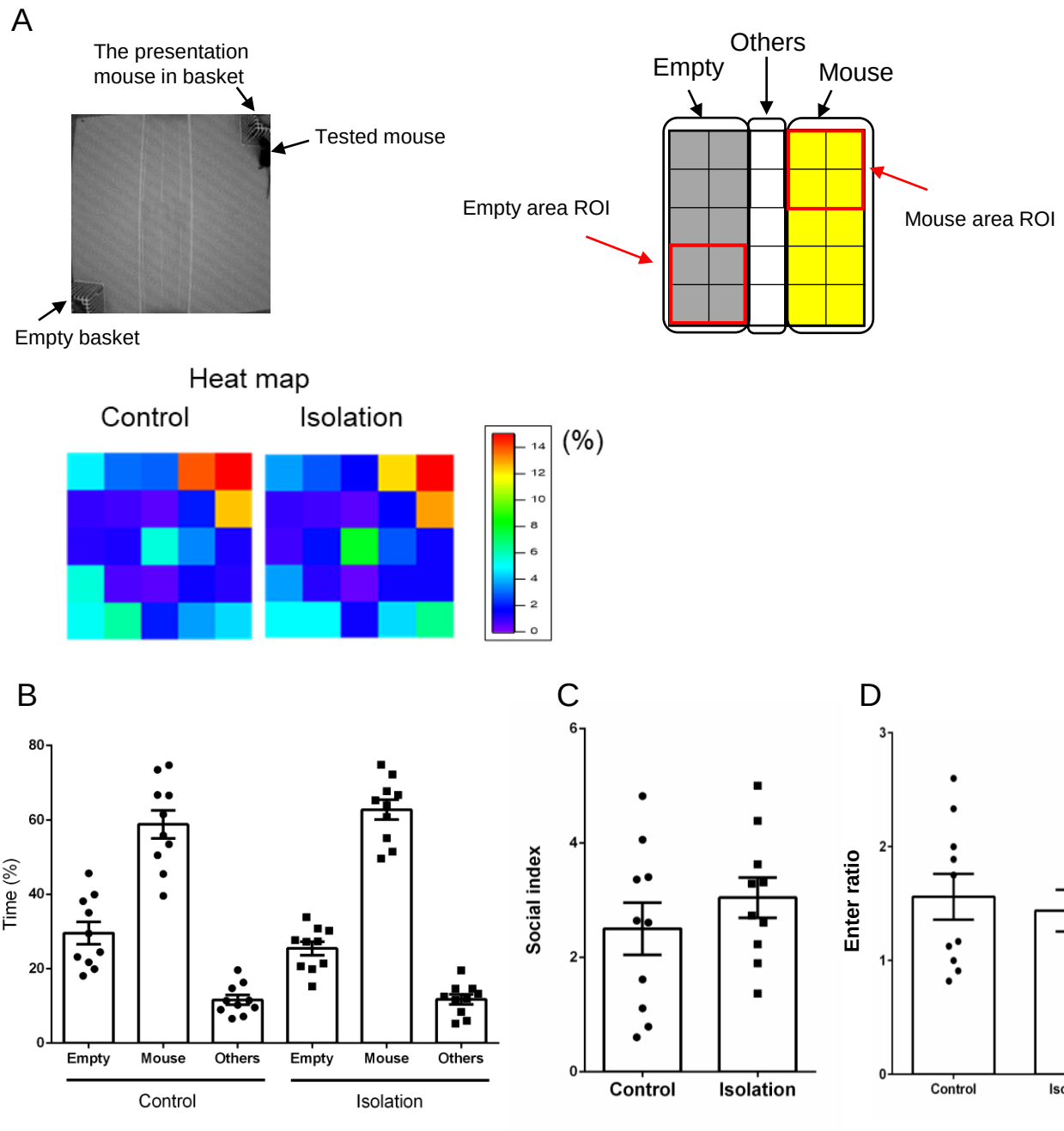

Figure 9. Analysis of social behavior in socially isolated mice

(A) The Empty Area and Mouse Area in the three-chamber test shown on the left. Heatmaps based on the average time spent at each block of Control mice and Isolation mice during 10 minutes of the recording. Empty area ROI and Mouse area ROI were defined for calculation of social index and enter ratio.
(B-D) The time in each area (B), the ratio of time spent at Empty area and Mouse area (social index) (C), the ratio of entry number to the Mouse Area and the Empty Area (Enter ratio) (D) during 10 min of recording. (Control n = 10 (mice), Isolation n = 10 (mice))
Data are presented as mean ± s. e. m, unpaired Student's t-test or two-way ANOVA with post hoc Bonferroni's test.

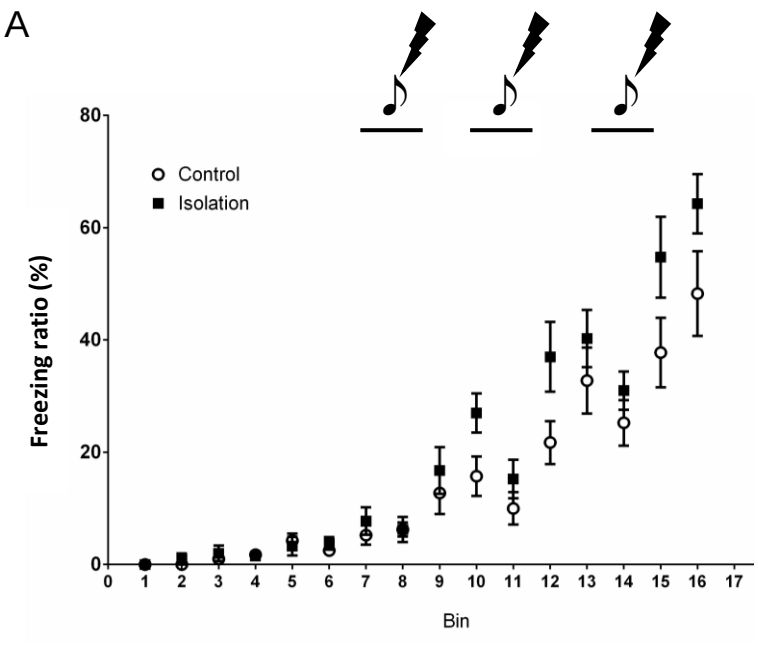

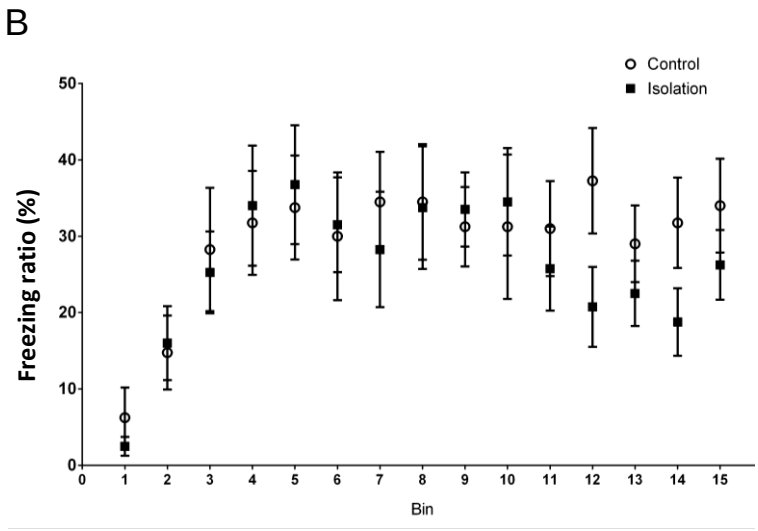

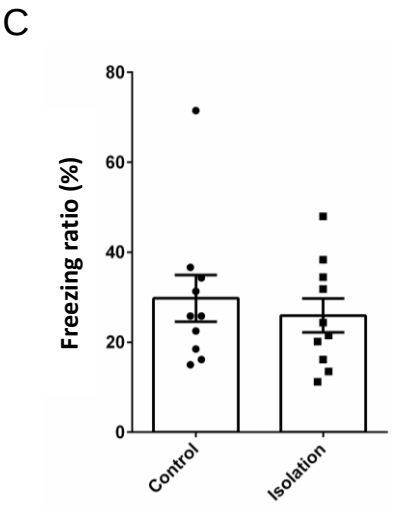

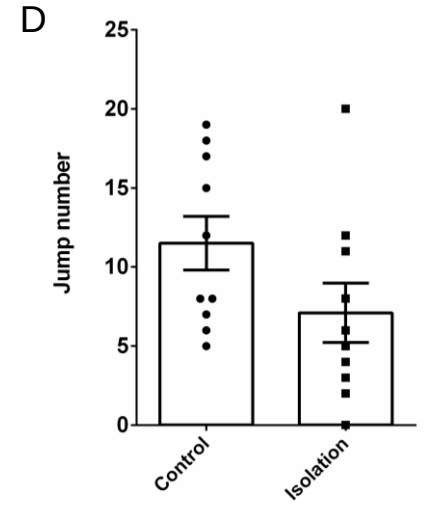

Figure 10. Retrieval of context-dependent fear memory in socially isolated mice

(A) The freezing time in each time bin of 20 seconds after placing mice in the conditioning environment and the presentation of tones coupled with the foot shock.
(B) The temporal profiles of freezing behavior along the time axis with 20-second bins in the context retrieval.
(C) The percent of freezing time during the context retrieval for 5 minutes of recording.
(D) The number of jumping behaviors during the context retrieval for 5 minutes recording.
(Control n = 10 (mice), Isolation n = 10 (mice) for A-D.)
Data are presented as mean ± s. e. m., unpaired Student's t-test or two-way ANOVA -with post hoc Bonferroni's test.

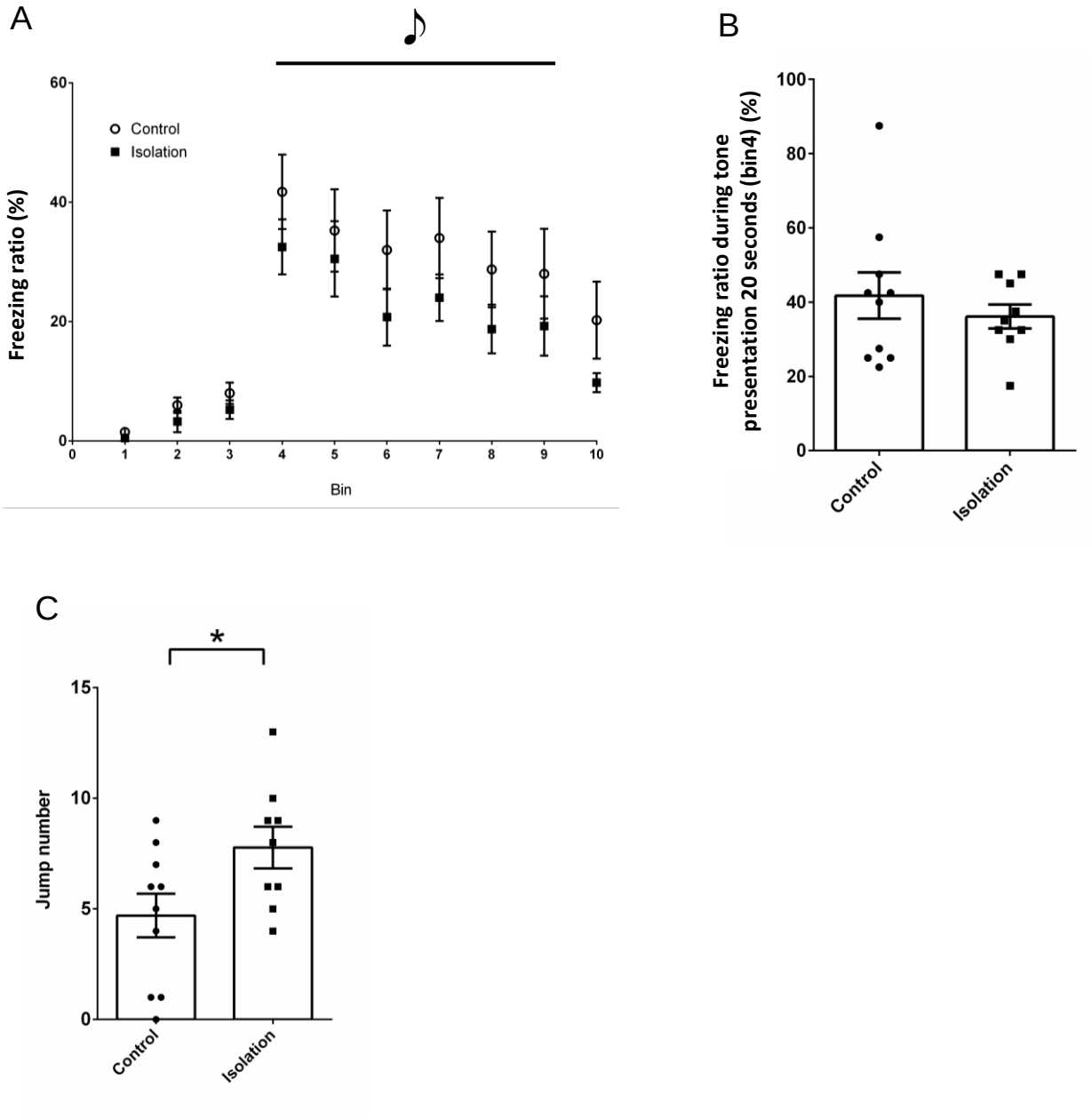

Figure 11. Tone-dependent fear memory retrieval of socially isolated mice

(A) The temporal profiles of the freezing behavior in response to the conditioned tone presentation. The temporal bins are 20 seconds.
(B) The fraction of time with freezing behavior in the tone retrieval test. The data are derived from bin 4 in (A).
(C) The total number of jumping behaviors during 120 seconds of the tone presentation.
(Control n = 10 (mice), Isolation n = 9 (mice) for A-C.)
Data are presented as mean ± s. e. m. *p < 0.05, unpaired Student's t-test or two-way ANOVA with post hoc Bonferroni's test.

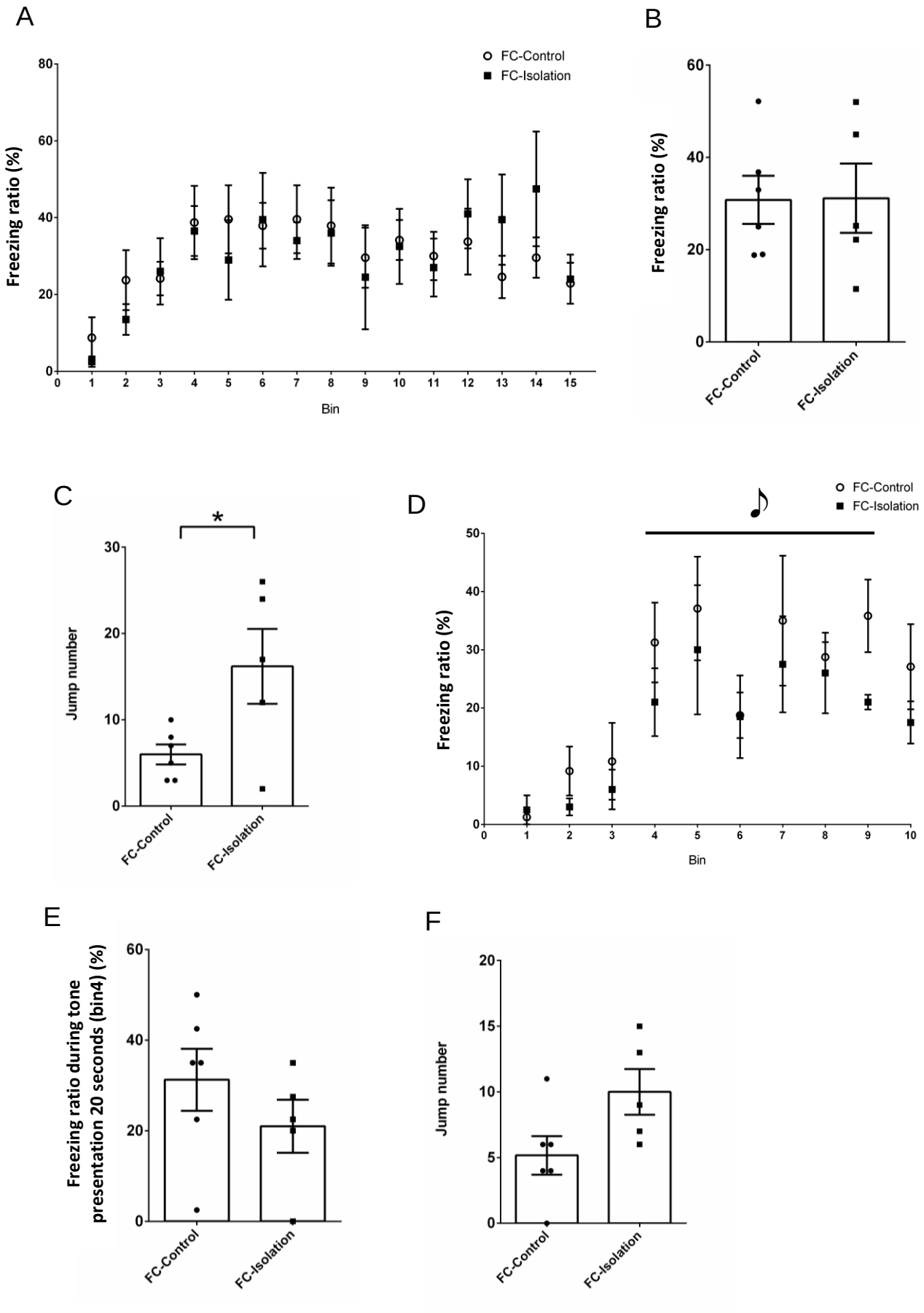

Figure 12

Figure legend was shown in next page.

Figure 12. Fear memory retrieval of socially isolated mice without prior behavioral tests

(A) The temporal profiles of the freezing behavior in the context retrieval test. The time bines are 20 seconds.
(B) The fraction of time spent in freezing behavior in the context retrieval test with 5 minutes of recording time.
(C) The number of jumping behaviors in the 5 minutes of the context retrieval test.
(D) The temporal profiles of the freezing behavior in the tone retrieval test. The time bines are 20 seconds.
(E) The fraction of time spent in freezing behavior in the tone retrieval test at bin 4 in (D).
(F) The number of jumping behaviors during 120 seconds of tone presentation in the tone retrieval test.
FC-Control n = 6 (mice), FC-Isolation n = 5 (mice) for A-F
Data are presented as mean ± s. e. m. *$p < 0.05$, unpaired Student's t-test or two-way ANOVA with post hoc Bonferroni's test.

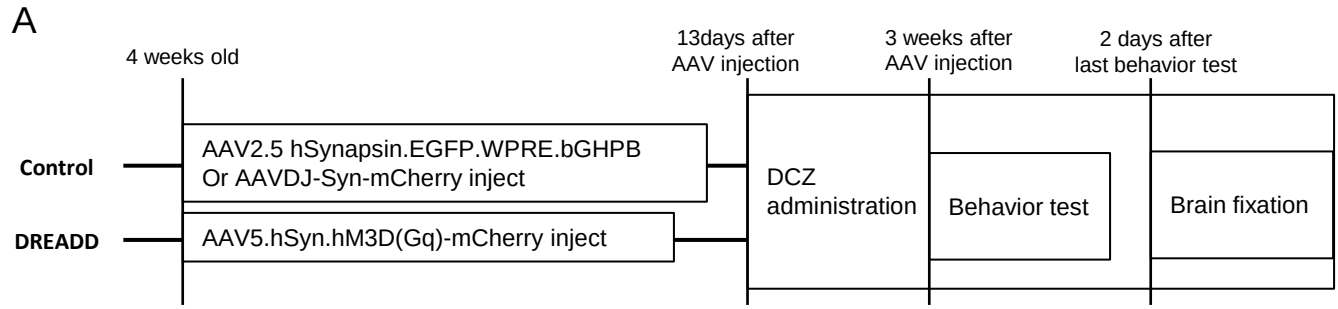

	Day1	Day2	Day3	Day4
#1	Open field test Mechanical Von flay test	Fear conditioning	Context retrieval	Tone retrieval
#2	Open field test	Generalized Fear conditioning	Unconditioned tone retrieval Conditioned tone retrieval	
#3	Open field test	3 chamber test	Electric von flay test	

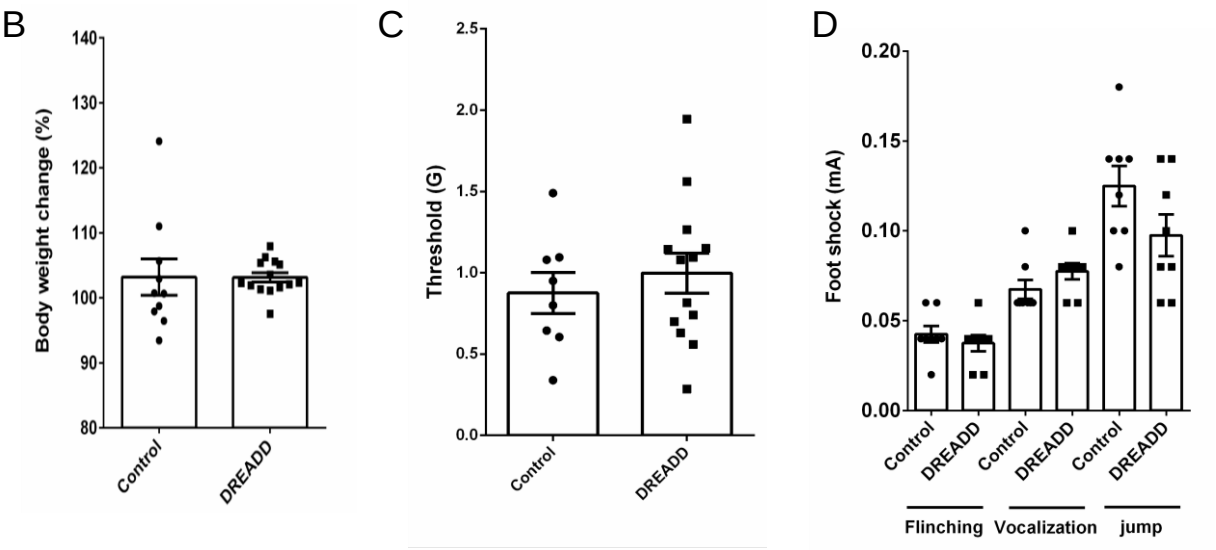

Figure 13. Analysis of anxiety-related behavior in mice with acute activation of the PB

(A) Timeline of experiments.
(B) Body weight changes in control mice and mice with DREADD on the first day of the behavioral experiment, compared to the first day of DCZ i.p. injection. Control n = 10 (mice), DREADD n = 14 (mice)
(C) The result of the mechanical von flay test. Mechanical pain thresholds of both hind legs were averaged. Control n = 8 (mice), DREADD n = 13 (mice)
(D) The result of the electrical von flay test. The data of pain thresholds for flinching, vocalization, and jump are presented. Control n = 8 (mice), DREADD n = 8 (mice)
Data are presented as mean ± s. e. m., unpaired Student's t-test or two-way ANOVA with post hoc Bonferroni's test.

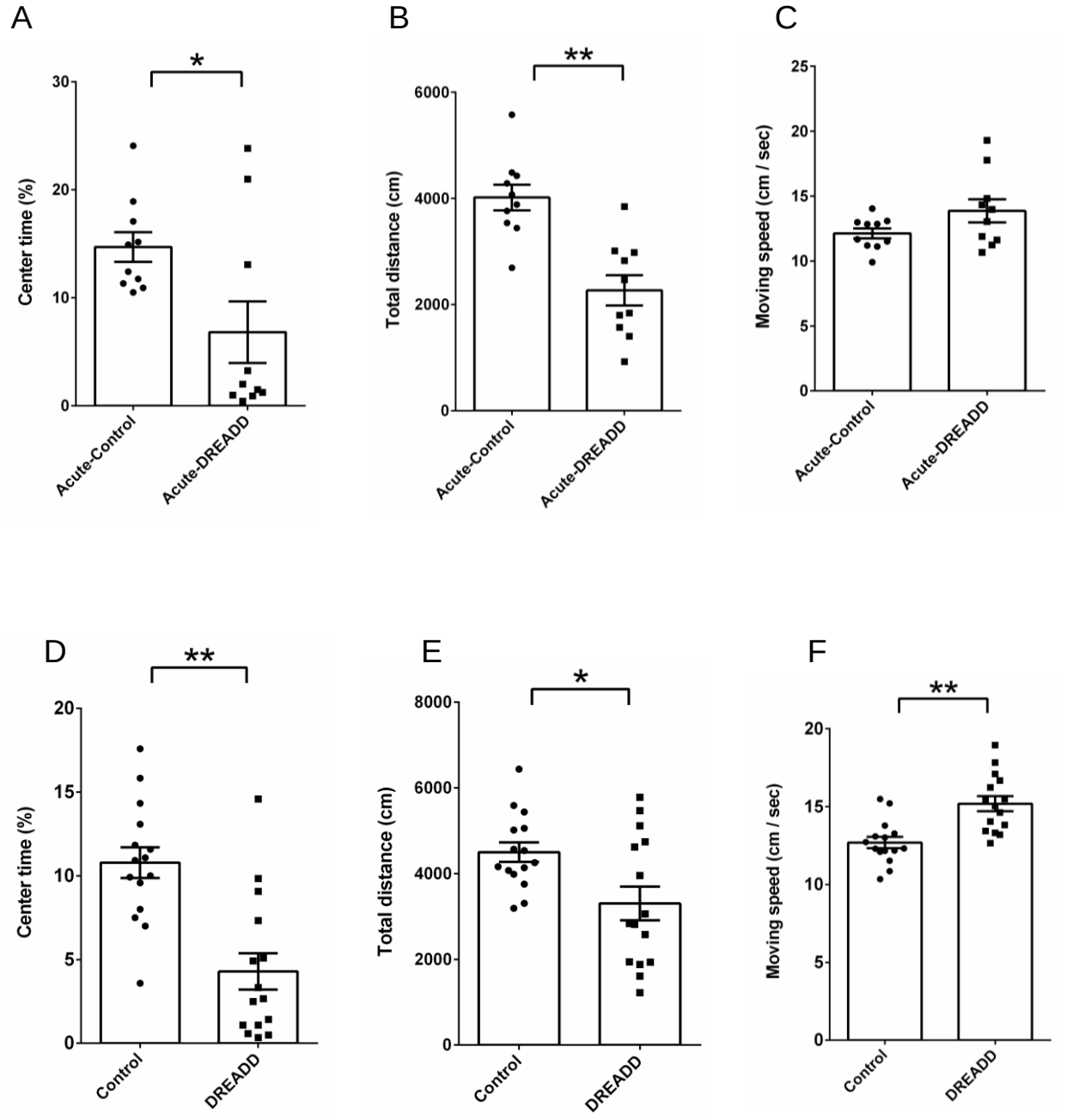

Figure 14. Analysis of anxiety-related behavior in mice with chronic activation of PB

(A-F) The ratio of time spent in the Center Area (A, D), the total distance traveled (B, E), and the speed of locomotion (C, F) in the open-field test for10 minutes of recording. Mice after single DCZ administration (A-C) and mice after chronic PB activation by DREADD (D-F) were analyzed. Control n = 15 (mice), DREADD n = 15 (mice).
Data are presented as mean ± s. e. m, *p < 0.05, **p < 0.01, unpaired Student's t-test.

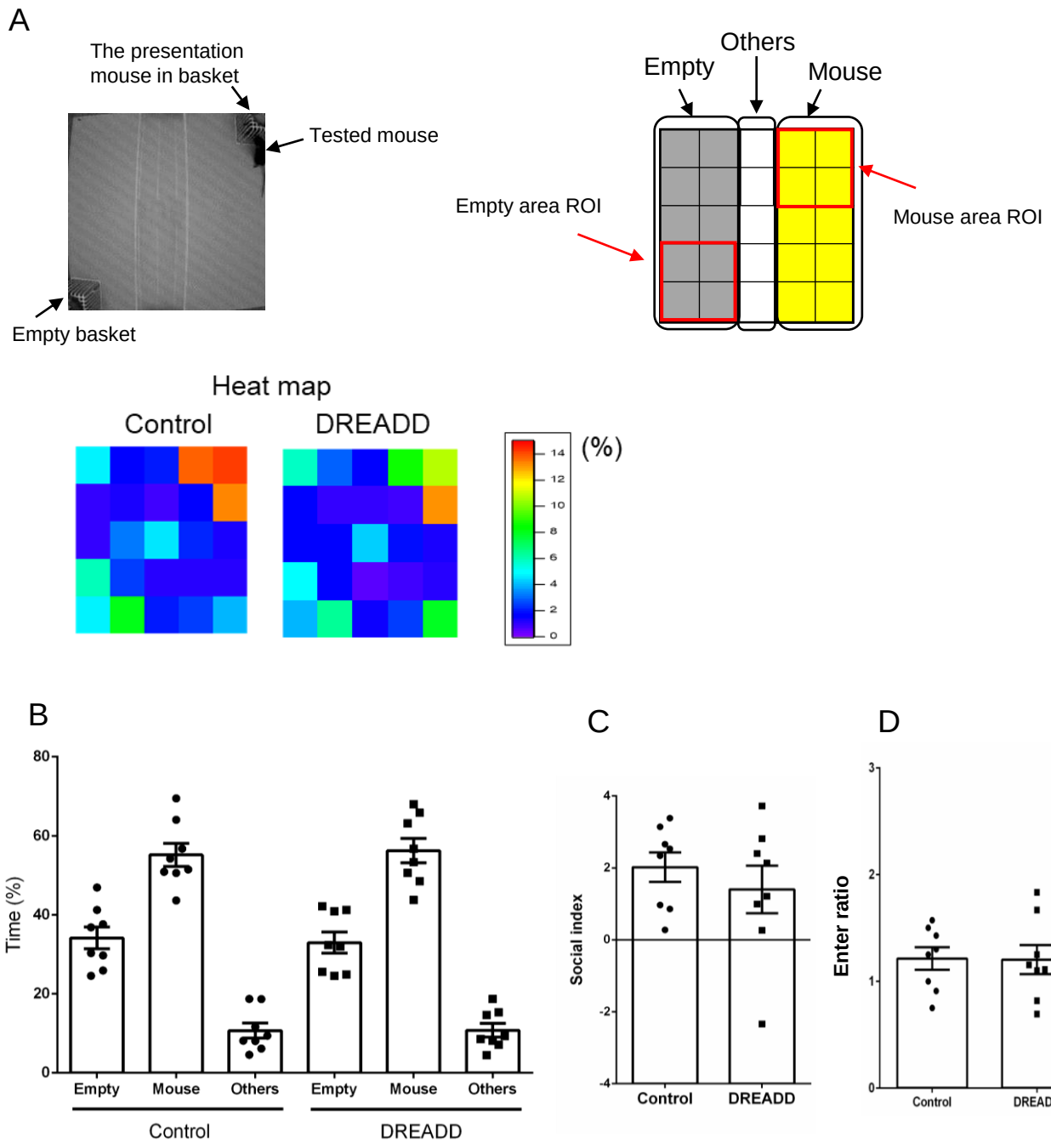

Figure 15. Analysis of social behavior in mice with chronic activation of PB

(A) The Empty Area and Mouse Area in the three-chamber test shown on the left. Heatmaps based on the average dwelling time of each group of mice during 10 minutes of the recording are shown on the right. Empty area ROI and Mouse area ROI were defined for calculation of social index and enter ratio.
(B-D) The time in each area (B), the ratio of time spent at Empty area and Mouse area (social index) (C), the ratio of entry number to the Mouse Area and the Empty Area (Enter ratio) (D) during 10 min of recording. Control n = 8 (mice), DREADD n = 8 (mice).
Data are presented as mean ± s. e. m, unpaired Student's t-test or two-way ANOVA with post hoc Bonferroni's test.

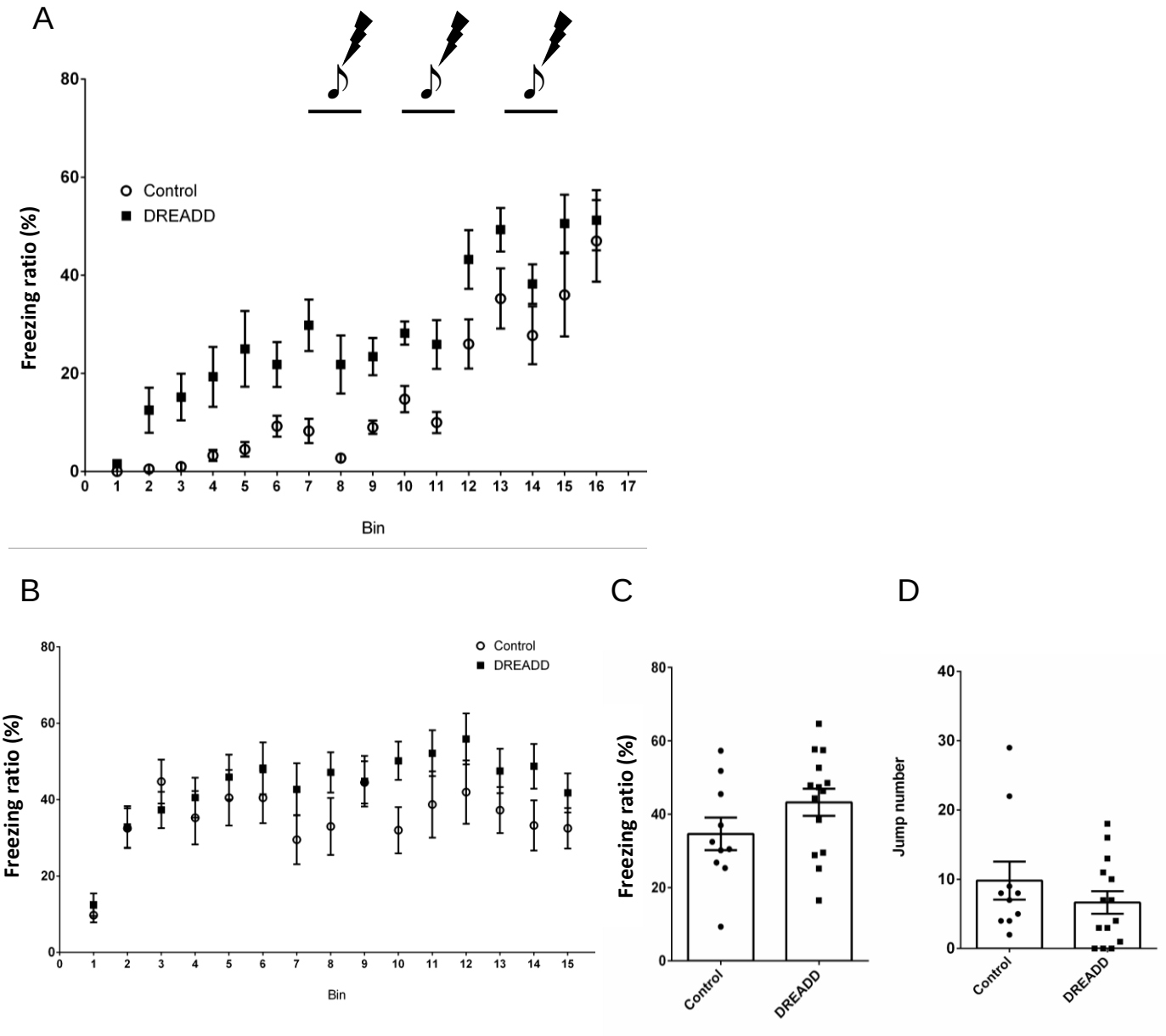

Figure 16. Context-dependent fear memory retrieval in mice with chronic activation of PB

(A) The freezing time in each time bin of 20 seconds after placing mice in the conditioning environment and the presentation of tones coupled with the foot shock.
(B) The temporal profiles of freezing behavior along the time with 20-second bins in the context retrieval.
(C) The percent of freezing time during the context retrieval for 5 minutes of recording.
(D) The number of jumping behaviors during the context retrieval for 5 minutes recording
Control n = 10 (mice), DREADD n = 14 (mice) for A-D.
Data are presented as mean ± s. e. m., unpaired Student's t-test and two-way ANOVA.

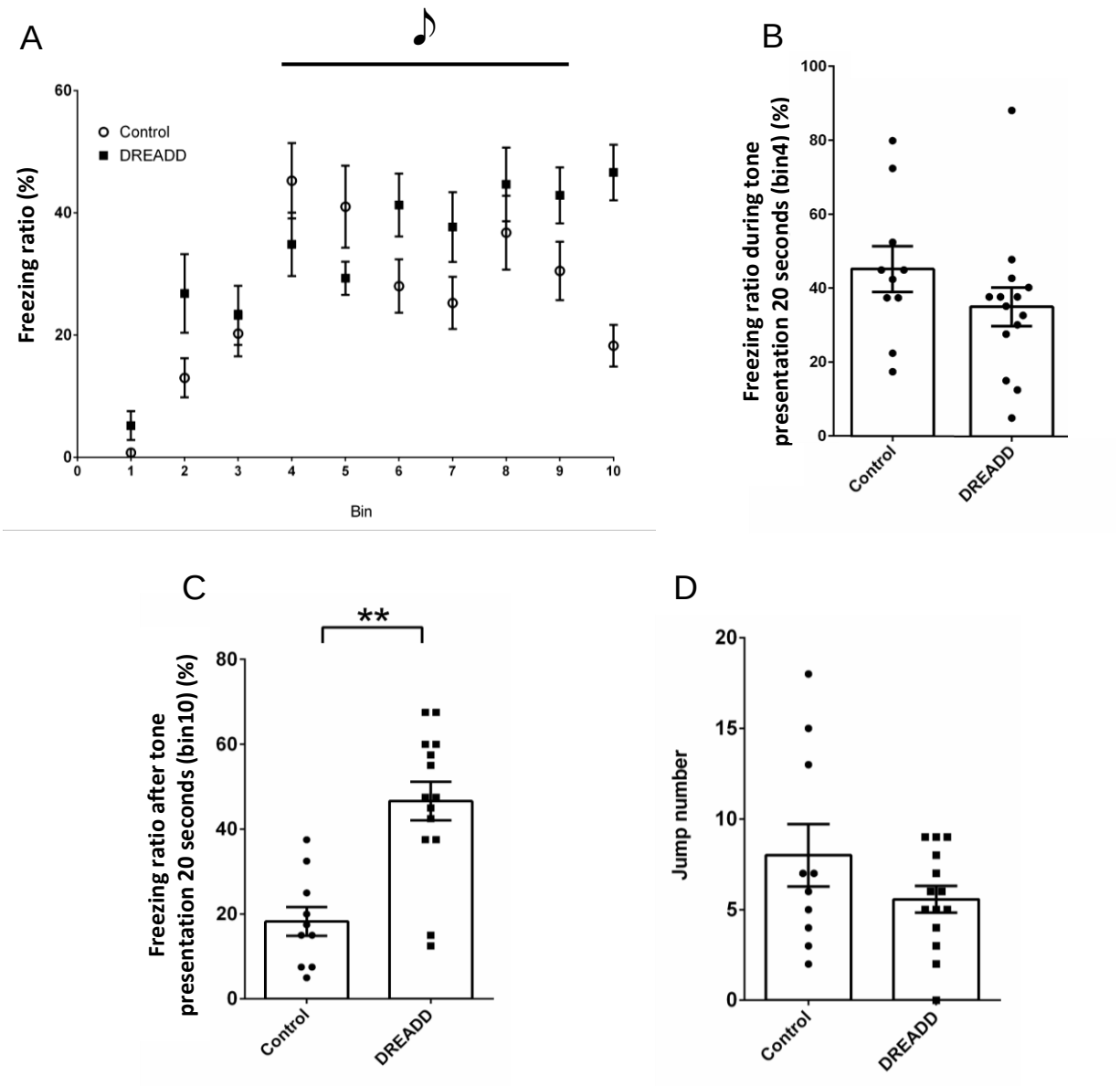

Figure 17. Tone-dependent fear memory retrieval in mice with chronic activation of PB

(A) The temporal profiles of the freezing behavior in response to the conditioned tone presentation. The temporal bins are 20 seconds.
(B) The fraction of time with freezing behavior in the tone retrieval test. The data are derived from bin 4 in (A).
(C) The fraction of time with freezing behavior in the tone retrieval test. The data are derived from bin 10 in (A).
(D) The total number of jumping behaviors during 120 seconds of the tone presentation.
Control n = 10 (mice), DREADD n = 14 (mice) for A-D.
Data are presented as mean ± s. e. m, *p < 0.05, unpaired Student's t-test or two-way ANOVA.

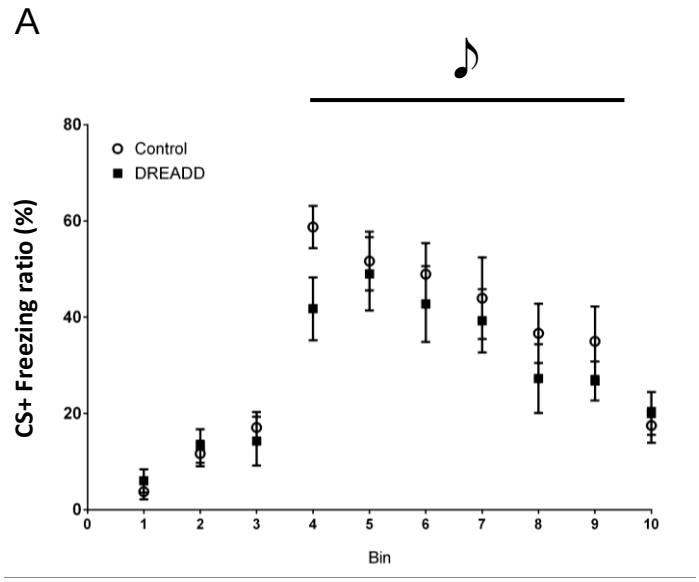

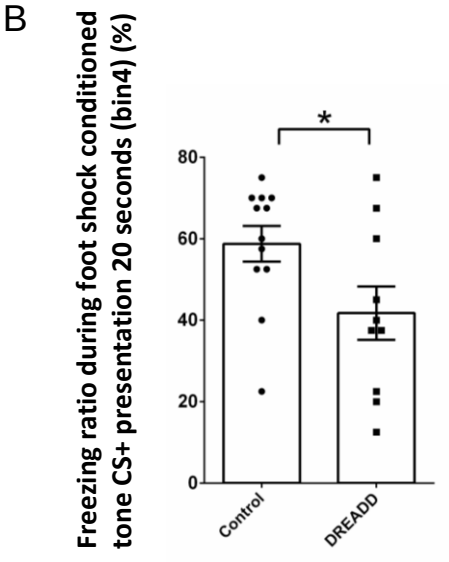

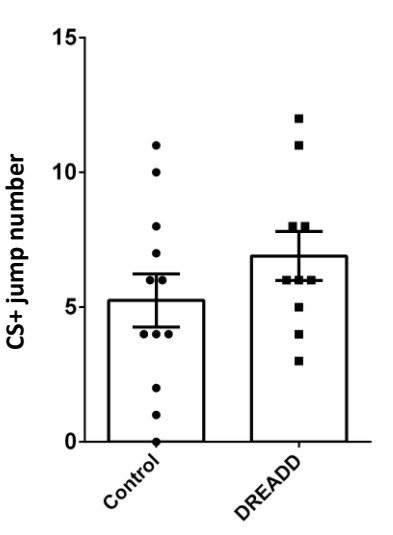

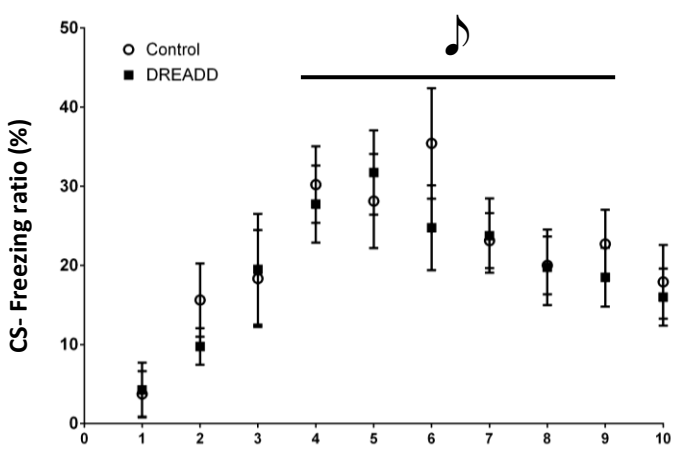

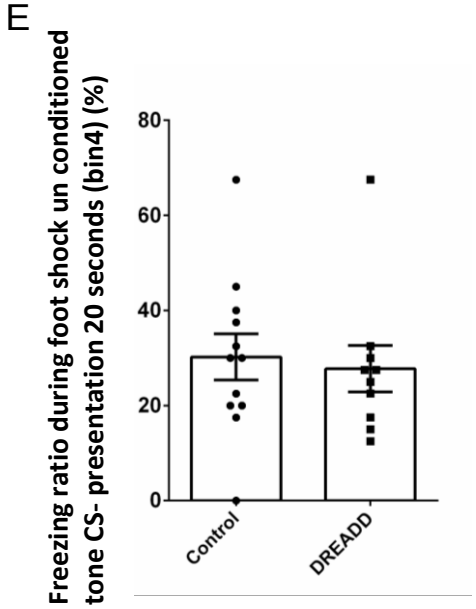

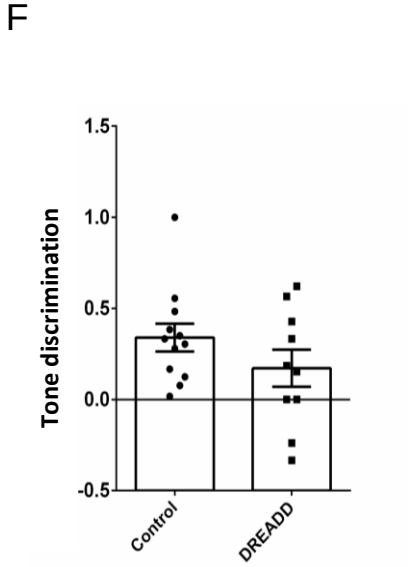

Figure 18

Figure legend was shown in next page.

Figure 18. Tone-dependent fear memory retrieval after generalized fear conditioning in mice with chronic activation of PB

(A) The temporal profiles of the freezing behavior in response to the conditioned tone (CS+) presentation. The temporal bins are 20 seconds.

(B) The fraction of time with freezing behavior in the tone retrieval test for CS+. The data are derived from bin 4 in (A).

(C) The total number of jumping behaviors during 120 seconds of the tone presentation (CS+).

(D) The temporal profiles of the freezing behavior in response to the conditioned tone (CS-) presentation.

(E) The fraction of time with freezing behavior in the tone retrieval test for CS-. The data are derived from bin 4 in (D).

(F) Freezing ratio between CS+ and CS- (Tone discrimination), calculated by each freezing ratio under the 20-second CS+ and CS- tone presentation.

Control n = 12 (mice), DREADD n = 10 (mice) for A-F.

Data are presented as mean ± s. e. m,*$p < 0.05$, unpaired Student's *t*-test or two-way ANOVA with *post hoc* Bonferroni's test.

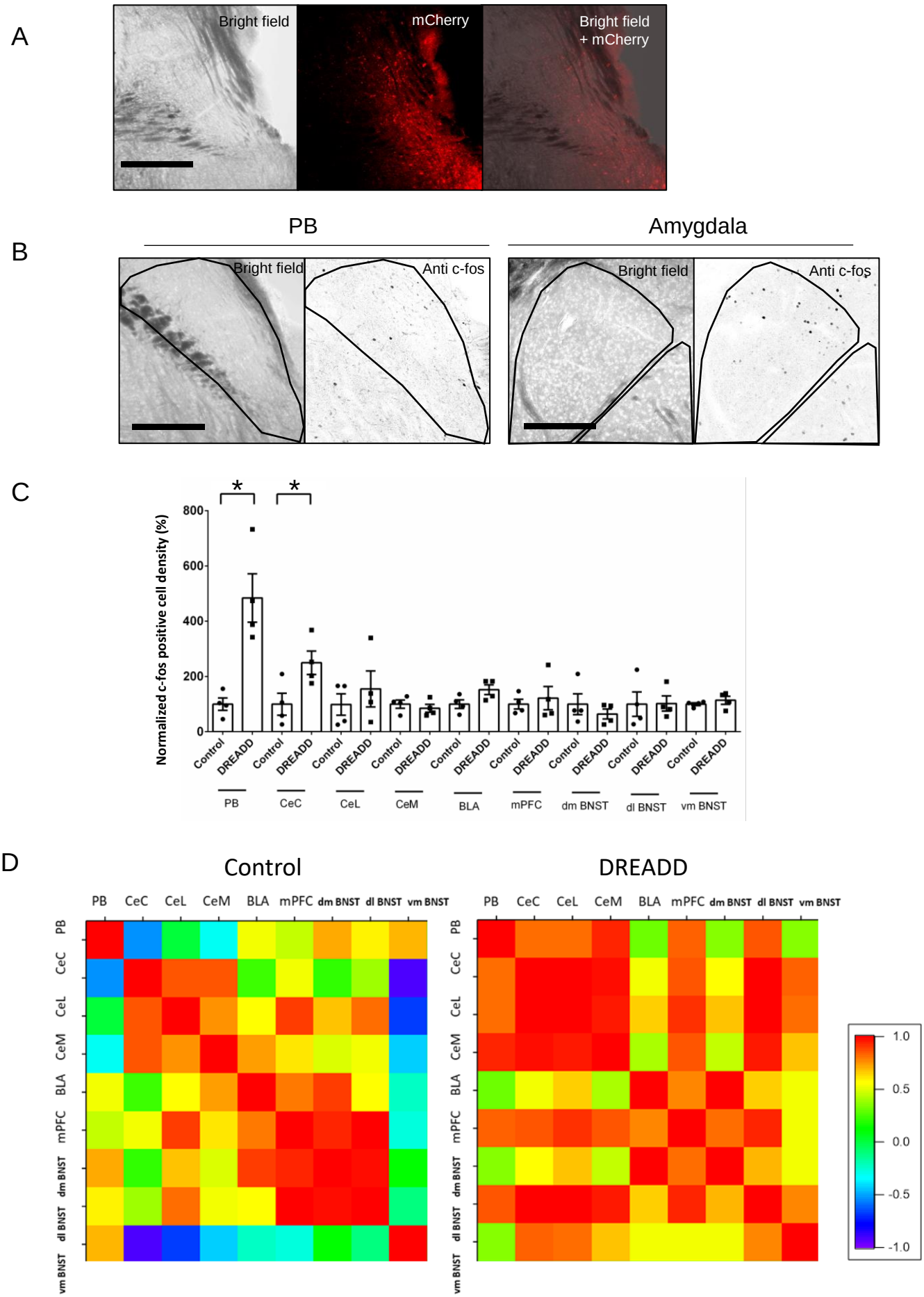

Figure 19

Figure legend was shown in next page.

Figure 19. c-Fos expression and interregional correlations in mice with chronic activation of PB

(A) Distribution pattern of mCherry positive (red) neurons in the PB of DREADD mouse.
(B) Distribution pattern of Anti-c-Fos positive neurons in PB and amygdala of control mouse.
(C) The density of c-Fos positive cells normalized by the average density of c-Fos positive cells in the control mice. The relative densities in PB, CeC, CeL, CeM, BLA, mPFC, dm BNST, dl BNST, and vm BNST are presented.
(D) Interregional correlations matrices based on Pearson's r.
Scale bars; 500 μm (A), 500 μm (B)
Control n = 4 (mice), DREADD n = 4 (mice) for C and D.
Data are presented as mean ± s. e. m., *p < 0.05 unpaired Student's t-test.

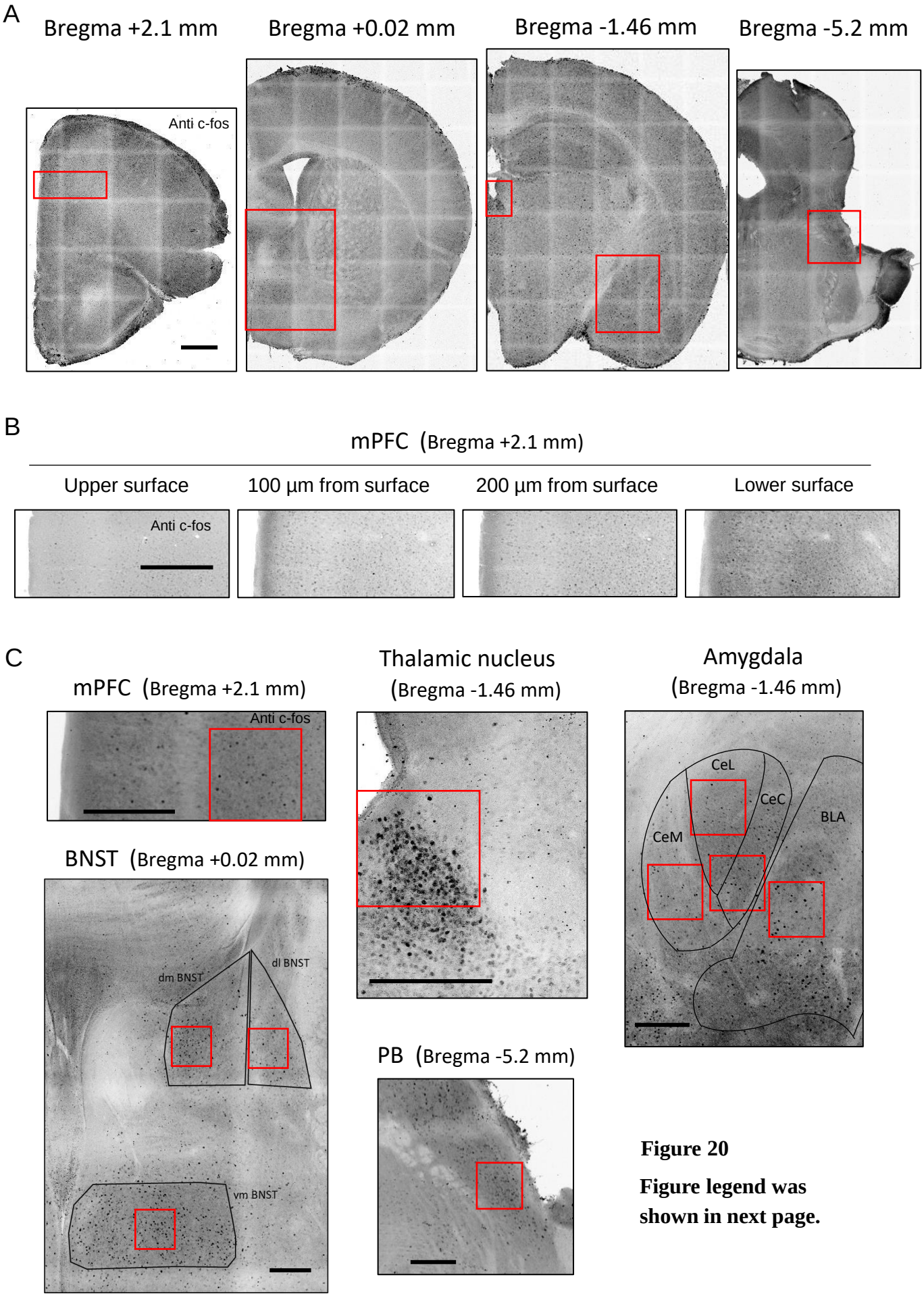

Figure 20

Figure legend was shown in next page.

Figure 20. Defined brain regions for c-Fos density analysis with Ab Scale method

(A) Coronal brain slices of the DREADD mouse stained with an anti-c-Fos antibody with their rostral-caudal positions at bregma +2.1 mm, bregma +0.02 mm, bregma -1.46 mm, bregma -5.2 mm.
(B) c-fos positive neurons in mPFC in the area marked by a red square in the slice at Bregma +2.1 mm slice in Figure 20A. Similar densities of neurons with c-Fos immunoreactivity across the depth of the thick brain slice were confirmed.
(C) Higher magnification images of mPFC, BNST, amygdala, PB and thalamic nucleus. The image areas correspond to the red squares in Figure 20A. The small red squares in these images indicate the positions of images in Figure 21A.
Scale bars; 1 mm (A), 200 μm (B), 200 μm (C)

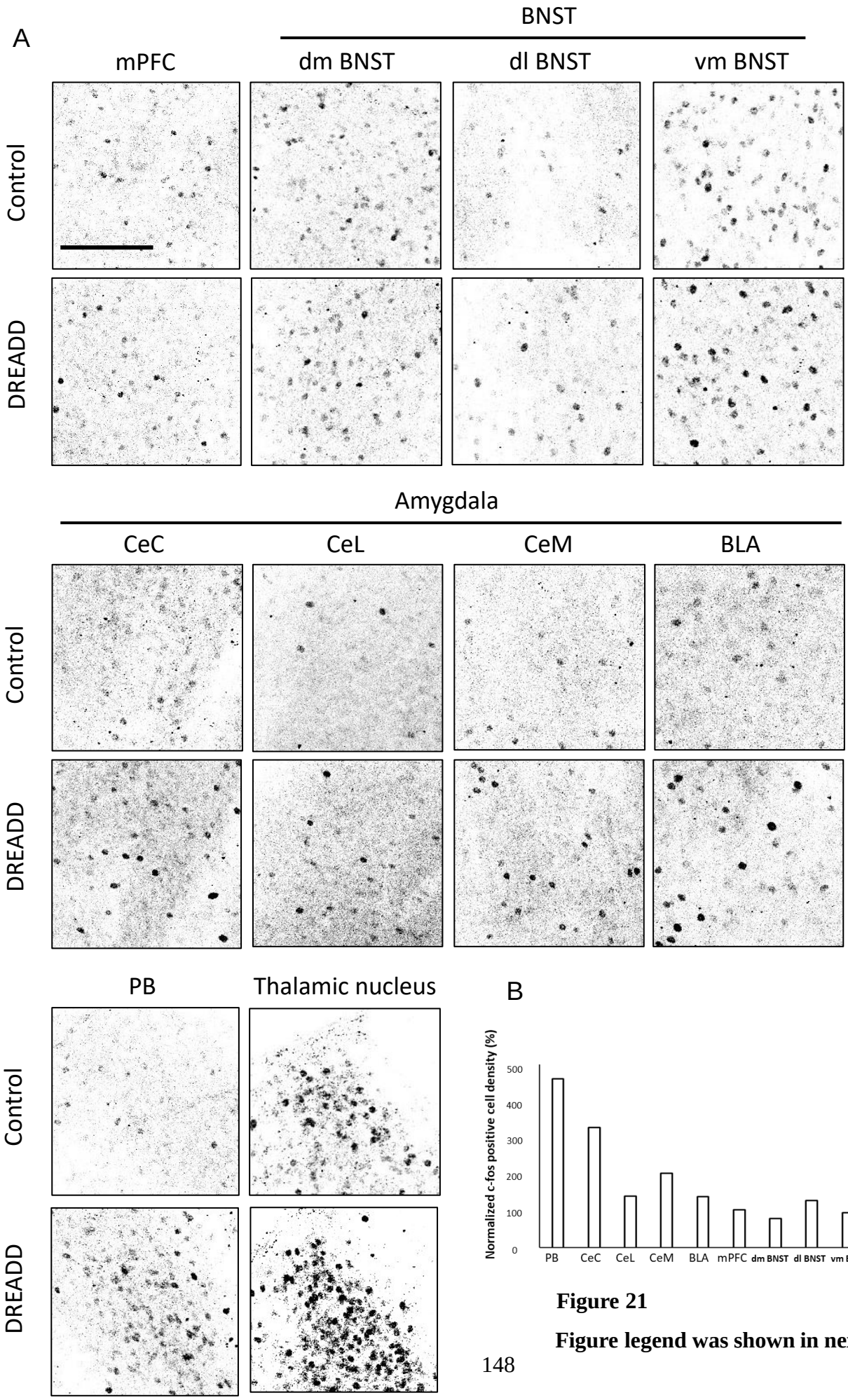

Figure 21

Figure legend was shown in next page.

Figure 21. c-Fos density analysis with Ab Scale method

(A) c-Fos positive cells in control mouse and DREADD mouse. Images represent the areas marked by red squares in Figure 20C.
(B) The density of c-fos positive cells in the DREADD mice normalized by the average density of c-Fos positive cells in the control mice. The relative densities in PB, CeC, CeL, CeM, BLA, mPFC, dm BNST, dl BNST, and vm BNST, thalamic nucleus are presented.
Scale bars; 100 μm

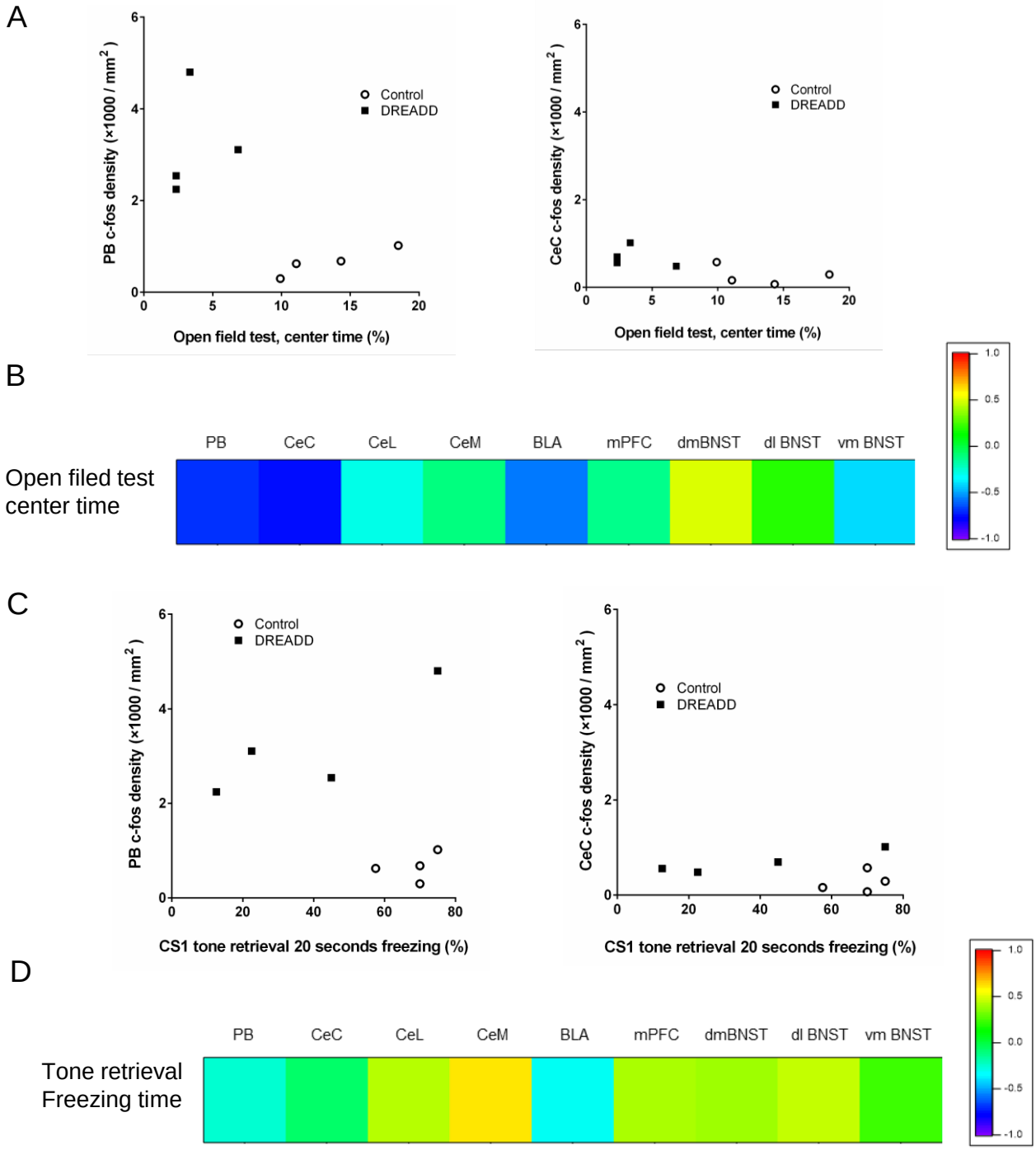

Figure 22. Correlations of c-Fos expression and behavior in mice with chronic activation of PB

(A) Plots of the relationship between total time spent in the central area at the open field test and c-fos positive neurons density in PB and CeC.
(B) Correlations of total time spent in the central area at the open field test and c-Fos positive neurons density based on Pearson's r
(C) Plots of the relationship between the freezing rate during CS1 tone presentation for 20 seconds and c-Fos positive cell density in PB and CeC.
(D) Correlations of the freezing rate during CS1 tone presentation for 20 seconds and c-Fos positive cell density based on Pearson's r.
Control n = 4 (mice), DREADD n = 4 (mice) for A and C.
8 mice including control n = 4 (mice), DREADD n = 4 (mice) for B and D